

Lawrence Berkeley National Laboratory

Recent Work

Title

The Morphological Development of the Nb₃Sn Phase in Multifilamentary Superconducting Wire

Permalink

<https://escholarship.org/uc/item/0p1448wh>

Author

Dietderich, D.R.

Publication Date

1987-12-01

UC-406
LBL-25625
c1

Center for Advanced Materials

CAM

RECEIVED
LAWRENCE
BERKELEY LABORATORY

MAR 3 1989

LIBRARY AND
DOCUMENTS SECTION

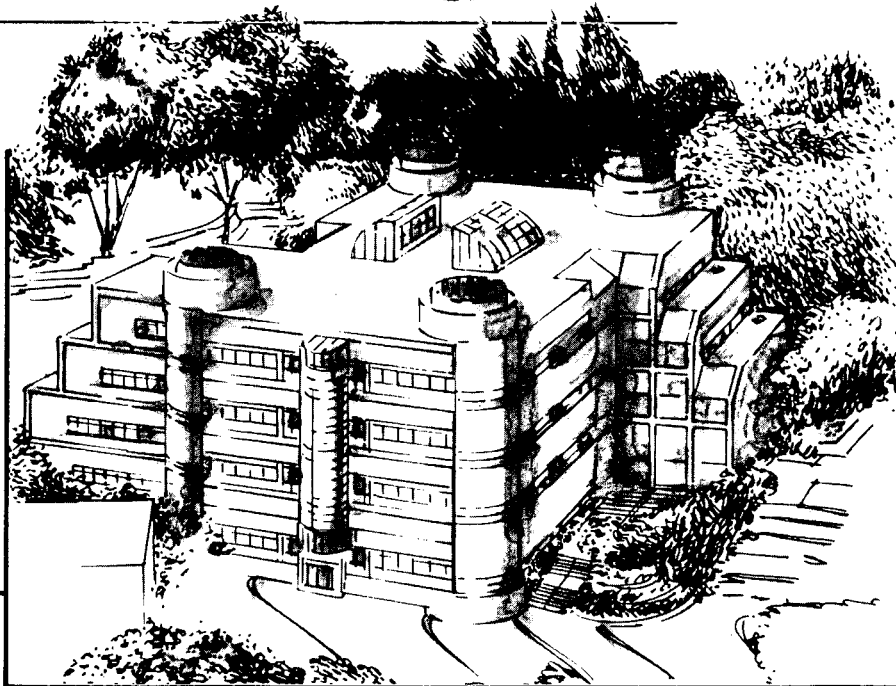
The Morphological Development of the Nb_3Sn Phase in Multifilamentary Superconducting Wire

D.R. Dieterich
(Ph.D. Thesis)

December 1987

For Reference

Not to be taken from this room



Materials and Chemical Sciences Division
Lawrence Berkeley Laboratory • University of California
ONE CYCLOTRON ROAD, BERKELEY, CA 94720 • (415) 486-4755

Prepared for the U.S. Department of Energy under Contract DE-AC03-76SF00098

LBL-25625
c1

DISCLAIMER

This document was prepared as an account of work sponsored by the United States Government. While this document is believed to contain correct information, neither the United States Government nor any agency thereof, nor the Regents of the University of California, nor any of their employees, makes any warranty, express or implied, or assumes any legal responsibility for the accuracy, completeness, or usefulness of any information, apparatus, product, or process disclosed, or represents that its use would not infringe privately owned rights. Reference herein to any specific commercial product, process, or service by its trade name, trademark, manufacturer, or otherwise, does not necessarily constitute or imply its endorsement, recommendation, or favoring by the United States Government or any agency thereof, or the Regents of the University of California. The views and opinions of authors expressed herein do not necessarily state or reflect those of the United States Government or any agency thereof or the Regents of the University of California.

**The Morphological Development of the Nb₃Sn Phase
in Multifilamentary Superconducting Wire**

**Daniel Robert Dieterich
Ph D Thesis**

**Department of Materials Science and Mineral Engineering
University of California**

and

**Center for Advanced Materials
Materials and Chemical Sciences Division
Lawrence Berkeley Laboratory
1 Cyclotron Road
Berkeley, CA 94720**

December 1987

**This work is supported by the Director, Office of Energy Research,
Office of Fusion Energy, Development and Technology Division of the
U. S. Department of Energy under Contract No. DE-AC03-76SF00098.**

The Morphological Development of the Nb₃Sn Phase in Multifilamentary Superconducting Wire

Daniel Robert Dietderich

Abstract

Multifilamentary superconducting wire is used to produce high magnetic fields. One of the materials utilized is Nb₃Sn produced by "bronze-type" processes. To achieve peak properties the wire fabrication technique and the Nb₃Sn grain morphology and composition must be optimized. This work investigated the variation in critical current of an internal-tin-processed wire and a bronze-processed wire to determine the source of the superior properties in the internal tin wire.

The internal tin process was found to have a much higher J_c at low fields, $\sim 10T$, than that produced in the bronze process. It was determined that either a temperature ramp or a multi-step heat treatment with distinct temperature steps could produce a high J_c . Both heat treatments incorporate the low temperature to high temperature schedule which gives good critical current properties due to its influence on the Nb₃Sn microstructure, stoichiometry and state of atomic order. Two factors, reduced filament modulation and the increased amount of small equiaxed grains, are the primary sources of the superior properties. The upper critical field of the internal tin wire is lower than that produced in the bronze process. The lower H_{c2} can have two origins, different strain states in the two wires or Nb₃Sn composition. These two factors are correlated to the different wire fabrication processes.

The distinct Nb₃Sn grain morphology (columnar, equiaxed, and coarse-grained) of "bronze-type" processes has been explained by two models. One attributes the formation of the columnar and equiaxed grained region to the tin supply in the bronze, while the other attributes it to the break up of the columnar grains. The bronze-processed wire of this work supports the break up model. Observations showed that the nucleation of new grains stops early in the reaction with the development of a columnar structure that subsequently reconfigures producing equiaxed grains. Two driving forces for reconfiguration are the instability of a columnar structure and/or the reduction in strain energy due to the reaction stresses. These stresses were modeled using a plane strain elastic approach in an attempt to isolate the controlling mechanism, recrystallization and polygonization of dislocations, have been eliminated due to the absence of dislocations and low angle boundaries. The columnar grains must reconfigure to relieve the reaction stresses using a global argument (Le Chatelier's principle). The microstructure will develop that can best relieve the stress; since an equiaxed structure can respond faster to stress than a columnar grain structure the microstructure goes in that direction.

Acknowledgement

I would like to express my deepest gratitude to my advisor, Professor J. W. Morris, Jr., for his close collaboration in this work, and for his guidance and inspiration, but about all for his patience.

I would also like to express my sincere thanks to Dr. I. W. Wu and J. T. Holthuis for valuable advice and collaboration in the early part of this work. The stimulating and in-depth discussion with Dr. Frear, J. Glazer and D. Tribula regarding fundamental aspects of the work was invaluable and made completion of this work possible. Additionally, without the "editor-in-chief" assistance and suggestions of J. Glazer during final dissertation preparation this work would not have been completed. To all the unmentioned members of the Morris group my heartfelt thanks for friendly assistance in unfamiliar areas of research needed to finish this work.

Most of all, I would like to express my deepest gratitude to my parents for their support, financially and emotionally, during my years of education.

This work was supported by the Director, Office of Energy Research, Office of Basic Energy Sciences, Materials Science Division of the U.S. Department of Energy under Contract No. DE-AC03-76SF00098.

TABLE OF CONTENTS

	page
Acknowledgment	i
I. Introduction	1
II. Background	
II.A. Superconducting Parameters	3
II.B. Wire Fabrication Processes	5
II.B.1. Bronze Process	7
II.B.2. Internal Tin Process	8
II.C. Factors That Affect the Critical Current of a Wire	9
II.C.1. Extrinsic Factors	10
II.C.2. Intrinsic Factors	11
III. Objectives and Synopsis	14
IV. Experimental Procedure	
IV.A. Materials	
IV.A.1. Internal-Tin-Processed Wire	16
IV.A.2. Bronze-Processed Wire	16
IV.B. Heat Treatment Technique	17
IV.C. TEM Sample Preparation and Technique	17
IV.D. Critical Current Testing	18
IV.D.1. Probes	19
IV.D.2. Measurement Technique	20
V. Internal-Tin-Processed Wire	
V.A. High Critical Current	22
V.A.1. Experimental Evidence	22
V.A.2. Factors Affecting the Critical Current	22

V.A.2.a.	Extrinsic Factors	23
V.A.2.b.	Intrinsic Factors	25
V.A.2.c.	Conclusions and Summary	28
V.B.	Microstructural Development in Manufacturer's Heat Treatment	
V.B.1.	Background	28
V.B.2.	Tin Distribution and Nb ₃ Sn Formation	30
V.B.3.	Direct to High Temperature Heat Treatment	34
V.B.4.	Porosity	34
V.B.5.	Conclusions and Summary	36
V.C.	Development of New Heat Treatments	
V.C.1.	Background: Heat Treatment and Critical Current	36
V.C.2.	New Heat Treatments	38
V.D.	Conclusions	40
VI.	Bronze-Processed Wire	
VI.A.	Results and Discussion	41
VI.A.1.	Nb ₃ Sn Layer Growth	42
VI.A.2.	Nb ₃ Sn Grain Morphology	44
VI.A.3.	Stresses in Nb ₃ Sn	47
VI.A.4.	Material Response to Stress	
VI.A.4.a.	General - Crystalline Materials	53
VI.A.4.b.	A15 Crystal Structure - Nb ₃ Sn	54
VI.A.5.	Mechanisms for Grain Reconfiguration	56
VI.A.5.a.	Polygonization	57
VI.A.5.b.	Recrystallization	58
VI.A.5.c.	Columnar Grain Instability	59
VI.B.	Conclusions	61
VII.	Overall Summary	63

VIII. Future Directions	66
IX. References	68
X. Appendices	
X.A. Stress Model	76
X.B. Upper Critical Field	79
XI. Figures	81

Tables

1. Heat treatment notation	17
2. Atomic volume of Cu-Sn phases	35
3. Relative diffusivities of Cu and Sn in Cu-Sn phases	35
4. Critical current, overall J_c , and J_c vs. heat treatment	124

The Morphological Development of the Nb₃Sn Phase in Multifilamentary Superconducting Wire

I. Introduction

Superconducting materials have been brought into the national spotlight with the recent discovery that certain oxides of the perovskite family are superconducting at high temperature (90-100K) and at high magnetic fields (150-200T). However, at this time these new materials in their polycrystalline form have a current carrying capacity which is several orders of magnitude below that of the commercially available superconductors such as NbTi and Nb₃Sn (Camps, 1987; Koto, 1987). In single crystal form, however, the oxide superconductors approach the commercial materials (Worthington, 1987) but processing limits their large scale applications. Furthermore, the mechanism for superconductivity in these new materials is not yet understood so it is not known if their current carrying capacity can be increased. In contrast, the current-carrying capacity of Nb-Ti alloys and Nb₃Sn superconductors can be improved by changes in microstructure. The mechanism is fairly well understood qualitatively; a high volume fraction of planar defects permits a large current. The Nb-Ti alloys utilize phase boundaries and dislocation cell walls for these planar defects, while Nb₃Sn employs grain boundaries.

Even though Nb-Ti alloy fabrication processes have been studied for 20 years, recent increases of 25-50% in the current-carrying capacity at 6T have been achieved by controlling chemical segregation in the starting ingot and the thermal and mechanical treatment of the Nb-Ti superconducting wire. Better metallurgical control produced a finer and more uniform distribution of phase boundaries and cell walls. The Nb₃Sn superconductors have a better current carrying capacity than Nb-Ti alloys at all magnetic

fields, but a similar improvement in the critical current capacity of Nb₃Sn through metallurgical manipulation has not been achieved. A fundamental understanding of the Nb₃Sn grain structure development could suggest guidelines for an improvement in the current carrying capacity.

II. Background

II.A. Superconducting Parameters

Soon after the discovery of superconductivity in metals by Onnes in 1911 solenoidal magnets were made of these metals. The results were very disappointing. The magnetic fields generated before the windings reverted into the normal state were low and of no engineering interest. However, these experiments showed that the superconductive state would be destroyed by an increase in temperature, current, or magnetic field to some critical value. This led to the realization that every superconductor has three parameters associated with it: a critical temperature, T_c , a critical current density, J_c , and an upper critical magnetic field, H_c . These three parameters are the intercepts of the critical surface in figure II.1 with the temperature, current density, and magnetic field axes of a three dimensional space. The critical surface separates the superconducting state, below, from the normal state, above.

If the state of the sample is altered this surface will be shifted. All three critical parameters are altered by strain or a change in the composition or microstructure, for example. If a material is in a strain-free state, application of an elastic strain (i.e. distortion of the lattice) shifts the surface to lower values (i.e. toward the origin). The strain can also produce structural changes in the sample which reduce the critical parameters by perturbing the state of the material. Altering the composition and/or microstructure of the sample can shift the critical surface to higher or lower values depending on the new state of the material. All of these points will be addressed in more detail in subsequent sections.

With time it was discovered that the elemental metals used in early solenoidal magnets belonged to a family of superconductors eventually called type I. Another family of superconductors, type II, discovered in the 1960's were of engineering interest due to

their ability to sustain a supercurrent in high magnetic fields. The type II materials, Nb-Ti and Nb₃Sn and now YBa₂Cu₃O_{6+δ}, have critical parameters much higher than the type I materials. The two families vary in their response to a magnetic field. Neglecting demagnetization factor effects due to sample geometry, a type I material is in the superconducting state up to H_c and in the normal state above it. Below H_c the magnetic field is excluded from the material – this is the Meissner effect (fig. II.2a) – and above H_c the magnetic field penetrates the material (fig. II.2c). With an increasing magnetic field the magnetization of the type I material follows the dashed curve in figure II.2d. A type II material, on the other hand, follows the solid magnetization curve of figure II.2d. A type II material has two critical fields, with superconducting type I behavior below H_{c1} (fig. II.2a) and normal state behavior above H_{c2} (fig. II.2c); between them the superconductor is in a mixed state (fig. II.2b). The remainder of this discussion will focus on type II superconductors because of their engineering importance.

All superconductors for high magnetic field application are in the mixed state (or vortex state) between H_{c1} and H_{c2} . In this state the superconducting and normal states coexist in the material. Each normal region has associated with it a flux quantum (or fluxoid). The fluxoids arrange themselves into a triangular array to minimize energy. This arrangement of fluxoids is called the flux line lattice (FLL). The lattice spacing, that is the separation between fluxoids, depends on temperature and the strength of the magnetic field. This magnetic field is the vector sum of the applied field and any self field due to a transport current. At H_{c2} the fluxoids overlap and the materials revert to the normal state.

When a supercurrent, a current made up of electrons in the superconducting state (i.e. Cooper pairs), passes along a sample the FLL experiences a displacing force, the Lorentz force. (figure. II.3) The magnitude and direction of the force is obtained from the cross product of the supercurrent and magnet field. For a superconductor to carry a large current it must prevent the motion of the fluxoid under this force; i.e. it must pin the lattice.

The motion of the fluxoids across the material is dissipative, generating heat which increases the temperature, driving the sample into the normal state. It has been observed experimentally that metallurgical defects in superconductors pin the FLL; a small grain size permits a large supercurrent (Scanlan, 1975; Livingston, 1977).

Not all defects are strong fluxoid pinning sites. Planar defects, such as grain boundaries and subgrain boundaries (dislocation cell walls), have the strongest interaction. The theoretical paper by Yetter (1982 and 1980) develops a model for the elemental interaction between a flux line and a grain boundary while those by Kramer (1973) and Zerveck (1981) deal with the summation of these elemental interactions. The importance of planar defects is related to the geometry of the flux line and the defect. For a strong interaction to occur the fluxoid must be almost parallel to the plane of the boundary. The presence of a grain boundary perturbs the superconducting state locally; similarly, the fluxoid is a perturbation (normal region) in the superconductor. The presence of either of these defects in the material increases its energy. When the fluxoid coincides with the boundary a lower energy configuration occurs.

II.B. Wire Fabrication Processes

There are usually conflicting requirements to be considered when designing a superconducting wire. As a rule, the main goal of wire design is to produce a wire that is thermally and magnetically stable with a high current carrying capacity. To achieve thermal and magnetic stability, Cu is incorporated into a composite with the superconductor. The thermal conductivity of a superconductor is poor compared to that of Cu. This, and the fact that magnetic field changes in the superconductor occur much faster than heat can be conducted away by thermal diffusion, requires that the superconductor be associated with a good thermal conducting material such as Cu (Stekly, 1971). It is this difference in

material behavior that makes Cu an effective stabilizer. The multifilamentary character of the wire improves the heat flow out of an individual filament because there is more surface area between the Cu and filament.

The brittle nature of Nb_3Sn does not permit it to be fabricated into a wire by a standard monolithic technique, e.g. ingot casting followed by homogenization and subsequent deformation. This brittleness is due to the A15 crystal structure of Nb_3Sn shown in figure II.4. The crystal structure can be viewed in two ways. The structure has Sn atoms at the eight corners and one in the center of the cube (in body centered cubic positions). All the Nb atoms are distributed in the cube faces, two in each face. They order in one half of the tetrahedral voids produced in the bcc Sn structure. This produces three orthogonal rows of Nb in the $\langle 100 \rangle$ directions. The other way to view the crystal structure is as a simple cubic lattice with a basis of eight atoms.

The second view of the Nb_3Sn crystal structure is informative in terms of its deformability. The A15 crystal structure, like the simple cubic, has a limited number of slip systems (i.e. 12) of the $\langle 100 \rangle (010)$ type. Out of these twelve slip systems only three are independent (i.e. any deformation produced by the other nine systems can be obtained from a combination of the three independent ones) (Groves and Kelly, 1963). It was first demonstrated by von Mises in 1928 (from Groves and Kelly, 1963) that for a material to undergo a general homogeneous strain by slip, five independent slip systems are necessary. Therefore, with no other mode to accommodate plastic deformation, five independent slip systems are required for deformation. As a result, wire fabrication requires that no Nb_3Sn be present in the deformation stages. To overcome these problems a family of processes have been developed, "bronze-type" processes. They will be discussed in the following sections.

II.B.1 Bronze Process

Due to the brittle nature of Nb_3Sn , elaborate fabrication techniques have been developed to manufacture this material into wire form. One of these processes is the bronze process (Kauffman, A.R. and Pickett, J.J., 1970; Tachikawa, 1970; Suenaga, 1981). A schematic of the process is seen in figure II.5. In its simplest form, elemental Nb rods are inserted into a Cu-Sn bronze billet, and deformed with anneals to final wire size; subsequent heat treatment converts the Nb filaments to the superconducting Nb_3Sn . Figure II.6 shows a typical bronze-processed wire. To obtain the maximum current from a wire it is desired that all of the Nb react to Nb_3Sn . However, the amount of Nb_3Sn is limited by the Sn concentration of the bronze. Due to deformation problems, this process is restricted to Sn concentrations of less than 9.1at.% (15.8wt.%), the solubility limit of Sn in Cu as seen in the Cu-Sn equilibrium phase diagrams, figure II.7 and figure II.8. Above this composition the formation of brittle Cu-Sn intermetallics render the bronze unworkable. For a bronze of this composition a bronze-to-niobium ratio of about three or greater will completely convert all the Nb to Nb_3Sn , while a ratio less than 3 will leave unreacted Nb. Therefore, the maximum Nb_3Sn area fraction that can be produced by this process is 0.25.

Besides the beneficial fabrication characteristics of the bronze process another reason for its success is the influence of Cu on the thermodynamics of the formation of Nb_3Sn and its lack of Nb-Cu intermetallic compounds. The Nb-Sn system, figure II.9, has three intermetallic phases, Nb_3Sn , Nb_6Sn_5 , and $NbSn_2$. When bulk samples of solid Nb react with bronze not all these phases are observed. For a bronze of less than 9at.% Sn only Nb_3Sn is produced. The schematic of the ternary Cu-Nb-Sn equilibrium phase at $-700^\circ C$ shows the tin diffusion path (fig. II.10). For higher Sn concentrations in the bronze, or Cu-Sn liquid, one or all of the Nb-Sn phases will appear in the reaction layer. Work by Zwicker and Rinder (1975) shows that the addition of as little as 10wt% Cu (17at%) to a tin melt accelerates the formation of all three phases at $700^\circ C$. Of more

importance, this Cu addition initiates the formation of Nb_3Sn at this temperature (Zwicker and Rinder, 1975; Yamasaki and Kimura, 1982). To suppress the formation of $NbSn_2$ and Nb_6Sn_5 and promote the formation of only Nb_3Sn at $700^\circ C$, the Cu concentration in liquid Sn is required to be ~ 55 at%Cu (Cu-45at%Sn) (Yamasaki and Kimura, 1982). Most commercial bronze-processed wire has a bronze with a tin concentration of 7-8at%; as a result only the Nb_3Sn forms during heat treatment. As mentioned in the preceding paragraph, the amount of Nb_3Sn that can be produced in a wire is limited by this low tin concentration. To overcome this problem an alternate process was developed, the internal tin process (also called the tin-core process).

II.B.2. Internal Tin Process

The internal tin process (Hashimoto, 1974) is a fabrication technique that makes possible an increase of the fraction of Nb_3Sn in a conductor cross section and thus increases the overall critical current density. This increase is achieved by decoupling the Sn supply from the fabrication procedure. If the Sn were uniformly mixed with the Cu the concentration would be ~ 18 at% (~ 27 wt%). The process starts with a Cu-Nb-Sn composite that can be deformed to final size without intermediate anneals since no bronze is present and the elemental units co-deform well. The process is shown schematically in figure II.5 and a representative conductor, which has a Nb diffusion barrier between the Cu-Nb-Sn composite and the Cu stabilizer, is shown in figure II.11.

Many different elaborate heat treatment schedules have been proposed for internal tin wire. (Schwall, 1983; Cogan, 1983; Higuchi, 1984; Zeitlin, 1985) The highest critical currents are achieved with multiple heat treatments at different temperatures with total heat treatment times of up to 20d (d=day). Part of this work was undertaken to simplify and shorten the heat treatment of the internal tin wire without degrading performance, and to

clarify and quantify the sources of the observed high overall critical current density. One result of this work is that a high overall J_c can be obtained with a short (2-3d) intermediate-temperature (580°C) heat treatment prior to 700°C, or with a 0.1°C/m (m=minute) temperature ramp from room temperature to 700°C. The high current carrying capacity seems to result from the fine equiaxed grained Nb₃Sn region which forms at intermediate temperatures.

II.C. Factors That Affect The Critical Current Of A Wire

The current carrying capacity is the total amount of current a wire can sustain before it reverts to the normal state; this is the critical current I_c of the wire. The critical current is only one of three current capacity parameters used to define a superconductor. The other two are critical current densities, the overall J_c and the J_c . The overall J_c is normalized with respect to the critical current (or I_c) by the Nb₃Sn plus bronze area while the J_c is normalized by the Nb₃Sn area in the wire (fig. II.12). When comparing the properties of a particular wire, either I_c or J_c can be used but when comparing two different wires the overall J_c or J_c should be used. The overall J_c in some work is normalized by the whole wire area. This is a good design parameter for magnet construction; it accounts for the effect of the Ta diffusion barrier and Cu stabilizer usually incorporated in a commercial wire. It relates the amount of current one can expect in the windings of a magnet. The overall J_c defined in this work is better for comparisons between different wire fabrication techniques. The critical current density of the Nb₃Sn, J_c , compares the quality of the Nb₃Sn that is produced by different heat treatments in the same wire or that produced in different wires.

II.C.1 Extrinsic factors

There are four factors that affect the overall critical current of a wire; two are extrinsic to the filament, while the other two are intrinsic to the filament. Each of these will be discussed in turn. The first extrinsic factor is the amount of Nb_3Sn in the wire cross section. Before the wire is fabricated the proportions of all the constituents (i.e. bronze and Nb or Cu, Sn, and Nb) are determined. This determines the maximum amount of Nb_3Sn that can be produced. The actual amount is determined by the heat treatment the finished wire receives. These proportions also affect the amount of thermal strain the Nb_3Sn experiences due to differential thermal contraction of these different components. The strain state of the Nb_3Sn is in part an extrinsic factor. The change in temperature, from 973K (700°C) to 4.2K, determines the amount of thermal contraction each component would undergo if unconstrained, but the volume fraction of the components determines the amount of thermally induced strain. The strain in the Nb_3Sn also depends on the heat treatment the wire has received, the residual tin content of the bronze and whether any unreacted Nb remains.

The second extrinsic factor, the amount of filament modulation, is produced during wire fabrication. The modulations are fluctuations in the filament diameter along its length. That segment of the filament with the smallest diameter will have the smallest critical current. When current is passed along the filament this constriction determines the critical current of the filament. This segment will reach J_c before the adjacent Nb_3Sn ; as a result, current is forced into the bronze. Since the bronze is in the normal state, local heating occurs and the sample prematurely reverts to the normal state due to the modulation (fig. II.13).

II.C.2 Intrinsic Factors

While the extrinsic factors are determined by processing before the bulk of the Nb_3Sn formation, the intrinsic factors are not. The two dominant intrinsic factors are the composition and microstructure of the Nb_3Sn . For optimum superconducting properties the Nb_3Sn composition should be near the stoichiometric ratio of 0.25. However, due to the layer growth process that forms Nb_3Sn an inherent composition gradient exists through the layer. Better conductor performance is obtained with flatter profiles that are obtained with higher heat treatment temperatures (Wu, 1983). The higher heat treatment temperatures produce a Nb_3Sn with a superior atomic order and composition through the layer near 25at%Sn. Having a composition that corresponds to exactly 25at%Sn may not give the best properties. For compositions between 24.5 and 25at%Sn Nb_3Sn is known to undergo a strain-induced cubic-to-tetragonal structural transformation which lowers T_c and H_{c2} . This point will be addressed in the internal tin section dealing with intrinsic factors that affect J_c . The second intrinsic factor is the superior morphology of the Nb_3Sn produced during heat treatment. This will be discussed in the next section dealing with microstructure and critical current.

All three superconducting parameters, T_c , H_{c2} , and J_c , depend on the material's processing history, but none more so than J_c . The critical current density of a superconductor can be increased in two ways: altering its microstructure or altering its strain state and chemistry. Increases in T_c and H_{c2} have been achieved in Nb-Ti and Nb_3Sn by the addition of third elements or by altering the strain state. If one could increase H_{c2} while retaining the same microstructure an increase in J_c would result, figure II.14a. The high field performance is improved. If H_{c2} is held constant and the microstructure is improved an increase in the low field J_c is obtained. If these two effects can be combined in the same sample the critical surface is shifted out to higher critical values (fig. II.14b). The critical current density, besides being a function of T_c and H_{c2} of the material, is a

strong function of the microstructure. Since T_c and H_{c2} are difficult to change significantly, most of the attention is focussed on the microstructure, which is amenable to metallurgical control

Microstructural observations on typical Nb_3Sn multifilamentary wires reveal morphologically distinct regions within each Nb_3Sn filament: a layer of small equiaxed grains located between columnar grains at the Nb interface and large coarsened grains at the bronze interface (Fig. II.15). The relative thickness of each of these regions varies with the particular conductor (e.g. bronze-to-niobium ratio, tin concentration in the bronze, third element additions, filament diameters) as well as with heat-treatment temperature and time. A three region morphology was observed by Wu (1983). Columnar and equiaxed regions were observed by Scanlan (1975), Togano (1979), and Pugh (1985). Shaw (1976) and West and Rawlings (1977) observed mostly columnar grains, while Livingston (1977) and Okuda (1983) only observed equiaxed grains. The optimum current-carrying capacity is expected with a uniform small grain structure (Scanlan, 1975; Wu, 1983). A conductor with such an idealized microstructure has yet to be realized; first, an understanding of the morphological development of the Nb_3Sn layer is essential.

Two schemes have been proposed to explain the grain morphology that develops in the Nb_3Sn layer of a bronze-processed wire. One scheme relates the grain structure to the tin supply in the bronze (Suenaga, 1981; Okuda, 1983). A high tin concentration in the bronze, present early in the reaction, is thought to promote nucleation of new grains at the Nb- Nb_3Sn reaction interface thus producing the equiaxed-grain region. Low tin concentrations, found late in the reaction, are expected to favor the growth of existing grains, resulting in a columnar grain structure. The second scheme attributes the equiaxed grains to a break up of columnar grains (Wu, 1983; Tribula, 1986; Johnson-Walls, 1985; Wallach and Evetts, 1986; Pugh, 1985). Its proponents argue that all grain growth at the reaction interface is columnar; those grains formed early in the layer growth process

eventually break up. This work investigates the probable operative scheme through transmission electron microscopy (TEM) on sections of multifilamentary wires at various stages of heat treatment, i.e. reaction to Nb_3Sn . Additionally, this work proposes possible driving forces and mechanisms responsible for the morphology change.

III. Objectives and Synopsis

The objective of this work is twofold. One is to determine if the high critical current in an internal-tin-processed wire can be achieved with shortened heat treatment times at low and intermediate temperatures and to ascertain or hypothesize the reason(s) for this high critical current. The increased area fraction of Nb_3Sn in the cross section, the first extrinsic factor, accounts for part of the increase in the critical current. The amount of filament modulation, the second extrinsic factor, of the internal tin wire is less than that in bronze-processed wire. However, only tentative conclusions are made about its quantitative effect on the amount of critical current improvement. The tin supply and concentration in the Cu affects the Sn concentration of the Nb_3Sn as well as the Nb_3Sn structure. The large tin supply of the internal tin wire promotes fast growth of the Nb_3Sn layer at intermediate temperatures. This reduces coarsening of the first Nb_3Sn grains that form during the reaction promoting the formation of a thick equiaxed grained shell.

This large volume of equiaxed grains is the second internal factor and, in part, accounts for the high critical current of the internal tin wire at intermediate magnetic fields. The importance of this equiaxed shell led to the second objective, the study of the development of the Nb_3Sn grain morphology in "bronze-type" processes. Two mechanisms have been proposed to explain the Nb_3Sn morphology, one due to nucleation of Nb_3Sn and the other due to the break up of the existing columnar Nb_3Sn grain structure. The purpose of this work is to determine which mechanism controls the morphological development of Nb_3Sn or, if they both operate, to determine the regime within which each is valid. Previous work on a bronze processed wire showed it developed a columnar grain structure early during the reaction heat treatment. This made it a good candidate to observe the operation of the nucleation or columnar grain break up mechanism. TEM observations showed that the nucleation of new Nb_3Sn grains stops early in the reaction and that columnar grains reconfigure producing equiaxed grains. Two driving forces are the

reduction in grain boundary energy associated with the instability of a columnar structure and/or the reduction in strain energy due to the reaction stresses. These stresses are modeled using a continuum elastic approach in an attempt to define the mechanism.

IV. Experimental Procedure

IV.A. Materials

IV.A.1. Internal Tin Process

The two internal tin wires utilized in this study were fabricated by Intermagnetics General Corporation. One, a 1.73mm (0.068in.) wire seen in figure IV.1, which was used for metallography and x-ray analysis, contained 61 subelements with nominal diameter of 0.12mm (0.005in.). The other wire, a 0.27mm (0.0105in.) wire (Fig. IV.2), was produced with a Ta barrier and Cu stabilizer specifically for critical current measurements. The internal dimensions and filament size of this wire approximated those in the larger conductor. The Ta barrier and Cu stabilizer of the subelement accounted for approximately 15% and 60% of the cross sectional area of the wire respectively.

Heat treatments were performed in sealed quartz tubes back-filled with argon such that the pressure in the tubes at the highest reaction temperature (650-700°C) would approximate ambient pressure. To ensure that no tin was lost both ends of the conductor were sealed by melting until a small alloy bead was created. At least 20mm at each end of the 0.27mm diameter conductor was removed prior to critical current measurements to insure that the material was not affected by the temperature rise.

IV.A.2. Bronze Process Wire

The bronze-processed wire used in this investigation was produced by the Hitachi Corporation. The wire with overall diameter of 1.2mm contains 10,261 Nb filaments (31 bundles of 331 filaments) in a bronze matrix of 7.5 at%Sn-0.4 at.%Ti. Each bundle is isolated from the copper stabilizer by a Nb diffusion barrier. Figure IV.3 shows a bundle of 331 filaments (a) and a single filament (b).

IV.B. Heat Treatment Technique

The heat treatment recommended for the internal tin wire by the manufacture, A, was 200°C for 200h + 375°C for 33h + 580°C for 216h and finished with 24 to 48 h at 700°C. The heat treatments developed in this work for the internal tin wire are given in Table 1 along with their notations. The heat treatments in Table 1 were followed by a 700°C to complete the heat treatment. The effects of two temperature ramps, 1.0 and 0.1°C/min. from room temperature to 700°C, were also investigated.

Table 1
Heat Treatment Notation

IVA	IVB	I
380°C/2d	380°C/2d	380°C/2d
+	+	+
580°C/3d	580°C/2d	580°C/9d
	+	
	625°C/1d	

IV.B. TEM Sample Preparation and Technique

Samples were prepared for transmission electron microscopic (TEM) observations by a combination of mechanical grinding and ion milling. The longitudinal samples were sequentially thinned with 240 and 600 grit SiC paper to a final thickness of 25-50mm (0.001-0.002in.) so that the sample came from the center of the wire. After grinding the samples were cut to lengths of about 2.5mm and mounted on 3mm Cu TEM holder with an oval hole 2mm by 1mm. The mounted sample was then thinned by ion milling in Gatan dual stage machine at ambient temperature. Two sets of ion gun parameters, voltage,

current and tilt, were used during thinning. For initial thinning the settings 7kV, 0.5mA, and 25° were used. After the filaments are broken in about 6-8h the gun conditions were changed to 4kV, 0.2mA, and 12°. The final thinning takes about 4-6h but this depends somewhat on the gun condition, i.e. older guns require longer milling time.

Conventional TEM and convergent beam microdiffraction techniques were used in this investigation. The two microscopes, EM301 and EM400, used in this study were manufactured by Philips Corporation. All observations were performed at an accelerating voltage of 100kV. The image rotation with respect to the diffraction pattern for different magnifications are seen in figure IV.4 and figure IV.5 for the EM301 and the EM400, respectively.

A typical TEM section through a partially reacted filament is seen in figure IV.6. Observations were made as near the center plane of the filament as possible, so that the layer morphology for the different samples observed was viewed in the same perspective. This is shown schematically in fig. IV.7. The average grain width and average grain size were obtained from TEM micrographs using a line intercept method. To obtain the average grain width lines were drawn parallel to the Nb-Nb₃Sn interface from the Nb interface to the bronze interface producing an array parallel of lines. The number of intercepts between a line and grain boundaries was divided by the line length, thus giving the average grain size. The average grain size of the equiaxed grain region was determined by drawing random lines through the region and counting the number of intercepts.

IV.C. Critical Current Testing

The critical current measurements were done in solenoidal magnets at the Francis Bitter National Magnet Laboratory (Rubin, 1983). The direction of the field is in the

upward direction. The radial homogeneity is not very important for I_c measurements, but the axial uniformity is. During testing the sample should be at the maximum field position. An error of $\pm 6\text{mm}$ ($1/4\text{in.}$) is tolerable.

IV.D.1. Probes

The probes provide the electrical connections and mechanical support needed at 4.2K. To obtain accurate measurements the probes must meet specific material and design requirements. The probe material and design must not strain the samples. There are two sources of sample strain. One is the differential thermal contraction of the wire and the support on cool down to liquid helium temperature. Certain fiber impregnated phenolic resin composites match the thermal contraction characteristics of the wire and therefore are used as a support material. The other source of strain is bowing of the sample due to the Lorentz force when a current is passed through the sample in the presence of a magnetic field. Bowing of the samples can be eliminated by correctly setting the polarity of the sample current in accordance with the magnetic field direction, so that the sample is forced into the support material. Figure IV.8 shows the probes used in this work. The low current probe ($<25\text{A}$) in fig. IV.8c measured 5 samples without removal from the cryostat. The 2 switches in the probe head assembly, right side of fig. IV. 8a, permitted changes of the voltage and current contacts externally. The sample positions are spaced 0.5in (12.5mm) apart. The probe height was adjusted for each sample, so that it was in the peak field of the magnet.

Procedures for soldering samples to the probe were developed to ensure reproducibility of the critical current. Joule heating at the current contacts can drive the sample into the normal state. To reduce heating a large contact area is desired since the heating is inversely proportional to the square of the contact area. To minimize heating of

the sample during mounting, which could damage the sample, a low melting point solder was used.

IV.D.2. Measurement Technique

The critical current (I_c) at 4.2K was measured in a transverse magnetic field with a potential criterion of $0.1\mu\text{V}/\text{mm}$ or less. The magnetic field was fixed and the current was ramped to above the transition point. A four point probe arrangement was used with 30mm long samples. The voltage taps were placed 5mm apart in the middle of the sample, equidistant from the current contacts. Obtaining reliable and reproducible data for I_c determination is not a simple task. The interpretation of the data depends on the testing geometry and the criteria used to obtain the I_c value. The paper by Goodrich and Fickett (1982) is an excellent source for methods of I_c data collection and interpretation.

The overall J_c was calculated using the active core area (i.e. area within the Ta barrier) which in the case of the IGC wire is $1.3 \times 10^{-2} \text{mm}^2$. The J_c was calculated using the Nb_3Sn in the wire cross section after heat treatment. The areas were measured from SEM micrographs using a CALCOMP 9000 SERIES digitizing tablet. To correct for magnification error, the active core areas were scaled by the ratio of the wire area obtained from the micrographs to the wire determined by a physical measurement of the wire diameter with a micrometer. At least five samples were measured for heat treatments with a high I_c ($700^\circ\text{C}/4\text{d}$, $0.1^\circ\text{C}/\text{min.} + 700^\circ\text{C}/1\text{d}$, $\text{IVB} + 700^\circ\text{C}/1\text{d}$, and $\text{I} + 700^\circ\text{C}/1\text{d}$) while a minimum of three tests were performed on low I_c samples (TVA , IVB , and I).

A Kramer plot can be used to estimate the upper critical field, H_{c2} . This upper critical field is designated H_{c2}^* since it is an estimate obtained from extrapolating low field data. The Kramer plot uses the high field flux pinning force developed by Kramer in 1973. The high field flux pinning force, which is related to the shearing of the flux line lattice, is proportional to $(h^{0.5}(1-h)^2)$, where h is $\frac{H}{H_{c2}}$. If this is equated to the Lorentz force, the

$J_c \times H$ product, exerted on the flux lines, a linear relationship is obtained, $(J_c^{0.5} H^{0.25}) = K(H_{c2} - H)$. When the left side of this equation goes to zero, H goes to H_{c2} . This value of H_{c2} from a Kramer plot to designated H_{c2}^* .

V. Internal-Tin-Processed Wire

V.A. High Critical Current

The principal results of this part of the work were to confirm the high overall critical current density and I_c of an internal tin wire that is properly heat treated, to clarify the development of the wire microstructure in the complex heat treatment suggested by the manufacturer, and to develop a simplified heat treatment that achieves the exceptional properties of the Nb_3Sn . The sources of the high overall J_c were clarified, and suggest that the two major sources of the good properties are less filament modulation and more Nb_3Sn with a small uniform equiaxed grain size.

V.A.1. Experimental Evidence

The Nb_3Sn in the cross section of an internal tin wire has a higher J_c in the 10-15T range than a bronze-processed wire. Figure V.1 plots the J_c of the internal-tin-processed wire used in this study (Dietderich, 1985) and the bronze-processed wire from the study by Wu (1983). This comparison shows that the current carried per unit area of Nb_3Sn is greater in the internal tin process. The high critical current density at 10T suggests the presence of a superior Nb_3Sn morphology to that produced by the bronze process, while the steeper decline with field suggests a lower H_{c2} .

V.A.2. Factors Affecting the Critical Current

As indicated in the Background Section the critical current I_c of an internal tin wire can be influenced by four factors: the amount, composition and microstructure of the Nb_3Sn , and nonuniformities along the length of the Nb_3Sn filament. The amount of Nb_3Sn in the wire cross section and its nonuniformity along the filaments – extrinsic factors – will be discussed first. In particular, the internal tin wire has more Nb_3Sn and

less filament modulation than a bronze-processed wire, both of which increase the critical current. The intrinsic factors, Nb_3Sn composition and morphology, will then be addressed. The composition of the Nb_3Sn is not measured directly, but is inferred from the critical properties. The Nb_3Sn layer morphology has a larger fraction of small equiaxed grains than that produced in the bronze-processed wire. The effect of heat treatments on I_c is interpreted on the basis of these two intrinsic properties. Each of these points will be addressed in more depth in the following sections. First, however, the general critical current behavior of the internal tin wire will be presented along with a summary of the principal results of this work.

V.A.2.a. Critical Current: Extrinsic Factors

As mentioned in the introduction the high critical current of the internal tin wire can have four sources; two are extrinsic to the filament, while the other two are intrinsic to the filament. The first extrinsic source is the increased amount of Nb_3Sn in the wire cross section. The second is a decrease in filament modulation produced during wire fabrication. The fabrication problems associated with the internal tin process are related to those of a nonreacting metal-metal filamentary composite, since Cu and Nb do not form intermetallic compounds. The main problem is modulation of the Nb filaments in the Cu matrix. The bronze-process, on the other hand, has these problems as well as filament irregularities introduced by Nb_3Sn formation. Annealing heat treatments required to soften the bronze produce a thin layer of Nb_3Sn which breaks up with subsequent deformation. This Nb_3Sn at the Nb-bronze interface forms hard undeformable particles which introduce filament irregularities (Fig. II.13). These irregularities reduce the critical current (Smathers, 1983). Some work has been done to quantify this effect and will be discussed below.

It has been observed that bronze-processed wires have an optimum Nb_3Sn filament size (i.e. diameter) that produces the maximum critical current (Kamata, 1984; Okuda,

1983). Filaments larger or smaller than this size give a lower critical current. Larger filament wires either have unreacted Nb, or Nb₃Sn that has undergone grain growth, due to the longer heat treatment times required to fully react the Nb. The result in both cases is a low I_c and J_c . Smaller filaments, on the other hand, react quickly with less grain growth. However, the filaments become modulated (i.e. nonuniform diameter along their length) during deformation, and with further deformation the variation increases. This effect has been quantified by Okuda (1983). Their work utilized two pairs of bronze-processed wires fabricated by Airco. One wire from each pair was deformed, such that the Nb filament diameter decreased from 6.3 μ m to 3.1 μ m (wire no. 222) and 7.8 μ m to 3.1 μ m (wire no. 223). This reduction increased the spread in the filament size; the standard deviation of their size distribution increased. The standard deviation increased from 14.4 to 17.8 (in arbitrary units) and from 12.4 to 17.4 for wires 222 and 223, respectively. Comparing the overall critical current of the large filament wires to their deformed counterparts – at peak properties for each wire – indicates a reduction in the critical current by ~15% for wire no. 222 and ~25% for wire no. 223. The larger decrease in current density occurred in the wire with the greater change in standard deviation (wire no. 223).

To make a direct comparison to other wires, however, the ratio $\left(\frac{\text{standard deviation}}{\text{mean}}\right)$ should be used, since Okuda's area and standard deviation are in arbitrary units. This ratio is ~12 for the large filament wires; and it increases to 15 to 16 in the small filament wires. The internal tin wire of this study has a standard deviation to mean ratio of ~12. If the standard deviation's effect on critical current is process independent, then the internal tin wire of this study could have a 15% to 25% higher J_c than the Airco bronze-processed wire studied by Wu (1983).

This illustration suggests that fabrication factors can reduce the maximum achievable I_c and may overshadow any improvements in I_c one can accomplish by

optimizing the intrinsic factors of Nb₃Sn, microstructure and composition. Nevertheless, given a particular wire fabrication technique, optimization of the critical current must be achieved through the intrinsic factors. The effect of these factors on the critical current will be discussed in the next section.

V.A.2.b. Critical Current: Intrinsic Factors

While the extrinsic factors that affect the critical current are encountered before Nb₃Sn formation, the intrinsic factors are not. The composition and microstructure of the Nb₃Sn are the two main intrinsic factors although the state of atomic order and the strain state of the Nb₃Sn also play an important role. They are of secondary importance without a good microstructure and a cubic Nb₃Sn at optimal stoichiometry.

As mentioned in the Background Section, the Nb₃Sn microstructure is important at low fields. Figure V.1 shows that the Nb₃Sn in the internal tin process carries substantially more current than the Nb₃Sn produced in a bronze-processed conductor at 10T. Prior work on a bronze-processed wire showed that the Nb₃Sn layer could be subdivided into distinct shells: columnar, equiaxed and coarsened. It was proposed that the equiaxed grain shell carried most of the current (Wu, 1983). The equiaxed grain size in the internal tin wire of this work is of comparable size to bronze-processed wire studied by Wu (1983). The equiaxed grain size as a function of heat treatment of the bronze-processed wire studied by Wu (1983) is seen in figure V.2 along with the grain size results of investigations by Scanlan (1975) and Shaw (1977) (S-S) for other bronze processed wire. All of them show the same trend, increasing grain size with increasing heat treatment temperature, but the grain size determined by Scanlan (1985) was larger for all temperatures. Shaw's values fall on the same trend line as those of Wu (1983). The grain size of the internal tin wire of this study is also plotted in figure V.2 and is seen to be

comparable to that in the Wu and Shaw studies. Even though the equiaxed grain size in the two conductors is similar an increase in critical current density results from a larger equiaxed shell in the internal tin wire. This intrinsic factor for the filaments in the internal tin wire by itself can account for a significant critical current increase at 10T. The development of the good microstructure is dependent on the heat treatment the wire receives; recognition of its importance motivated much of the work described in the next section.

The steeper drop at high magnetic fields of the J_c of the internal tin wire (fig. V.1) implies a lower H_{c2} . The influence of the process on strain state and the effect of strain state on critical current is discussed below with particular emphasis on high field properties. The strain state of the Nb_3Sn is difficult to define since it is affected by two factors. One is the reaction stresses that develop during the Nb_3Sn layer growth while the other is due to differential thermal contraction of the wire components (i.e. Ta, Nb_3Sn , and bronze). The reaction stresses, and their effect on the morphology of the Nb_3Sn layer, will be addressed in the second part of this dissertation, which focuses on morphology changes in Nb_3Sn . The strains that result from thermal effects will be discussed briefly due to their interplay with the Nb_3Sn composition and structure. The relationships between these intrinsic factors and the critical current are discussed and compared to those in a bronze processed wire.

In fact, the extrapolated upper critical field, H_{c2}^* , of the internal tin wire is less than that in a bronze-processed wire. Figure V.3 compares the extrapolated upper critical fields of both wires using a Kramer plot (see experimental procedure: measurement technique). The extrapolated field for a bronze wire heat treated at 700°C for 2d is 20.7T (4.2K) and for the internal tin wire given heat treat I+700°C for 1d (Table 2) is 18.9T (4.2K). Both of these values are less than the measured upper critical field of 26T for a cubic stoichiometric strain-free Nb_3Sn (Foner and McNiff, 197?). This difference could result from the state of

atomic order, the strain state, or the composition of the Nb_3Sn , or from the structural transformation that Nb_3Sn undergoes at low temperature. The state of atomic order in the two wires should be comparable due to the 700°C heat treatment temperature. However, strain in the Nb_3Sn due to thermal contraction of the different components of the wire will suppress H_{c2} . Two factors must be considered: the volume fraction of each component and the yield strength of the bronze. The higher the residual tin composition in the bronze after the reaction, the higher its yield strength at low temperature. Taken by itself the higher yield stress would impose larger strains on the Nb_3Sn of the internal tin wire. However, the bronze to niobium ratio in the internal tin wire is lower (less bronze), but not by much (2.5 vs. ~ 3.0). Additionally, the bronze distribution is different in the two wires which would alter the strain distribution through the filament region. The bronze process has the filaments uniformly distributed in the bronze matrix (uniform strain), while the filaments in the internal tin process are localized to a bronze annulus which has a bronze core (strain profile). The two effects, yield strength and component volume fraction, are difficult to separate. Another potential source of H_{c2} suppression is the strain-induced cubic-to-tetragonal crystal structure transformation ($c/a=1.02$) that Nb_3Sn undergoes at $\sim 40\text{K}$ when it has a composition between 24.5-25at% Sn (Flükiger, 1981; King, 1968, Devantay 1984). The tetragonal phase has an H_{c2} of 19T at 4.2K, $\sim 6\text{T}$ less than the cubic structure (Flükiger, preprint IEEE) but almost identical to the measured H_{c2}^* value for the internal tin wire. Foner's measured H_{c2} value for stoichiometric cubic strain-free Nb_3Sn is 26T (4.2K). For the transformation to be a factor in the internal tin wire the Nb_3Sn would need to be more stoichiometric. See the appendix titled, Upper Critical Field, for further discussion of this point. The H_{c2}^* value of 18.9T for the internal tin wire may be fortuitous; too many factors are involved to say the reduction in H_{c2} is only due to the transformation.

V.A.2.c. Conclusions and Summary

The internal tin wire has a higher critical current at low fields due two factors. One is extrinsic to the filament, filament modulation, and the other is intrinsic to the filament, Nb₃Sn grain morphology. The modulation can account for a large part of the increase if the critical current dependence is process independent. The increased amount of fine grains further increases the low field performance. The lower J_c at high field can be due to several factors, state of atomic order, stoichiometry, and strain, each of which alter the state of the Nb₃Sn. They can operate alone or concurrently making it difficult to isolate the dominant one(s).

V.B. Microstructural Development in the Manufacturer's Heat Treatment

The Nb₃Sn morphology and stoichiometry that develop in an internal tin conductor are a function of its heat treatment, as in all "bronze-type" processes. However, an internal-tin processed wire does not start with a homogeneous Cu-Sn solution. The tin must be distributed from the core of the subelement to the filament array. The Sn distribution heat treatments with their associated Cu-Sn phase development are presented in the next section. The subsequent section correlates these heat treatments to the wire critical current.

V.B.1. Background

The predecessor to the internal tin process was the external tin process, figure II.5. As the name implies, the Sn was supplied externally after the Cu-Nb composite was deformed to final size. The external tin process deforms a Cu-Nb composite to final wire size. It is plated with Sn and heat treated to distribute the Sn and react the Nb forming Nb₃Sn. The heat treatments used must retain all the material in the solid state; otherwise

gravity effects and beading of the liquid tin will produce a nonuniform tin distribution. The heat treatments (several temperatures, each for a fixed time) also have to be chosen to prevent delamination of the Cu-Sn intermetallics due to reaction stresses and void formation (ref Ames, Verhoven, MIT, Cogan). Two factors require that the wire diameter be kept small. One is the limited amount of tin that can be uniformly plated onto the wire and still fully react the Nb. The other restriction is to permit Sn diffusion to occur in a reasonable time. Since the diffusion distance is proportional to time to the one half power ($x=2\sqrt{Dt}$); a wire with twice the diameter would take ~4 times as long to heat treat. This usually keeps wire diameters to less than 10mil (0.25mm). Initially, these heat treatments were applied directly to the internal tin wire, although it does not share all of these problems.

The internal tin process confines the tin to the core, so no loss of tin results. The diffusion distance in the wires of this study is kept small by the use of subelements with a diameter of 5mil (0.125mm) seen in figures IV.1 and IV.2. The best heat treatment sequence to radially diffuse the Sn outward from the core, or Cu inward to the core is still not known. However, several heat treatments determined somewhat empirically have been proposed to be the optimum. Some of the heat treatments are remnants of the external tin process. To obtain the high critical current density at 10T, previous work has used elaborate multi-step heat treatments that include long times, ~200h, at relatively low temperature, 200°C, or intermediate temperature 580°C (Schwall, 1983). Other heat treatments (340°C for 200h followed by 500°C for 100h and finished with 650-725°C for 2d to 4d), first used by Cogan (1983) on external tin conductors, were used by Higuchi (1985) on IGC internal tin wire similar to the one used in this work, but result in some loss (5-12%) of critical current. This led to the effort described here to correlate the critical current of a conductor to the Sn distribution heat treatments, and ultimately to the microstructural and chemical state of the Nb₃Sn.

The three-step heat treatment A, (200°C for 200h, 375°C for 33h followed by 580°C for 216h) recommended by IGC, was taken as the reference, or benchmark, heat treatment for a metallurgical study of the wires, since it produced a 15-20% better overall J_c at 10T for a 700°C final treatment temperature than wires heat treated directly at 650°C, 700°C and 730°C (fig. IV.4). However, this treatment is long, 449h plus 1d or 2d at 700°C, giving a total heat treatment time of about 500h (20.8d). A better understanding of the overall microstructure that results from the Cu-Sn interdiffusion led to the selection of shortened heat treatments that retained the peak J_c . The microstructure of the benchmark heat treatment was observed at different stages of the heat treatment sequence and conclusions made from these observations led to shortened heat treatments which gave the same high J_c . The results of the initial study will be presented with discussion, after which the conclusions about the reference heat treatment will be used to propose the shortened treatments.

V.B.2. Tin Distribution and Nb_3Sn Formation

The 200°C heat treatment produces two intermetallic layers around the tin core (fig. V.5a). Each layer is about 5-6 μ m thick giving a total of 10-12 μ m. Before the reaction the copper layer between the tin center and first row of niobium filaments is about 10 μ m. After the reaction a 5 μ m layer of unreacted copper remains. The two intermetallic layers have been identified as the ϵ (Cu_3Sn) and η (Cu_6Sn_5) phases by SEM/EDS. It is assumed that the compositions observed correspond to the equilibrium phases. Since these two phases are stable at 375°C the sample is ready for the next temperature of the treatment. If the volume of tin in the core of this internal tin wire were plated on the surface of an external tin wire of equal volume the tin thickness would be ~12 μ m. An external tin wire would have consumed all the Sn forming both the ϵ and η phases.

The second step, 375°C for 33h, produces an all ϵ core. The ϵ -Cu interface is 10-15 μm (or 5-10 rows) into the filaments (fig. V.5b). Porosity is observed at this stage of the diffusion heat treatment. Most of the porosity is at the periphery of the core and in the filament region. The pore size in the filament region was kept small, apparently due to the growth restraint presented by the filament array. This porosity could originate from two sources, a volume difference between the initial phases (Cu and Sn) and the final phase (ϵ), and/or the Kirkendall effect. This will be discussed at the end of this section.

The temperature of the third step is 580°C. This is the most important step of the heat treatment. At this temperature the radial diffusion of Sn is accelerated due to its exponential dependence with temperature, and a substantial amount of Nb_3Sn forms. This temperature is also associated with the most complicated region of the Cu-Sn equilibrium phase diagram (fig. II.7). The β and ζ phases decompose eutectically at 586°C and 582°C respectively, with $\beta \rightarrow \alpha + \gamma$ and $\zeta \rightarrow \gamma + \epsilon$. Between the ϵ and α phases there are four phases, ζ, δ, γ , and β , all within 6°C of 580°C. This suggests that a slight variation in temperature could have important effects on the microstructure. Therefore, future experiments should study the temperatures of 560°C and 600°C. The ϵ phase is still stable at 600°C and the three phases, ζ, γ , and β can form (although they may not all appear due to kinetic limitations), while the 560°C treatment should give similar results to 580°C, since the only phases that can form are δ and γ . This would be informative with respect to porosity formation since the intrinsic diffusion data for Cu and Sn in these two phases (γ and δ) is available. (Ebeling and Wever 1967).

After 48h at 580°C the ϵ phase has disappeared leaving the α phase (Cu-Sn solid solution with ~8.5at.% Sn) throughout the filament region and a high tin phase(s) in the core (fig. V5c). There also appear to be isolated islands of a high tin phase(s) in the filament region. The porosity which was in the core region and first few rows of filaments has now moved to the outer filaments leaving the core void free. The Nb filaments are

~40% reacted. The composition, determined by SEM/EDS, of the high tin region is (15-16at% Sn). This corresponds to either the γ phase, or possibly the β phase, but the microstructure of these regions appears two phase (fig. V.6).

This work is concerned with the high temperature Cu-Sn phases that are present during the high temperature heat treatment, not the phases that form on cooling. However, by observing the phases present at low temperature, one may be able to infer which phases are present at high temperature. Work performed to identify the high temperature phases will be discussed due to their possible influence on the Nb_3Sn formation. This digression illustrates the importance of the Cu-Sn phase progression during heat treatment to the eventual Nb_3Sn microstructure. The lath-like appearance of the microstructure in the high tin islands may be a result of a phase transformation on cooling. Below 520°C the γ phase decomposes to the α and δ phases eutectically with the δ phase subsequently undergoing a eutectoid transformation below $\sim 350^\circ\text{C}$ to the α and ϵ phases. However, the eutectoid reaction $\delta \rightarrow \alpha + \epsilon$ is too slow to occur on cooling from the heat treatment temperature (Wang and Hansen 1951). The lath-like appearance of the microstructure suggests a martensitic transformation on cooling, which the β phase and the γ phase are known to undergo (Breedis, 1973; Kuwano and Wayman, 1983; Shimizu, 1975). The lath-like microstructure of the two phase region is identical to that in figure 12 of Smith 1948 for the β phase. On cooling β and γ form ordered orthorhombic martensite, either internally faulted (β') or twinned (γ'). A sample given heat treatment A, but with only 12h at 580°C , develops the Cu-Sn microstructure seen in the TEM₁ micrograph of figure V.7a. The microstructure is a two phase mixture with one phase having twins or faults. This phase is observed to be in contact with faceted grains (arrows fig. V.7b). The faceted grains are observed by SEM at longer heat treatment times, 72h (fig. V.8). The presence of the high tin phase may be important to the formation of the large grains, since less time at 580°C reduces the number of large grains. These grains are believed to be Nb_3Sn , but work done

on the formation of Nb-Sn compounds from Sn-Cu liquids shows that Nb_6Sn_5 can also form at 660°C . Therefore, some doubt remains as to the initial Nb-Sn phase to form at 580°C in the internal tin wire. The melt must have a tin concentration of greater than 35at% (Yamasaki and Kimura, 1982). However, as the reaction to form Nb-Sn phases proceeds, the tin content of the Cu-Sn liquid decreases until either the γ or ϵ phases forms. If one extrapolates the data of ref. to 580°C the Nb_6Sn_5 phase can form from a bronze of ~20at% Sn. At the start of the 580°C treatment the Nb filament is in contact with the ϵ phase (Cu_3Sn) which is 25at% Sn. It is possible that a two phase tie line between Cu_3Sn and Nb_6Sn_5 exists at this temperature. Figure V.9 shows a schematic of a proposed Cu-Nb-Sn ternary equilibrium phase diagram at 580°C if this tie line exists. The ternary phase diagram studies done on Cu-Nb-Sn have been for temperatures of 1000°C or higher and for tin concentrations on the Cu-Nb side of the phase diagram (Hopkins, 1977). As stated earlier, this is an interesting and complicated region of the Cu-Sn phase diagram due to the number of phases. In addition the crystallography of these Cu-Sn phases is still not well known. A definitive answer as to which phases are present can not be obtained without further TEM and x-ray diffraction analysis.

Returning to the discussion of the evolution of the wire microstructure during heat treatment, completion of heat treatment A (after 218h at 580°C) removes the high tin phase leaving only the α phase. The filaments are ~85% reacted (fig. IV.1). The filaments near the core are almost completely reacted while those at the subelement periphery are not. A ring of porosity through the filament region develops in some of the subelements but not in all (fig. V.10). This porosity could have a strong effect on the strain sensitivity of the critical current of the conductor. The filament adjacent to porosity will experience more strain during a uniaxial test due to the decohesion of the filament and matrix at these points. The variation of critical current with applied axial strain for different heat treatments (i.e.

different porosity distributions) is presently being investigated at LLNL by M. Strum and L.T. Summers.

V.B.3. Direct to High Temperature Heat Treatment

A different overall wire microstructure is obtained when the conductor is taken directly to 700°C. Figure V.11 shows a wire that has been heat treated 2d at 700°C. Substantial porosity is seen in the core regions but not in the filaments. The porosity is present as early as 3h into the heat treatment when a high-tin phase is still observed in the core. The presence of porosity and its location this early during the heat treatment will inhibit radial diffusion. Figure V.12 shows a longitudinal view of the wire heat treated at 700°C for 2d; the porosity is adjacent to the first row of filaments. This porosity distribution is not observed in wires heat treated at 580°C. The microstructure of a wire heat treated at 650°C is expected to be similar. This porosity, or lack of porosity is believed to have an effect on J_c . As can be seen in fig. V.4 the J_c of the 650°C heat treatment is a little higher than that of the 700°C and 730°C heat treatments.

V.B.4. Porosity

As stated earlier, porosity in the internal tin process is unavoidable due to the volume difference between Sn phase in the core and the Cu-Sn phases that form during the heat treatments. Each particular choice of heat treatments will produce different Cu-Sn phases, which will produce a different void distribution. This is due to the Kirkendall effect, i.e. the diffusivity of Cu and Sn are different in the Cu-Sn intermetallics. In other words, the presence of porosity is intrinsic to this process while the distribution is not. The atomic volumes of the different phases are given below:

Table 2

Crystal Structure	$\left(\frac{A^3}{\text{atom}}\right)$
Sn(β)	- 27
Cu (fcc)	- 11.7
γ , δ , β , and ϵ	- 12 to 15
η , ζ	- N/A

When the Sn core reacts with the Cu to form an all ϵ core, the difference in crystal structure volume (10%) will produce porosity in the core.

The difference in intrinsic diffusivities of the different crystal structures is responsible for the porosity distribution. This difference in intrinsic diffusivities produces the Kirkendall effect (da Silva and Mehl, 1951). The relative intrinsic diffusion rates of Sn and Cu in the different crystal structures are listed below.

Table 3

Sn	- 10 to 20 times faster in Cu-Sn solid solution (Hoshino, 1980)
	- 100 to 200 times faster at 580°C and 500°C, respectively in δ . (Ebeling and Wever, 1967.)
Cu	- 25 to 10 times faster at 580°C and 700°C, respectively in γ . (Ebeling and Wever, 1967.)
Sn, Cu	- about the same in ϵ and η . (deduced from Cogan, 1981 data)
	Unknown for β and ζ .

The heat treatment at 580°C moves the porosity to the opposite side of the growth interface. The removal of the porosity from the core requires Cu diffusion into the core. Without information about the intrinsic diffusivity in the β phase, the only phase in which

this diffusion could occur in γ phase. Nevertheless, copper diffuses 25 times faster than Sn in the γ phase at 580°C. The large intrinsic diffusion rate of Sn in δ (100 times faster than Cu) at 580°C would remove Sn from the core such that more porosity would result. Since γ and δ can both form at 580°C and each will disappear to form α it is not clear which will dominate.

V.B.5. Summary of the Manufacturer's Heat Treatments

Several conclusions can be made about the reference heat treatment; one is that the 200°C for 200h heat treatment does not consume the Sn core or contribute much to Sn distribution. This treatment is unnecessary in the internal tin wire and will not be included in further heat treatments in this work. Nevertheless, the manufacturer still recommends this temperature as a precaution against tin leakage, (the volume increase when tin becomes molten could rupture a region of the wire); however, the time has been shortened to 48h. The core region is all ϵ phase after the 200°C for 200h + 375°C for 33h treatment. It was determined that an equivalent ϵ phase microstructure can be obtained after 48h at 380°C. This was therefore adopted as the first step in future heat treatments. The treatment at 580°C for 216h was too long on practical grounds, i.e. heat treatment of a magnet, as well as for, fundamental reasons, i.e. optimum microstructure of the Nb₃Sn. This will be discussed in the next section.

V.C. Development of New Heat Treatments

V.C.1. Background

The heat treatment to optimize the critical current of a bronze-processed superconducting wire depends on the particular wire characteristics. However, in general the highest critical current at low magnetic fields is obtained with a low temperature treatment while a high temperature treatment optimizes the high magnetic field regime. The

low temperature produces a small Nb_3Sn grain size, important at low fields, but poor stoichiometry and atomic order. The Nb_3Sn formed at high temperature has better stoichiometry and state of atomic order, necessary for good high field properties, but a larger grain size. The beneficial effects of both temperatures can be achieved in a wire by utilizing a two step heat treatment. Work by several groups has shown that a low temperature followed by a high temperature can improve the critical current in both field regimes. Work by Wu et al (1984) investigating a bronze wire fabricated by Airco showed that the optimum low-high temperature treatment for this conductor was 700°C for 4d followed by 730°C for 2d. While others researchers (Schaur and Schelb, 1981; Ochiai, 1987) have used heat treatment temperatures of 700°C followed by 800°C . In these studies good high field performance was obtained but the low field critical current was reduced by excessive grain growth during the second step at 800°C . Evaluation of all the two-step heat treatments reveals that the first step should be at 700°C or less and that the second step should begin before all of the Nb has been consumed. The temperature of the second step should not exceed 750°C .

The second step, at the higher temperature, increases the layer growth rate. This increases coarsening (i.e. grain growth) of the Nb_3Sn . Any grain growth that does occur is in part compensated for by the remainder of the Nb being converted to Nb_3Sn . The higher temperature also increases the bulk diffusion rate of Sn in Nb_3Sn , accelerating the approach to stoichiometry and a state of perfect atomic order. The intrinsic diffusivity of Sn in Nb_3Sn is less than that of Nb, which makes it rate controlling for the achievement of stoichiometry and a state of atomic order. The activation energy for diffusion of Sn in Nb_3Sn is between 5-10eV (Welch 1987). Therefore a small increase in temperature can have a large effect on diffusion due to the exponential dependence. It is a trade-off between a longer time at the lower temperature or a shorter time at the higher temperature.

V.C.2. New Heat Treatments

The multi-step heat treatment of the internal tin wire incorporates these principles. A low or intermediate temperature heat treatment to distribute the tin also initiates Nb₃Sn formation; it is the first step of a two step heat treatment for the Nb₃Sn. However, the long time at the intermediate temperature of 580°C is detrimental to the Nb₃Sn microstructure. A small grained Nb₃Sn is produced, but the long time promotes grain growth of the Nb₃Sn grains at the filament periphery (the first grains to form). Two heat treatments were chosen to test this hypothesis. One heat treatment (IVA) was 380°C for 2d followed by 3d at 580°C prior to the 700°C final temperature. The other (IVB) was 380°C for 2 days, 580°C for 2d, and 625°C for 1d prior to the 700°C final heat treatment. The overall critical current density and the critical current density of the Nb₃Sn are given in Table 4. The overall critical current density of IVB+700°C for 1d (16.6×10^2 A per mm²) is plotted in figure V.13 along with the I+700°C for 1d (16.9×10^2 A per mm²). Heat treatment I (380°C for 2d followed by 580°C for 9d (216h) replaced the reference heat treatment A. These two heat treatments are 15-20% higher than wires heat treated directly to 700°C for 4d (14.0×10^2 A per mm²), also listed in Table 4 and plotted in figure V.13.

The increase in the critical current density with the final heat treatment at 700°C is higher than would be expected if more Nb₃Sn was produced with the same J_c. The critical current density increases by 40-45%, when heat treatments IVB and I are given the final step, 700°C for 1d. These increases are achieved with increases in Nb₃Sn area of only a 15% for heat treatment I and a 25% for heat treatment IVB. The second step at 700°C has improved several of the intrinsic factors.

The porosity ring observed in the direct to 700°C heat treatment may not occur in practice. The rapid heating rate (10-15m) used in this study could not be implemented for a magnet that undergoes a wind and react treatment. The thermal mass of a large magnet

would produce a temperature ramp to 700°C which one might expect to be beneficial since it is a low-high heat treatment. This concept led to the final heat treatments, two temperature ramps. The first is a slow ramp to 700°C, $0.1 \frac{^{\circ}\text{C}}{\text{m}}$, to distribute the tin and give the Nb₃Sn a low-high temperature heat treatment. The other ramp, a factor of ten faster, $1.0 \frac{^{\circ}\text{C}}{\text{m}}$, would be similar to the direct heat treatment but with some time at intermediate temperature to distribute the tin. The fast ramp took 12h to reach 700°C, while the slow ramp required 117h (4.9 days). The slow ramp time to 700°C is the same as the multi-step heat treatments IVA and IVB (5 days). However, one should not expect the same Cu-Sn microstructure to result from the two treatments. The Cu-Sn phase formation and disappearance will occur at different rates due to the difference in interdiffusion rates in each phase with temperature. The overall critical current of both ramps is included in figure V.13 and is listed in Table 2. The overall critical current of the slow ramp treatment (16.3×10^2 A per mm²) is as good as the multi-step heat treatments IVB+700°C for 1d (16.6×10^2 A per mm²) and I+700°C for 1d (16.9×10^2 A per mm²). To the best of my knowledge a ramp heat treatment for this conductor or any superconducting wire had not been implemented prior to this work.

The success of the ramped heat treatments is good for practical magnet heat treatments and is being recommended to some of IGC's internal tin wire customers. This is in part due to a magnet's size. It would be difficult to heat treat with fixed temperature steps and obtain uniform properties throughout the magnet. The high critical currents obtained with the slow ramp suggest that the benefits of the two step temperature concept were achieved with this heat treatment. The ramp to 700°C distributes the Sn and starts the formation of a small-grained Nb₃Sn. The final treatment at 700°C completes the reaction and improves the state of atomic order and the composition of the Nb₃Sn. The ramp treatments treatment behaved as expected using the low-high temperature heat treatment concepts.

V.D. Conclusions

In summary, the internal tin wire was found to have a much higher critical current density than bronze-processed wire. The sources are a more uniform filament size (i.e. diameter) and more small-grained Nb_3Sn . The heat treatment time can be shortened without loss of current carrying capacity using the understanding of microstructural development acquired during the first stage of the research. The alternate heat treatments also produce a different porosity distribution which should affect the strain state of the conductor. The high critical current can be achieved by utilizing discrete temperature steps or a temperature ramp.

VI. Bronze-Processed Wire

VI.A Results and Discussion

The previous half of this work showed how certain factors affected the critical current of an internal tin wire. There are four dominant factors, two of which are extrinsic to the filament and two of which are intrinsic. One intrinsic factor of the internal tin process, the microstructure of the Nb_3Sn , was superior to that observed in the bronze process. The development of this microstructure is of interest since it produces such a high J_c at low fields. Several morphological studies of Nb_3Sn produced by "bronze-type" processes have observed differing microstructures, not necessarily in conflict. The typical layer microstructure consists of three Nb_3Sn regions that differ in grain morphology: columnar, or equiaxed, or coarsened grain shells. Columnar grains are present at the Nb- Nb_3Sn growth interface while coarsened grains are present at the bronze interface. Between each of these regions is an equiaxed grain shell. The relative proportions of each region depends on the particular wire design and the heat treatment it has received. Since a small equiaxed grain morphology is the preferred microstructure there is interest as to how it develops. Two mechanisms have been proposed to explain the observed morphologies. One attributes the observed layer morphology to nucleation and growth of Nb_3Sn early during the reaction heat treatment (Suenaga, 1981). It is proposed that early in the heat treatment the high tin supply in the bronze provides a high tin concentration at the growth interface. This high tin concentration facilitates the nucleation of new grains at the interface instead of the growth of existing grains. Later during the reaction when the tin concentration in the bronze is low, the growth of existing grains is preferred producing columnar grains. The second mechanism proposes that columnar grains form early during the reaction and that with subsequent layer growth they reconfigure (i.e. break-up) producing the equiaxed grain shell (Wu, 1983; Wallach and Everts, 1986).

A bronze-processed wire fabricated by Hitachi was shown to have columnar grains at the Nb interface, an equiaxed shell, and coarse grains near the bronze (Johnson-Walls, 1985). Therefore, this made it a good choice for a study to observe the microstructural change. TEM observations of this wire reveal that columnar grain formation starts early during the Nb₃Sn layer growth. These columnar grains break up (i.e. reconfigure) with further layer growth producing the equiaxed region. Several mechanisms could be responsible for the grain morphology change. These possible mechanisms require either dislocations (recrystallization and polygonization) or grain boundary motion (columnar grain instability). The likelihood of each mechanism is correlated to the observed microstructure and the ability of the process to relieve the reaction stresses that arise due to layer growth.

VI.A.1. Nb₃Sn Layer Growth

The variation of the Nb₃Sn layer growth rate with heat treatment time has been measured in an attempt to correlate it to the layer morphology. The layer thickness variation with heat treatment time can be used to determine the mechanism of layer growth. The variation is usually characterized by the two parameter equation $d=Kt^n$ where d is the layer thickness, t is the time, K is the rate constant and n is the time exponent. The rate constant K varies with temperature and may not have a simple exponential character typical of a diffusion coefficient, $\exp\left(\frac{-E}{k_B T}\right)$, where E =activation energy, k_B =Boltzmann's constant and T =temperature, which gives an Arrhenius plot. The complex dependence of K with temperature is due to K being related the difference of two diffusivities each of which is weighted by a composition gradient (Kidson, 1961). The time exponent n reveals information about the mechanism controlling growth. The values of n and K are obtained from a plot of layer thickness vs. log time. The slope gives the value of n and the intercept with the y axis gives log K . For a time exponent of 1 the reaction at the growth interface is

thought to be controlling the layer growth and for a growth exponent of 0.5 diffusion through the layer is rate controlling. Values between 1 and 0.5 suggest a regime where both rates are comparable and values < 0.5 suggest the Sn supply in the bronze is limiting (Farrell, 1974; Agarwal, 1984)

Figure VI.1 shows the Nb_3Sn layer thickness vs. log of the heat treatment time at 700°C for the Hitachi wire. The slope for times less than 24h is 0.52 while for times greater than 24h it is 0.19. The value of K^2 is $1.2 \times 10^{-11} \frac{\text{cm}^2}{\text{s}}$ when $n=0.52$. The units of K^2 make it like a diffusivity; however, as mentioned above it can not directly be interpreted as a diffusivity in most cases. These layer growth observations show that the Hitachi wire is in the diffusion-controlled regime when heat treated at 700°C for less than 24h. Since Nb_3Sn has a high melting temperature (2130°C) and the ordered A15 crystal structure, diffusion through the bulk by a vacancy mechanism can not account for much mass transport. (Welch, 1987) This poor bulk diffusivity combined with the small Nb_3Sn grain size implies the majority of the mass flow to the Nb interface is along Nb_3Sn grain boundaries (Togano, 1979). The behavior of Nb_3Sn wires doped with Ti is further evidence of this. The addition of Ti to the Nb core increases the growth rate of Nb_3Sn by 2-3 times. From data obtained by Tribula (1986) the ratio of K^2 between a Ti-doped bronze wire and a Ti-free control wire is 2.5. Since the n value of each wire is about the same, $n \approx 0.6$ near the diffusion controlled regime, the addition of Ti must alter the diffusion rate through the Nb_3Sn layer. The layer growth is controlled by the rate Sn diffuses along the Nb_3Sn grain boundaries. Since the grain size in Ti doped wire is about the same, if not slightly larger, than that in an undoped wire, Ti must increase this rate.

In the Hitachi wire, the kinetic regime where $n=1$ dominates, is not seen due to the pre-reacted layer ($\sim 0.15 \mu\text{m}$) of Nb_3Sn that formed during fabrication. Once a thin layer of Nb_3Sn has formed, the rate of Sn diffusion through this layer dominates the growth. It may

be possible to infer the layer morphology from the layer growth mechanism, i.e. whether the nucleation of Nb_3Sn grains or the growth of existing grains is occurring. When $n=1$ nucleation of grains is occurring, for $1 > n > 0.5$ nucleation of grains and growth of existing grains compete, and when $n=0.5$ the growth of existing grains predominates. Subsequent microstructural observations will be related to the layer growth rate in this manner.

VI.A.2. Nb_3Sn Grain Morphology

As mentioned earlier, past work on the Hitachi wire showed it produces a columnar grain structure. This made it a good candidate in which to observe the evolution of the Nb_3Sn grain morphology from one that is columnar to one that is equiaxed. In an attempt to determine the mechanism responsible for the morphological changes TEM studies were performed. Observations were made at the Nb- Nb_3Sn interface to investigate the occurrence of nucleating grains or the formation of columnar grains. The tails of the columnar grains were studied for information leading to a break-up mechanism (i.e. the presence of recrystallization, dislocations, and low angle or high angle boundaries). The majority of the results will be presented with only a brief discussion as to their importance. An in-depth discussion will follow.

Every compound layer goes through a nucleation and growth sequence as it forms. A new phase first nucleates (with random or oriented nuclei) at the boundary between the parent phases, in this case, Nb and Cu-Sn bronze. Those nuclei or grains that are favorably oriented for faster growth advance into the Nb. There can be a regime where there is a competition between the growth of existing grains and the nucleation of new grains as discussed in the section on layer growth. The absence of the kinetic-controlled layer growth regime (reaction controlled $n-1$) in the Hitachi wire may be due to the

formation of Nb_3Sn during the fabrication anneals at $\sim 550^\circ\text{C}$ to soften the bronze. As a result of these anneals, the thickness of the Nb_3Sn layer is already $0.15\mu\text{m}$ even before the 700°C reaction heat treatment. Obviously the nucleation stage has begun and finished by this time. The competition between nucleation of new grains and growth of existing grains seems to be of short duration in the Hitachi conductor, less than two hours. As early as one to two hours into the reaction a well-developed columnar grain morphology has formed (fig. VI.2). Observations of the interface of this sample near the edge of the foil (fig. VI.3) show no new grains even at favorable nucleation sites such as the three grain junction between two adjacent Nb_3Sn grains at the Nb interface. A schematic of the interface microstructure in figure VI.3 is seen in figure VI.4 with the favorable points identified. Behavior at these sites should indicate whether grain growth or grain nucleation is occurring. Since the tin supply is high at the junction and the surface energy barrier to nucleation is reduced there.

With further heat treatment to 7h columnar grains of about the same length as those observed at 2h are still found at the Nb interface. However, the columnar grain structure formed at 2h has broken up, forming a more equiaxed structure (fig. VI.5). The tails of the columnar grains appear to break up producing equiaxed grains of comparable width to that of the parent columnar grain. Figure VI.6 shows the average grain width vs. distance from the Nb- Nb_3Sn interface. The average grain width is uncorrected for grain shape (i.e. columnar or equiaxed). If this effect is accounted for the average size of the equiaxed grains would increase. A deflection in the curve is observed at the columnar grain to equiaxed grain transition region indicating some form of grain reconfiguration. Three possible sources for the observed columnar-to-equiaxed grained reconfiguration are: polygonization of dislocations, recrystallization, and columnar grain instability.

To determine which of these mechanisms operates TEM observations were performed. Polygonization of dislocations and recrystallization typically require a

measurable dislocation density. No dislocations are observed in the interior of the columnar or equiaxed grains even when tilted to different orientations. The only dislocations observed are at grain boundaries to accommodate crystallographic mismatch between adjacent grains (fig. VI.7). Observations were performed in the columnar-equiaxed grain region to determine the misorientation between the columnar grains and their neighboring equiaxed grains. A high angle character ($>10^\circ$) was generally observed which suggests polygonization is not likely. Also, no fine grains are observed at the tail of the columnar grains that could be interpreted as new grains due to a recrystallization process.

The columnar grain texture (preferred orientation) was determined since this would have an influence on the break up mechanism. The preferred growth direction of the columnar grains was determined using convergent beam electron diffraction and microdiffraction. The preferred direction was determined to be $[210] (\pm 5^\circ)$ for about 50-60% of the grains examined (fig. VI.8). This is shown schematically in figure VI.9. For these grains, the A15 (210) planes are parallel to the Nb surface. If dislocations or grain boundary motion were instrumental in the break-up of the columnar grains the columnar grain orientation would be important. Since the A15 crystal structure has only three slip systems the orientation of the columnar grain will determine which one(s) can operate in the stress state that develops from the reaction. Also, the mobility of a boundary depends on the misorientation between the grains.

Work by Tachikawa and Togano (1979) showed that bronze-processed Nb_3Sn developed a $(100)[011]$ preferred orientation when grown on a flattened Nb filament (a tape character) with a $(100)[011]$ bcc rolling texture. Therefore any texture that develops in the Nb filament would play a role in determining the Nb_3Sn layer morphology. The Nb filaments in the Hitachi conductor also develop a preferred orientation, a strong $\langle 110 \rangle$ bcc fiber texture. The texturing is observed in both TEM diffraction (fig. VI.10) and x-ray diffraction (fig. VI.11). Several Nb grains contributed to the TEM selected area diffraction

pattern of figure VL.10. The diffraction spot associated with [110] direction that is parallel to the filament axis is split into two spots. They are separated by $\sim 5^\circ$. At this time it is not known if the filaments have developed a cylindrical texture, [110] fiber texture with (100) planes around the surface (i.e. circumference) of the filaments, like a rolling texture.

It should be mentioned that the Nb filaments have been heavily cold worked and as a result are highly dislocated (fig. VL.10) in addition to having a strong [110] fiber texture. At this time it is not known how the homogeneous dislocation distribution in the Nb will affect the Nb₃Sn layer morphology. However, it has been reported that the nucleating grain size depends on the degree of deformation in the filaments (Blum, 1977). The degree of deformation in part determines the dislocation density in the Nb. During the long heat treatment times at 700°C (about 4-8 days) for a bronze-processed wire the Nb is undergoing recovery. This will produce a different dislocation substructure in the filament center, later in the reaction, than at the filament surface earlier in the reaction. If the dislocation density and its distribution in the Nb play a role in determining the Nb₃Sn layer morphology a wire with a faster layer growth at a given temperature such as an internal tin wire should benefit from the increased dislocation density.

Each of the three possible columnar grain break up mechanisms mentioned above (polygonization of dislocations, recrystallization, and columnar grain instability) will be discussed in more detail. First, however, the stresses that develop in the Nb₃Sn layer due to the Nb-Sn reaction must be discussed since each of these possible mechanisms relies on the reaction stresses in one way or another to provide a driving force.

VI.A.3. Stresses In Nb₃Sn

It has been known for over a hundred years that stresses develop in thin films which are produced by plating (Stoney, 1909). Films produced by other techniques also

have internal stresses. Both the film growth mechanism and the thermal expansion differences between the film and substrate produce the stresses. The film growth produces what will be called "intrinsic stresses" to distinguish them from thermal stresses. Thermal stresses are not encountered during the Nb₃Sn layer growth; however, they do play an important role in determining the superconducting properties as discussed in the previous part of this work. The model that is developed below, to analyze the intrinsic stresses, could approximate thermal stresses with the appropriate changes of boundary and initial conditions (see the appendix titled Stress Model). Due to the multifilamentary wire geometry a measurement of the intrinsic stresses is impossible. Therefore, a model is developed to determine the magnitude and functional form of these stresses.

To model the intrinsic stresses certain assumptions and approximations must be made about the Nb₃Sn layer growth. First, current understanding has Sn diffusing from the bronze along the Nb₃Sn grain boundaries to the Nb-Nb₃Sn interface where it reacts with the Nb. Second, the conversion of Nb to Nb₃Sn produces a 37% volume increase in the filament. The volume change is calculated by comparing the volume of the Nb unit cell before the reaction to the volume of Nb₃Sn produced, keeping the number of Nb atoms constant. This volume calculation is analogous to the Pilling-Bedworth ratio for oxide film growth, $\left(\frac{V_{\text{oxide}}}{V_{\text{metal}}}\right)$ where V_{oxide} is the volume of oxide produced when the volume of metal, V_{metal} , reacts with oxygen. Lastly, one assumes that all of the volume increase occurs at the reaction interface.

A linear elastic model is used to model the stresses in the Nb₃Sn layer. Even though the layer growth requires a moving boundary solution a static model is developed. The layer is permitted to grow to some thickness and the stress state of the system is determined assuming no stress relaxation has occurred. In this model the volume increase mentioned above is equated to $3\epsilon_0$, where ϵ_0 is the unconstrained linear transformation

strain the Nb_3Sn undergoes. The volume of a material can be expressed in terms of the strain by the product $(1+\epsilon_r)(1+\epsilon_\theta)(1+\epsilon_z) = (1+\epsilon_r+\epsilon_\theta+\epsilon_z) + [\epsilon_r\epsilon_\theta+\epsilon_r\epsilon_z+\epsilon_\theta\epsilon_z+\epsilon_r\epsilon_\theta\epsilon_z]$. In linear elastic theory strains of second order or larger are assumed to be small, and neglected (sum in brackets). In cylindrical coordinates the dilatation is the sum of the principal strains ϵ_r , ϵ_θ , and ϵ_z , $(\epsilon_r+\epsilon_\theta+\epsilon_z) = 3\epsilon_0$.

The stress state of the material is obtained by using the appropriate initial conditions and boundary conditions between the Nb- Nb_3Sn and the Nb_3Sn -bronze. The material is assumed to be initially strain free. It is assumed that the bronze does not inhibit the expansion of the Nb_3Sn at the reaction temperature of 700°C (i.e. it is perfectly plastic with a yield strength of zero). The boundary conditions at the Nb- Nb_3Sn interface require that the displacements and radial stresses be equal.

Figure VI.12 shows the idealized model which assumes that the Nb_3Sn (region II) forms on the surface of an isolated Nb filament (region I) in an infinite bronze matrix. An annulus of Nb is removed from the material, allowed to transform to Nb_3Sn and replaced into the original volume. The geometry (cylindrical plane strain) and the surface tractions (boundary conditions) determine the stress distribution in the material. Force balance considerations from the core to the bronze interface require that the following differential equation holds:

$$\frac{d\sigma_r}{dr} + \frac{\sigma_r - \sigma_\theta}{r} = 0$$

To solve this equation the two stresses (σ_r and σ_θ) can both be expressed in terms of the radial displacement u . The strains in the radial ϵ_r and circumferential ϵ_θ directions can be expressed in terms of u .

$$\epsilon_r = \frac{du}{dr} \quad \text{and} \quad \epsilon_\theta = \frac{u}{r}$$

The elastic equations (generalized Hooke's law) which relate the strains and stresses for plane strain are:

$$(\epsilon_r - \epsilon_0) = \frac{1}{E} [\sigma_r - \nu(\sigma_\theta + \sigma_z)]$$

$$(\epsilon_\theta - \epsilon_0) = \frac{1}{E} [\sigma_\theta - \nu(\sigma_z + \sigma_r)]$$

$$(\epsilon_z - \epsilon_0) = \frac{1}{E} [\sigma_z - \nu(\sigma_r + \sigma_\theta)] \quad \Rightarrow \text{for plane strain } \epsilon_z = 0,$$

$$\sigma_z = \nu(\sigma_r + \sigma_\theta) - E\epsilon_0$$

Solving for σ_r and σ_θ :

$$\sigma_r = K[(1-\nu)\epsilon_r + \nu\epsilon_\theta - (1-\nu)\epsilon_0]$$

$$\sigma_\theta = K[(1-\nu)\epsilon_\theta + \nu\epsilon_r - (1-\nu)\epsilon_0], \quad \text{where } K = \frac{E}{(1-2\nu)(1-\nu)}$$

Using these equations for σ_r and σ_θ and the relations for ϵ_r and ϵ_θ in the displacements in the force balance equation an ordinary differential equation of second order in terms of the displacements is obtained:

$$\frac{d^2u}{dr^2} + \frac{1}{r} \frac{du}{dr} - \frac{u}{r^2} = 0$$

Its general solution is:

$$u(r) = C_1 r + \frac{C_2}{r}$$

In the Nb core the displacement $u \Rightarrow 0$ as $r \Rightarrow 0$. This requires that $C_2 = 0$. The displacement in the Nb core and the Nb₃Sn annulus (primes are for the Nb₃Sn) are the following:

$$u(r) = C_1 r \quad \text{Nb core}$$

$$u'(r) = C_1' r + \frac{C_2'}{r} \quad \text{Nb}_3\text{Sn annulus}$$

The strains in each region become:

$$\epsilon_r = C_1, \quad \epsilon_\theta = C_1 \quad \text{Nb core}$$

$$\epsilon_r = C_1' - \frac{C_2'}{r^2}, \quad \epsilon_\theta = C_1' + \frac{C_2'}{r^2} \quad \text{Nb}_3\text{Sn annulus}$$

The stress equations in each region are the following (see the appendix titled Stress Model for determination of constants):

Nb core

$$\sigma_r = KC_1$$

$$\sigma_\theta = KC_1$$

$$\sigma_z = 2\nu KC_1$$

Nb₃Sn shell

$$\sigma_r' = K' \left[C_1' - \frac{C_2'}{r^2} (1-2\nu') - (1-\nu') \epsilon_0 \right]$$

$$\sigma_\theta' = K' \left[C_1' + \frac{C_2'}{r^2} (1-2\nu') - (1-\nu') \epsilon_0 \right]$$

$$\sigma_z' = K' [2\nu' C_1' - (1-\nu') \epsilon_0]$$

Using the above mentioned boundary and initial conditions a state of triaxial tension is obtained in the Nb core while the Nb₃Sn shell is in biaxial compression in the axial and circumferential directions and tension in the radial direction (fig. VL13). The large tensile radial stress in the Nb₃Sn is a result of the boundary condition that the Nb-Nb₃Sn interface retain coherency. The expansion of the Nb₃Sn shell is analogous to the thermal expansion of a tube when heated. The tube undergoes an unconstrained volume increase; the inner and outer radii both increase. This radial displacement of the inner interface will always place it in radial tension, if constrained at the inner surface by a material with a small

expansion with temperature, regardless of the elastic moduli of the materials. Two effects that can alter these results will be discussed in more detail later with respect to their influence on the development of the grain morphology. One is that the Nb filaments have a strong $\langle 110 \rangle$ fiber texture; as a result, the elastic modulus is different than the randomized modulus used in these calculations. Secondly, Nb_3Sn is elastically anisotropic and the columnar grains are preferentially oriented, again making it difficult to assign an elastic modulus.

The functional form and sign of these results differ from those of Pugh et al. (fig. VI.14), the only other published work for this system. Their solution gives a linear profile for σ_θ which is slightly compressive at the Nb- Nb_3Sn interface and increases to a large tensile value at the bronze interface. The radial stress, σ_r , on the other hand, has an r^2 dependence which is compressive at the Nb interface and zero at the bronze interface. They claim to have used a shrink fitting model, in which an annulus of Nb_3Sn was shrunk over a Nb core. However, in a cylindrical geometry no stress can have a linear profile like the one they obtained for σ_θ . The solution requires a $\frac{1}{r^2}$ dependence. A linear profile is only obtained with a planar geometry.

The magnitude of the stresses in both models is unrealistically large. The stresses that develop if a Nb filament with an initial radius of $3\mu\text{m}$ reacts producing a $1\mu\text{m}$ layer of Nb_3Sn – that remains elastic – are shown in figure VI.13. The radial stress, hoop stress, and axial stress at the Nb interface are 2.8GPa, -9.4GPa and -6.0GPa, respectively. These values are 10-15% of the shear modulus of Nb_3Sn , which is ~62GPa. However, these results give an indication of the direction mass would flow to help relieve the stress. Material would move from regions of compression (i.e. sides of the columnar grain) to regions of tension (i.e. ends of the columnar grains). Unfortunately, a distinct mechanism for the grain reconfiguration can not be inferred from these results. However, a global argument can be invoked based on Le Chatelier's principle. To lower the overall energy of

the system the microstructure must evolve in such a way as to relieve the stress. Since an equiaxed grain morphology facilitates mass flow at high homologous temperatures, the microstructure is expected to evolve toward that morphology from the columnar morphology formed initially due to growth kinetics. If one compares the theoretical strain rates for an equiaxed microstructure, i.e. spheres (Herring, 1950) to that of a columnar microstructure, i.e. square rods (Nabarro, 1948), the equiaxed structure can respond to a stress by creep about 4 times faster.

VI.A.4. Material Response to Stress

The viability of the three possible break up mechanisms, recrystallization, polygonization of dislocations, and instability of a columnar grain, will be discussed with respect to relief of the intrinsic stresses. First however, a crystalline materials response to stress in general will be discussed. Then the stress response of Nb_3Sn will be discussed.

VI.A.4.a. General - Crystalline Materials

A polycrystalline material can respond to stress in several ways. The manner or mechanism by which the material responds depends on the stress level and microstructure, as well as the temperature and strain rate (or loading rate). Polycrystalline materials can deform by three mechanisms: 1) glide or climb of dislocations, 2) mass diffusion, and 3) shear of, or adjacent to, grain boundaries. Each mechanism has its own regime of operation depending on the aforementioned parameters. If a material is loaded with a stress below its yield stress it will plastically deform over time due to creep if given enough time at a high temperature. Thermally activated processes (i.e. dislocation climb and mass diffusion) are creep phenomena. For larger stresses, above the yield stress, the material deforms plastically by the generation and glide of dislocations. Regardless of the deformation mechanism, shear at the grain boundaries (i.e. grain boundary sliding) is

required to retain material coherency there. If the material deforms by slip and has an adequate number of slip systems, grain boundary shearing is not necessary. On the contrary, grain boundary sliding is an inevitable result of a creep process. These deformation processes are discussed below as possible stress relief mechanisms in Nb₃Sn.

VI.A.4.b. A15 Crystal Structure - Nb₃Sn

There is very little experimental data on the deformation of A15 materials. What is available was obtained at high temperature (>1200°C) for single crystal V₃Si (Mahajan, 1978) and (>1300°C) for large-grained Nb₃Sn, grain size ~60μm (Eisenstatt and Wright, 1980). In addition the microstructure was not sufficiently well characterized to allow identification of the deformation mechanism, i.e. diffusional creep or dislocation glide. Deformation of the A15 crystal structure by slip (dislocation glide) is difficult. Besides the limited number of slip systems, discussed in the introduction, the energy to nucleate a dislocation and the force to move it by glide are large. This is due to the crystal structure's large Burgers vector and shear modulus. To test the feasibility of dislocation glide to deform Nb₃Sn a simple deformation model can be used.

If one assumes the presence of a mobile dislocation in a columnar grain one can estimate the force required to move it. As discussed previously, stresses from the reaction would move any mobile dislocation that was present. The dislocation will bow out under this force since it is pinned at its ends by the grain boundary. At a certain bowing radius, the dislocation will spontaneously move the remaining distance across the grain. This bowing stress can be estimated from the material properties and simple dislocation theory. The shear stress depends on the grain width l , the shear modulus G , and the Burgers vector b of the Nb₃Sn. Neglecting internal forces that may be present, the shear stress is given by,

$$\tau \sim \frac{Gb}{2l}$$

If one assigns values of 0.53nm and 53nm to the parameters b and l , respectively, $\tau_{\max} = \frac{G}{200}$. This is 5% of the theoretical shear stress $\frac{G}{10}$. Thus, it is possible for a dislocation to slip across a columnar grain if the stresses are large enough and one of the slip systems of the grain is oriented properly. As a result mobile dislocations would be move across the grains and would not be observed. Nevertheless this does give a lower limit to the shear stress. However, this does not address the problem of nucleation of a mobile dislocation.

Several models for the generation of dislocations have been proposed. The first and perhaps the most well known is the Frank-Read source (Frank and Read 1950, Read-Hill, 1973). This mechanism requires the existence of mobile dislocations and enough slip systems to permit double cross slip. This may not always be the case, especially in the small-grained Nb₃Sn (50-100nm) produced in the bronze process where space limitations make double cross slip difficult. In addition, the A15 crystal structure has only 3 independent slip systems, making cross slip difficult. Given these limitations mentioned, the F-R source probably can not operate in this case.

Other dislocation generation mechanisms which are experimentally observed utilize grain boundaries as the source of mobile dislocations. Models for dislocation generation at a grain boundary ledges have been developed for edge dislocations (Li, 1963) and for screw dislocations (Price and Hirth, 1972). Both models show the feasibility of the mechanism but neither model gives an estimate of the stress or energy required to generate a dislocation. Theoretical calculations by Frank (1950) and Hirth (1963) on Cu indicated that the critical resolved shear stress required for the nucleation of a dislocation at a surface step is $\sim 0.025G$ (25% of the theoretical shear stress) at a temperature of 900K ($\sim 0.8T_m$ of Cu). Both calculations assume a large dislocation nucleation rate, which would probably not exist in Nb₃Sn. If one nonetheless applies this result to obtain a lower limit for Nb₃Sn, then the critical resolved shear stress for the nucleation of a dislocation at a grain boundary would be greater than 1,500MPa. This large value suggests that dislocation nucleation

occurs infrequently at best and other mechanism(s) such as diffusional creep must be responsible for the deformation that does occur.

The ultra-fine Nb_3Sn grain size 50-100nm (0.05-0.1 μm) that forms in "bronze-type" processes is one to two orders of magnitude less than most material which undergo creep by grain boundary diffusion. The Nb_3Sn can respond to reaction stresses by diffusional creep at low homologous temperature (~ 0.4 for a typical heat treatment) and low stress levels.

As mentioned in the section dealing with modeling of the reaction stresses (i.e. intrinsic stresses) the layer growth is a dynamic process. When the Nb_3Sn layer initially forms there is very little stress. As the layer grows the stresses will get larger until stress relief mechanisms in the Nb_3Sn produce a steady state condition. The feasibility of possible relief mechanisms, dislocation glide and creep, has been discussed above. Microstructural observation should determine which mechanism(s) operates.

VI.A.5. Mechanisms of Grain Reconfiguration

Three possible mechanisms that can produce the observed columnar grain reconfiguration are: recrystallization, polygonization of dislocations, and the instability of columnar grains. Significant dislocation densities are needed for either polygonization or recrystallization to occur. It has been shown above that the nucleation of dislocations in Nb_3Sn is difficult. This fact, along with the observation that few dislocations are observed in the interior of grains suggests that reconfiguration processes that require dislocations are unlikely. However, other relevant observations relevant to assessing their likelihood are discussed below. The wavy lateral boundaries of the columnar grain suggest reconfiguration by opposing boundaries moving together, subdividing the grains. This requires grain boundary motion.

Typically, recrystallization and polygonization are associated with a measurable dislocation density. The required dislocation density in the grains is not observed in the Nb_3Sn (fig.VI.15). However, it is nonetheless possible that there is a high dislocation density driving the reaction that is not observed by TEM. Loss of dislocations during sample preparation is unlikely due to the limited dislocation mobility in the very small-grained Nb_3Sn but cannot be ruled out entirely. This point is worthy of further investigation.

VI.A.5.a. Polygonization

Polygonization is a process by which a heterogeneous distribution of dislocations will rearrange itself to reduce the energy of the system. During this process dislocations rearrange themselves by climb (edge dislocations) and cross slip (screw dislocations). Due to the interaction of their strain fields the dislocations form arrays or annihilate. When dislocations of opposite sign meet they annihilate forming a perfect lattice, while those with the same sign form a low angle boundary, thus reducing the energy associated with their long range strain fields. This polygonized array of dislocations forms a low angle boundary ($<10^\circ$) between dislocation free regions. Therefore, if columnar grains break up by a dislocation polygonization process, low angle boundaries should separate them from the adjacent equiaxed grains. The typical angular relationship, i.e. misorientation, between a columnar grain and the equiaxed grains is seen the figure VI.15. These observations were obtained from the columnar-equiaxed region of the sample shown in figure VI.8. Even when the best possible assumption is made, the smallest angle between the two zone axis patterns, the misorientation is near (9°) or above (25° or 15°) the low angle boundary criterion ($<10^\circ$). This is shown schematically in figure VI.16. This is strong evidence against a polygonization process occurring in this material. The proposed break up

mechanism of Wu, (1983), nucleation of dislocations and their subsequent polygonization, does not operate in this case.

VI.A.5.b. Recrystallization

Another process by which columnar grain break up could occur is recrystallization. Recrystallization requires that a material have a high dislocation density. There is an energy barrier to the formation of a dislocation-free grain since new grain boundary area is created. However, the stored energy in the dislocations (particularly high for Nb₃Sn) helps to overcome this barrier. In general a microstructure which has undergone recrystallization will have randomly oriented grains if the parent structure was random. Consequently, the boundaries separating the grains will be high angle boundaries. Therefore, if high angle boundaries ($>10^\circ$) separate the columnar grains from the adjacent equiaxed grains, recrystallization may be a viable break up mechanism. Another piece of evidence that would support recrystallization are fine grains at the tails of the columnar grains. However, fine grains, nuclei, at the tails of the columnar grains that would suggest the formation of new grains are not observed.

Based on the microstructural evidence neither polygonization or recrystallization appear to be viable mechanisms. The few dislocations that are observed in the Nb₃Sn layer appear to accommodate crystallographic mismatch between adjacent grains (fig. VI.7). The absence of small grains at the columnar-equiaxed region rejects recrystallization as a possible mechanism. Therefore, an alternate mechanism for the morphology change must be found.

VI.A.5.c. Columnar Grain Instability

There must be a direct mechanism for the break up of the columnar grains. If the columnar grains reconfigure without polygonization or recrystallization, some type of instability must be responsible which must be assisted by the reaction stresses. To relieve these stresses the microstructure develops that can best relieve them, the principle of Le Chatelier's. The wavy lateral boundaries of the columnar grains suggest the grains pinch off by the merger of opposing sides. This mechanism requires grain boundary motion (i.e. migration). A possible driving force that can account for grain boundary motion is the reduction of surface energy (i.e. grain growth) associated with the instability of a columnar grain. The former arises from the instability of a long rod (i.e. column) to decompose into spheres to reduce its specific surface energy. This phenomenon is observed frequently with fluid columns (Lord Rayleigh, 1879) and filaments of one phase in a matrix of another (Courtney, 1979, Carter, 1986). To model this phenomenon a column of diameter $2r$ is given a sinusoidal surface perturbation with a wavelength λ and a small amplitude δ . Energy and kinetic considerations give two results as to which wavelengths will grow. One is a minimum decomposition wave length [$\lambda_{\min} = \pi(2r)$] which will grow. The other is the fastest growing wave length [$\lambda_{\text{fast}} = 4.5(2r)$]. This phenomenon can occur in single phase materials, but additional constraints must be considered. These constraints would increase both λ 's (Carter, 1986). Therefore, a direct extension to the columnar Nb_3Sn grains may not be accurate. Nevertheless, the grain width, which is like $2r$, of the columnar grains near the equiaxed region is about 40nm (fig. VI.6). This produces a λ_{\min} and a λ_{fast} of ~125nm and ~180nm, respectively. The columnar grain length is between 200-300nm when they break up (fig. VI.6). This value is a little larger than the fastest growing wave length, as would be expected in a single phase material.

For the reconfiguration described above to occur grain boundaries must move. One driving force for boundary motion is chemical potential difference across a curved

boundary. In a homogeneous strain-free material grain boundaries move due to the chemical potential difference across a curved boundary, as occurs in secondary recrystallization (i.e. grain growth). The Gibbs-Thomson equation for a cylindrical grain is, $\Delta\mu = -\frac{\gamma\Omega}{r}$, where $\Delta\mu$ is the chemical potential difference across the boundary, γ interfacial energy (isotropic), and Ω is the atomic volume (Shewmon, 1969). The relation shows that the smaller the curvature the larger the driving force for boundary motion and that for a planar boundary ($r = \infty$) $\Delta\mu = 0$. Using this relation one can deduce the direction of motion of the columnar grain boundaries favored due to the chemical potential difference. To achieve this the grain shape must be viewed in three dimensions. The axial view as well as the longitudinal view shown in figure VI.8 must be taken into account for the columnar grains. Figure VI.17 which is a schematic of the columnar grain in figure VI.8 will clarify this point. In this orientation the columnar grain boundary has the larger radius of curvature r_1 , shown in part a of figure VI.17. However, if this grain could be viewed along axis, at the point of smallest columnar grain diameter, it would have the smaller radius of curvature r_2 , shown in part b of the figure VI.17. Since the chemical potential difference across the boundary is negative, $\Delta\mu_2 < \Delta\mu_1$. As a result, the grain boundary motion is dominated by the smaller radius which ultimately would favor pinch off of the columnar grain.

The Gibbs-Thomson argument above does not consider the influence of the number of sides (i.e. facets) a columnar grain has and its stability. In polycrystalline material (that is assumed to have an isotropic surface energy) a three grain junction with 3 angles of 120° has no net force on it. If the angles are different from this, the grain boundaries are curved and boundary motion occurs. If one assumes a stack of columnar grains like the hexagonal pencils shown end-on in figure VI.18a then there is no net force on the grain boundaries. However, if one of the grains has less than six sides, the situation is different. The five-sided grain will be consumed by the adjacent grains. The force balance between

boundaries a, b, and c is such that a net force exists on boundaries a and b to move them into the pentagonal grain (fig. VI.18b). This is a grain growth type phenomena that could account for some of the break up if some of the columnar grains have less than six lateral sides. By itself the equiaxed structure that would be produced from this mechanisms would have a grain size twice the columnar grain width. It is experimentally observed that the equiaxed grain size is comparable to the columnar grain width. The driving force is in the same direction as break-up by "Rayleigh-type" instability described above, so they can act together.

Both of these mechanisms can reconfigure the columnar grains with only atomic motion across the boundaries. However, relief of the reaction stresses would require long range diffusion, (i.e. creep). At this time it is not known how grain boundary motion would relieve stress, but only that the boundaries will move to help accommodate the stress. This is related to Le Chatelier's principle: if a system is displaced from equilibrium through application of a force, it will then move in the direction that will reduce that force (Devereux, 1983). But as mentioned previously fine grains can respond to a stress more quickly than columnar grains.

VI.B. Conclusions

Microstructural observation of Nb_3Sn as it forms in a bronze-processed wire reveals that nucleation of new grains stops early in the layer growth process and that columnar grains form early. Observations of the columnar grains as the layer grows show that they break up to form equiaxed grains. Several phenomena that could account for this grain reconfiguration were investigated. Even though the specific mechanism remains unclear, two processes, polygonization and recrystallization, have been excluded due to the rarity of intragranular dislocations in the Nb_3Sn . Two probable driving forces for columnar grain reconfiguration are reduction of surface energy and/or strain energy. The

instability of the columnar grain structure in a strained environment seems the most probable mechanism.

VII. Overall Summary

The objective of this work was twofold: to shorten the heat treatment time of an internal tin wire while clarifying the factors that influence its critical current and to determine the mechanism(s) controlling the Nb₃Sn grain morphology in "bronze-type" processes.

The long time multi-step heat treatment normally used to obtain a high critical current in this wire was shortened from ~20 days to ~6 days. The shorter heat treatments were achieved by obtaining a better understanding of the Cu-Sn phase formation during heat treatment which facilitated tin distribution. The high critical current was retained by using two shorter heat treatments, either a temperature ramp or a multi-step heat treatment with distinct temperature steps. Both heat treatments incorporate the low temperature to high temperature schedule which gives good critical current properties due to its influence on the Nb₃Sn microstructure, stoichiometry, and state of atomic order.

The factors that affect the critical current of any Nb₃Sn multifilamentary wire were subdivided into two groups. Those which are external to the Nb₃Sn filament (i.e. extrinsic factors) are the amount of Nb₃Sn in the wire cross section and filament diameter modulation along the length of the wire. To optimize the critical current of a wire the area fraction of Nb₃Sn needs to be maximized while the filament modulation needs to be minimized. The internal-tin-processed wire optimizes both of these factors compared to a bronze-processed wire. The other group consists of intrinsic factors, parameters internal to the Nb₃Sn filament. The intrinsic factors are the composition and grain morphology of the Nb₃Sn. A thermodynamic argument was presented which indicated that the tin composition in the Nb₃Sn produced in the internal tin process is higher than that in a bronze processed wire. This alters the structure and the high magnetic field characteristics, specifically the upper critical magnetic field. Most "bronze-type" processes produce a

Nb_3Sn microstructure with three distinct grain morphologies: columnar, equiaxed, and coarse grained. The grain morphology of the internal tin wire was superior to that produced in a bronze-processed wire due to the increased areal fraction of the equiaxed grain region. The combination of these factors, chiefly reduced filament modulation and the increased amount of small equiaxed grains, produced a high critical current in the internal tin wire. However, the 10-15% higher overall J_c for the heat treatment that optimizes the intrinsic factors can be overshadowed by a 15-25% reduction in overall J_c due to poor control of extrinsic factors during fabrication (i.e. filament modulation).

The increased amount of equiaxed grains of the internal tin wire led to the second objective: understanding the morphological development in "bronze-type" processes. The distinct Nb_3Sn grain morphology of "bronze-type" processes described above has been explained by two models. The coarse grained region is due to grain growth at high temperature according to both models. The dispute concerns the formation of the columnar and equiaxed regions. One model attributes it to the tin supply in the bronze. Early in the heat treatment the tin supply in the bronze is high which produces a high tin concentration at the Nb- Nb_3Sn growth interface, promoting the nucleation of new grains at the interface. Later in the reaction the tin supply in the bronze decreases, reducing the tin supply at the growth interface which promotes the growth of existing grains producing a columnar structure. The other model correlates the formation of the equiaxed region to the break up or reconfiguration of the columnar grains. The columnar grains form early in the layer formation and reconfigure with subsequent layer growth. The Nb_3Sn layer in the particular bronze-processed wire investigated was known to produce columnar and equiaxed region thus making it a good candidate in which to observe the morphology change with layer growth. TEM observations showed that the nucleation of new grains stopped early in the layer growth and that columnar grains reconfigured. Three mechanisms (recrystallization, polygonization of dislocation, and instability of columnar grains) that could be responsible

for the break-up were investigated. Two driving forces for reconfiguration are the reduction in grain boundary energy associated with the instability of a columnar structure and/or the reduction in strain energy due to the reaction stresses. These stresses were modeled using a plane strain elastic approach in an attempt to isolate one of the three as the controlling mechanism. Even though a specific mechanism was not determined, two of the mechanisms, recrystallization and polygonization of dislocations, have been eliminated due to the absence of dislocations and low angle boundaries. The columnar grains must reconfigure to relieve the reaction stresses using a global argument, i.e. Le Chatelier's principle. The microstructure will develop that can best relieve the stress. Since an equiaxed structure has a faster stress response than a columnar grain structure, the microstructure goes in that direction.

VIII. Future Directions

Nb₃Sn superconducting wire produced by the internal tin process was found to have a high critical current in comparison to conventional bronze-processed wires because it has more uniform filaments and a superior Nb₃Sn grain morphology. Both of these factors vary with details of wire processing and heat treatment and therefore warrant further study aimed at optimizing this class of Nb₃Sn wire.

(1) Critical Current and Filament Modulation

To better quantify the influence of filament modulation on J_c , an in-depth experimental study should be performed since any filament modulation can reduce the maximum achievable J_c of a wire. The characterization effort should be accompanied by the development of a theoretical model of the effect of filament modulation on the I-V characteristics (and, by implication, critical current) of a superconducting wire.

(2) Cu-Nb-Sn Equilibrium Ternary Phase Diagram

To better understand how the layer morphology of the Nb₃Sn that forms in "bronze-type" processes is affected by heat treatment a study of Nb-Sn phase formation from high tin Cu-Sn intermetallics such as ϵ and η is necessary. This requires exploration of the Cu-Nb-Sn ternary diagram for Cu-Sn and Nb-Sn alloys with compositions between 15-50 at% Sn and 25-50 at% Sn, respectively. This investigation should focus on determining the equilibrium two-phase fields and the tie lines that might be followed in a diffusion couple between Nb and a bronze intermetallic phase.

(3) Measurement of Reaction Stresses

The Nb₃Sn layer morphology was observed to undergo a columnar grain to equiaxed grain reconfiguration. The direct mechanism(s) that produces this reconfiguration

is not known. However, it is believed to result from strain-induced grain boundary motion, with the stresses due to the formation of Nb₃Sn driving the reaction. The bulk reaction stresses might be measurable experimentally using a planar diffusion couple of niobium coated with a thin layer of bronze. As the layer grows during heat treatment, stresses will develop, causing the couple to bow. The amount of deflection (or equivalently, change of curvature) can be measured at various stages of the reaction to estimate the stress by an in situ laser interferometry techniques. The biaxial stress state that develops in the Nb₃Sn in a planar geometry will be proportional to

$$E \left(\frac{t_{\text{Nb}}^2}{t_{\text{Al5}}} \right) \left(\frac{\delta}{R^2} \right)$$

where E is the modulus of the Nb, t_{Nb} is the Nb substrate thickness, t_{Al5} is the Nb₃Sn layer thickness, δ is the measured deflection, and R is the radius of a round Nb wafer or the reference length of a Nb foil. The Nb substrate is assumed to be much thicker than the Nb₃Sn layer produced. The bronze is expected to contribute little to the bowing of the wafer. The initial deflection introduced with the ramp to 700°C will be recovered due to creep processes in the bronze since it is at about 0.8 of its melting point.

IX. References

- Agarwal, S.K., 1984, S.B.Samanta, V.K. Batra, A.V. Narlikar, J. Mat. Sci., 19, 2057.
- Blum, P., Gregory, E., and Coffey D.L. 1977, Adv. Cry. Eng. 22, 362.
- Breedis, J.F., 1973, Nonferrous martensitic structures, ASM Metals Handbook, 8th ed., vol. 8, 200.
- Camps, R.A. 1987, J.E. Evetts, B.A. Glowacki, S.B. Newcomb, R.E. Somekh and W.M. Stobbs, Microstructure and critical current of superconducting $\text{YBa}_2\text{Cu}_3\text{O}_{7-x}$, Nature, 329, Sept. 17, 229.
- Carter, W.C. 1986, The morphological stability of continuous intergranular phases: thermodynamic considerations, Acta Met. (submitted), work done as M.S Thesis, University of California, Berkeley.
- Charlesworth, J.P., 1970, I. Macphail, and P.E. Madsen, Experimental work on the Nb-Sn constitution diagram and related studies, J. of Material Science, 5, 580.
- Cogan, S.F. 1979, D.S. Holmes, I.M. Puffer, T.W. Eagar, and R.M. Rose, On the micromechanics of multifilamentary superconducting composites, IEEE Trans. Magn. MAG-15, 684.
- Cogan, S.F. 1983, J.D. Klein, S. Kwon, H. Landis and R.M. Rose, On the mechanical properties of Sn-core processed Nb_3Sn filamentary composites, IEEE Trans. Magn., MAG-19, 917.
- Courtney, T.H. 1979, "Thermal and mechanical Stability in finely divided structures," in New Developments and Applications in Composites, ed. D. Kuhlmann-Wilsdorf and W.C. Harrigan, Jr., The Metallurgical Society of AIME.

- da Silva, L.C.C. and Mehl, R.F. 1951, Trans. AIME, 191, 155.
- Devantay, H. 1984, J.L. Jorda, M. Decroux, J. Muller and R. Flukiger, J. Mat. Sci., ???
- Devereux, O.F., 1983, "Topics in Metallurgical Thermodynamics", John Wiley & Sons, New York, p. 465.
- Dietderich, D.R., 1985, J. Glazer, C. Lea, W.V. Hassenzahl and J.W. Morris, Jr., The critical current density and microstructural state of an internal tin multifilamentary superconducting wire, IEEE Trans. Mags., MAG-21, 297.
- Eisenstatt L.R. and Wright R.N., 1980, Plastic deformation in polycrystalline Nb₃Sn, Met. Trans., 11A, 1132.
- Ekin, J.W., 1984, Strain effects in superconducting compounds, in: "Adv. in Cry. Eng.", Plenum, New York, vol. 30.
- Farrell, H.H. 1974, G.H. Gilmer, and M. Suenaga, Grain boundary diffusion and growth of intermetallic layers: Nb₃Sn, J. Appl. Phys., 45(9), 4025.
- Flükiger, R. 198?, The stress induced cubic-to-tetragonal phase transformation, IEEE Magn. (preprint).
- Flükiger, R. 1981, W. Schauer, W. Specking, B. Schmidt, and E. Springer, Low temperature phase transformation in Nb₃Sn multifilamentary wires and the strain dependence of their critical current density, IEEE Trans. Mag., MAG-17(5), 2285.
- Frank F.C. and W.T. Read, 1950, Phys. Rev., 79, 722.
- Frank, F.K., 1950, in "Symposium on Plastic Deformation of Crystalline Solids," Carnegie Institute of Technology, Pittsburgh, p. 89; reference from, Hirth, J.P.

- and Lothe, J. 1982, "Theory of Dislocations" (2^{ed.}), John Wiley & Sons, New York, p. 758.
- Goodrich, L.F. and Fickett, F.R., 1982, Critical current measurements: a compendium of experimental results, *Cryogenics*, May, 225.
- Groves, G.W. and Kelly, A. 1963, Independent slip systems in crystals, *Phil. Mag.*, ??? , 877.
- Haselton D.W., 1985, G.M. Ozeryansky, M.S. Walker, B.A. Zeitlin, K. Hemachalam and E.N.C. Dalder, L. Summers, Internal tin process Nb₃Sn superconductors for 18T, "Adv. in Cry. Eng., vol. 30, Plenum Press.
- Hashimoto Y. 1974, K. Yoshizaki, and M. Tanaka, Processing and properties of superconducting Nb₃Sn filamentary wires, in: "London ICEC Proceedings," IPC Science and Technology Press, London, p. 332.
- Herring, C. 1950, *J. Appl. Phys.*, 21, 437.
- Higuchi, H. 1985, K. Tsuchiya, C.J. Klamut, and M. Suenaga, Superconducting Properties of Nb₃Sn Multifilamentary Wires Fabricated by Internal Tin Process, in: "Advances in Cryogenic Engineering," vol. 30.
- Hirth, J.P., 1963, "Relation between Structure and Strength in Metals and Alloys," H.M. Stationery Office, London, p. 218; reference from, Hirth, J.P. and Lothe, J. 1982, "Theory of Dislocations" (2^{ed.}), John Wiley & Sons, New York, p. 758.
- Hopkins, R.H. 1977, G.W. Roland, and Michael R. Daniels, Phase relations and diffusion layer formation in the systems Cu-Nb-Sn and Cu-Nb-Ge, *Met. Trans.*, 8A, 91.

- Hoshino, K 1980, Y. Iijima, and K. Hirano, Interdiffusion and Kirkendall effect in Cu-Sn alloys, *Trans. JIM*, 21(10), 674.
- Johson-Walls, P.E. 1985, D.R. Dietderich, W.V. Hassenzahl, J.W. Morris, Jr., The microstructural state of Nb₃Sn in a multifilamentary titanium doped bronze-processed wire, *IEEE Trans. MAG-21*, 1137.
- Kamata, K. 1984, N. Tada, K. Itoh, and K. Tachikawa, High-field current-carrying capacities of "titanium bronze" processed multifilamentary Nb₃Sn conductors with pure and alloy cores, in: "Adv. in Cry. Eng.", Plenum, New York, vol.30.
- Kauffman, A.R. and Pickett, J.J., 1970, *Bull. Am. Phys. Soc.*, 15, 838.
- Kidson, G.V. 1961, Some aspects of the growth of diffusion layers in binary systems, *J. of Nuclear Materials*, 3(1), 21.
- King, H.W. 1968, "The mechanism of phase transformations in crystalline solids", Monograph No. 33, *Inst. Metals (Manchester)*, p. 196
- Kramer, E.J., 1973, Scaling laws for flux pinning in hard superconductors, *J. Appl. Phys.*, 44(3), 1360.
- Kuwano, N. and Wayman, C.M. 1983, Precipitation processes in a β -phase Cu-15 at%Sn shape memory alloy, *Trans. JIM*, 24(8), 561.
- Li, J.C.M., 1963, *Trans. AIME*, 227, 239.
- Livingston, J.D., 1977, *Phys. Stat. Sol.(a)*, 44, 295.
- Lord Rayleigh, (Strutt, John William) 1879, On the instability of jets, *London Math Soc.*, 10, 4.

- Mahajan, S. 1978, Wernick J.H., G.Y. Chin, S. Nakahara, and T.H. Geballe, Plastic deformation of V_3Si single crystals at elevated temperature, *Appl. Phys. Lett.*, 33(11), 972.
- Nabarro, F.R.N. (1948), Report of conference on strength of solids, Phys. Soc. London.
- Noto, K. 1987, K. Watanabe, H. Morita, Y. Murakami, I. Yoshii, I. Sato, H. Sugawara, N. Kobayashi, H. Fujimori, And Y. Muto, Current carrying properties in high T_c Y-Ba-Cu-O system, International Workshop on Novel Mechanisms of Superconductivity, "Novel Superconductivity", ed. S.A. Wolf and V.Z. Kresin, Plenum Press, New York, p. 801.
- Ochiai, S, 1987, K. Osamura, and M. Ryoji, Influence of two-stage annealing treatment on critical current of bronze-processed multifilamentary Nb_3Sn superconducting materials, *Acta. Met.*, 35(7), 1433.
- Okuda, S. 1983, M. Suenaga, and R.L. Sabatini, *J. Appl. Phys.*, Influence of metallurgical factors on superconducting current densities in "bronze-processed" Nb_3Sn multifilamentary wires, 54, 289.
- Price C. W. and J.P. Hirth, 1972, A mechanism for the generation of screw dislocations from grain-boundary ledges, *Mater. Sci. Eng.* 9, 15.
- Pugh N.J. 1985, J.L.M. Robertson, E.R. Wallach, J.R. Cave, R.E. Somekh, and J.E. Evetts, *IEEE Trans. Magn.* MAG-21, 1129.
- Read-Hill R.E., 1973, in: "Physical Metallurgy Principles" second ed., D. Van Nostrand Co, New York, p. 158

- Rubin, L.G., 1983, R.J. Weggel, M.J. Leupold, J.E.C. Williams, and Y. Iwasa, High field facilities at the Francis Bitter National Magnet Laboratory, in "High Field Magnetism", ed. M. Date, North-Holland Publishing Company, p. 249.
- Scanlan, R.M. 1975, W.A. Fietz, and E.F. Koch, J. Appl. Phys., 46, 2244.
- Schaur, W. and Schelb, W. 1981, IEEE Trans Mag. MAG-17, 374.
- Schwall R.E. 1983, G.M. Ozeryansky, and D.W. Hazelton, Properties and performance of high current density Sn-core process multifilamentary Nb₃Sn, IEEE Trans. Magn., MAG-19, 1135.
- Shaw, B.J., 1976, J. Appl. Phys., 47, 2143.
- Shimizu, K. 1975, H. Sakamoto, and K. Otsuka, On the crystal structure of the banded martensite in Cu-24.5 wt% Sn alloy, Trans. JIM, 16, 581.
- Smathers, D.K. 1983, K.R. Marken, D.C. Larbalestier, and R.M. Scanlan, IEEE Trans. Mag. MAG-19, 1417.
- Smith, C.S. 1948, Grains, phases, and interfaces: An interpretation of microstructure, AIME Tech. Paper 2387, Metals Tech., p 15.
- Stekly, Z.J.J., 1971, State of the art of superconducting magnets, J. Appl. Phy., 42, 65.
- Stoney, G.G. 1909, The tension of metallic films deposited by electrolysis, Proc. Royal Soc. of London, 82A, 172.
- Suenaga M. 1981, Metallurgy of Continuous Filamentary A15 Superconductors, in: "Superconductor Materials Science," ed. S. Foner and B. Schwartz, Plenum Press, New York, p. 201.

- Tachikawa, K., 1970, Proc. of the Third ICEC, Berlin, Germany, Iliffe Sci. and Tech. Pubs., Surrey, England, p. 339.
- Togano, K. and Tachikawa K. 1979, Textures in diffusion-processed superconducting Nb₃Sn and V₃Ga layers, J. Appl. Phys. 50(5), 3495.
- Togano, K., 1979, Y. Asano, and K. Tachikawa, J. Less Com. Met., 68, 15.
- Tribula, D. 1986, M.S. Thesis, University of California, Berkeley.
- Wallach, E.R. and Evetts, J.E. 1986, in: Advances in Cryogenic Engineering, ed. R.P. Reed and A. F. Clark, Plenum Press, New York, vol. 32, p. 911.
- Wang, C.C. and Hansen, M 1951, Eutectoid decomposition of the δ -phase of the Cu-Sn system, Trans. AIME, J. of Metals, Dec., 1212.
- Welch D.O. 198?, G.J. Dienes, O.W. Lazareth, Jr., and R.D. Hatcher, Theoretical studies of point defects and diffusion in Nb₃Sn, BNL #32274 (IEEE preprint).
- West, A.W. and Rawlings. R.D., 1977, J. Mat. Sci., 12, 1862.
- Worthington, T.K. 1987, W.J. Gallagher, T.R. Dinger, and R.L Sandstrom, Anisotropy in single-crystal Y₁Ba₂Cu₃O_{7-x}, International Workshop on Novel Mechanisms of Superconductivity, "Novel Superconductivity", ed. S.A. Wolf and V.Z. Kresin, Plenum Press, New York, p. 781.
- Wu, I.W. 1983, D.R. Dietderich, J.T. Holthuis, M. Hong, W.V. Hassenzahl, and J.W. Morris, Jr., J. Appl. Phys., 54, 7139.
- Yamasaki, H. and Kimura, Y. 1982, Fabrication of Nb₃Sn superconductors by the solid-liquid diffusion method using Sn rich CuSn alloy, Cryogenics, February 1982, 89.

Yetter, W.E., 1982, D.A. Thomas, and E.J. Kramer, *Phil. Mag.B*, **46**, 523, Yetter, W.E., 1980, Ph.D. thesis, Cornell University, Ithaca, New York.

Yoshizaki K. 1982, O. Taguchi, F. Fujiwara, M. Imaizumi, Y. Hashimoto, K. Wakamoto, T. Yamada and T. Satow, Properties of Multifilamentary Nb₃Sn Wires Processed by Internal Tin Diffusion, in: "Advances in Cryogenic Engineering," vol. 28, p. 380.

Zeitlin, B.A. 1985, G. Ozeryansky, K. Hemachalam, An overview of the IGC internal tin Nb₃Sn Conductor, *IEEE Trans. Magn.*, **MAG-21**, 293.

Zerveck, G. 1981, *J. Low Temp. Phys.*, **42**, 1.

Zwicker, U. and Rinder, L. 1975, Investigations on the formation of the Nb₃Sn A15 phase at temperatures below 800°C, *Z. Metallkde*, **66(12)**, 738.

X.A. Appendix: Stress Model

To determine the constants in these equations the initial and boundary conditions are used. The constants will first be solved for the intrinsic stresses. At the end of this section the procedure to extend this analysis to thermal stress is discussed. The stress equations in each region (assuming different elastic constants in each region) are the following:

$$\begin{aligned} \sigma_r &= KC_1 & \sigma_r' &= K'[C_1' - \frac{C_2'}{r^2}(1-2\nu') - (1-\nu')\epsilon_0] \\ \sigma_\theta &= KC_1 & \sigma_\theta' &= K'[C_1' + \frac{C_2'}{r^2}(1-2\nu') - (1-\nu')\epsilon_0] \\ \sigma_z &= 2\nu KC_1 & \sigma_z' &= K'[2\nu' C_1' - (1-\nu')\epsilon_0] \end{aligned}$$

Using the boundary conditions

$$r = a: \quad u(a) = u'(a), \quad \sigma_r(a) = \sigma_r'(a)$$

$$\text{From the displacements:} \quad C_1 a^2 = C_1' a^2 + C_2' \quad (1)$$

$$\begin{aligned} \text{From the stresses:} \quad KC_1 &= K'[C_1' - \frac{C_2'}{a^2}(1-2\nu') - (1-\nu')\epsilon_0] \\ C_1 &= \frac{K'}{K}[C_1' - \frac{C_2'}{a^2}(1-2\nu') - (1-\nu')\epsilon_0] \quad (2) \end{aligned}$$

$$r = b: \quad \sigma_r'(b) = 0$$

$$\begin{aligned} \text{From the stresses:} \quad K'[C_1' - \frac{C_2'}{b^2}(1-2\nu') - (1-\nu')\epsilon_0] &= 0 \\ C_1' &= \frac{C_2'}{b^2}(1-2\nu') + (1-\nu')\epsilon_0 \quad (3) \end{aligned}$$

Solving this system of three equations, (1), (2), and(3), for the constants C_1 , C_1' , and C_2' :

$$C_1 = \epsilon_0(1-\nu') (1-2\nu') \left(\frac{K'}{K}\right) \left(1 - \frac{a^2}{b^2}\right) \left(\frac{1}{1 - (1-2\nu') \left(\frac{K'}{K} - 1\right) \frac{a^2}{b^2} + (1-2\nu') \frac{K'}{K}}\right)$$

$$C_1' = \epsilon_0(1-\nu') \left(1 + (1-2\nu') \left(\frac{K'}{K}\right) \left(1 - \frac{a^2}{b^2}\right)\right) \left(\frac{1}{1 - (1-2\nu') \left(\frac{K'}{K} - 1\right) \frac{a^2}{b^2} + (1-2\nu') \frac{K'}{K}}\right)$$

$$C_2' = -\epsilon_0 a^2 (1-\nu') \left(\frac{1}{1 - (1-2\nu') \left(\frac{K'}{K} - 1\right) \frac{a^2}{b^2} + (1-2\nu') \frac{K'}{K}}\right)$$

These simplify to the following values when the regions have the same elastic constants:

$$C_1 = \frac{\epsilon_0}{2} (1-2\nu) \left(1 - \frac{a^2}{b^2}\right)$$

$$C_1' = \frac{\epsilon_0}{2} \left((1-2\nu) \left(1 - \frac{a^2}{b^2}\right) + 1 \right)$$

$$C_2' = \frac{\epsilon_0}{2} a^2$$

Using the elastic modulus for Nb and Nb₃Sn, numbers can be assigned to each constant:

$$E = 100\text{GPa} \quad E' = 165\text{GPa}$$

$$\nu = \nu' = 0.33$$

Thermal Stresses

To extend this model to thermal stresses that arise on cooling from the reaction temperature 973K (700°C) to 4.2K, the filament region should be subdivided into hexagonal cells. The boundary planes between each cell will be at half the distance between the Nb filament centers. The outer hexagonal boundary should be approximated by a cylinder with a radius such that the bronze volume is conserved. This introduces a third cylindrical shell into the model. This new shell for the bronze must be treated with an elastic-plastic model, since the bronze yields on cooling to liquid helium temperature (4.2K).

The strains are now related to $\alpha\Delta T$ terms, where α is the linear coefficient of thermal expansion and ΔT is the temperature change the material undergoes. Each region has its own α ; this is the origin of the thermal stresses.

X.B. Appendix: Upper Critical Field

Using the variation in critical current density with applied axial tensile strain the two factors, yield strength and thermal strains, can be isolated. To determine the amount of compressive strain on the Nb₃Sn due to differential thermal contraction uniaxial tension loads are applied during critical current measurements. The axial loading of the wire removes the compressive strain which increases the critical current. The bronze and internal tin processed wires behave similarly. The critical current density of a bronze-processed wire reaches a peak for an axial strain (ϵ_m) of ~ 0.3 . The critical current increases by about 25% at 14T (Ekin, 1984). An internal tin wire similar to the one in this study – it had no Ta diffusion barrier – had a critical current increase of 25% at 14T for a strain of 0.28 (Schwall, 1983). The absence of the Ta diffusion barrier will impose a higher strain on the Nb₃Sn in the wire studied by Schwall. Since the wire in this study has a Ta barrier that makes up about 15% of its cross section, the Nb₃Sn will be in a lower strain state. Since the wire studied by Schwall and the one in this work are very similar, the yield strength of the bronze should be comparable. Therefore, the extrapolated upper critical field of the internal tin wire should be larger than that in a bronze processed wire if differential thermal contraction alone decreases H_{c2}^* .

From the above argument, the low H_{c2}^* is most likely not caused by strain differences between the two wires. However, porosity produced during these heat treatments could alter H_{c2} due to strain localization. Also, the strain distribution in the filament arrays of the two wires is different due to overall geometry differences. This could have a large effect. However,, all things considered, the cubic-to-tetragonal structural transformation could be a major source for the H_{c2}^* reduction. This suggests the Nb₃Sn composition between the two wires is different.

The narrow composition range, 24.5-25at% Sn, of the Nb_3Sn for which the tetragonal phase will form implies that a small change in the composition of the Nb_3Sn could induce the transformation. The Nb_3Sn in the internal tin wire should have a more stoichiometric composition than that produced in the bronze process from a diffusion couple argument. Two Nb-bronze diffusion couples with different tin concentrations in the bronze will produce Nb_3Sn with a different tin concentration. This occurs since the diffusion paths of the two couples can not cross. The bronze with the higher tin concentration will follow a path which produces a Nb_3Sn with a higher tin concentration than that followed by a low Sn concentration bronze. Therefore, the internal tin process could have a higher tin concentration in the Nb_3Sn . If this is the case more of the Nb_3Sn in the internal tin wire undergoes the structural transformation when cooled to low temperature, resulting in a lower H_{c2} . The low temperature (<40K) in situ x-ray diffraction experiment to observe this would be difficult. To overcome this H_{c2} reduction, Ti has been added to suppress the structure transformation and increase H_{c2} (Flückiger, 198?). The high field J_c of internal tin wire was increased by the addition of Ti (Hazelton, 1985).

XI. Figure Captions

II. Background

- Fig. II.1 The critical surface for a superconducting material. Below this surface the sample is in the superconducting state. XBL 836-5778
- Fig. II.2 The magnetic properties of type II superconducting material. (a) In a weak magnetic field, less than H_{c1} , the magnetic field is excluded from the sample except for a shallow region at the surface. (b) In an intermediate magnetic field, between H_{c1} and H_{c2} , the field penetrates the sample producing the vortex state. (c) In a high magnetic field, above H_{c2} , the field fully penetrates the sample. It is now in the normal state. (d) The magnetization of the sample (assuming a cylinder parallel to the field) vs. the applied magnetic field.
- Fig. II.3 A schematic of the vortices being pinned by metallurgical defects in a type II material.
- Fig. II.4 The A15 crystal structure.
- Fig. II.5 Schematic (axial view) of three processes used to produce Nb_3Sn in wire form: The standard bronze process (top), the external tin process (center), and the internal tin process (bottom).
- Fig. II.6 A scanning electron micrograph of a bronze-processed wire produced by the Airco Corporation. The sample has been deeply etched to better reveal the features. The etching solution was 50% nitric acid and 50% water. XBB 831-546A
- Fig. II.7 Cu-Sn binary alloy phase diagram from Hansen.
- Fig. II.8 Cu-Sn binary alloy phase diagram from ASM Metals Handbook vol. 8, p.299
- Fig. II.9 Nb-Sn binary alloy phase diagram (Charlesworth, 1970). XBL 833-5407

- Fig. II.10 Schematic of the Cu-Nb side of the Cu-Nb-Sn ternary alloy diagram at -700°C .
- Fig. II.11 Micrograph of an internal tin wire that has not been heat treated. The axial view of the wire (top) reveals the 61 subelements in the core, the Nb diffusion barrier, and Cu stabilizer. At higher magnification (bottom), the composite nature of the subelement is visible. In each subelement about 1100 Nb filaments in a Cu matrix surround a Sn-1wt%Cu core. XBB 838-7631
- Fig. II.12 Definition of critical current density.
- Fig. II.13 Filament modulation in a bronze-processed wire due to reaction during fabrication anneals. XBB 870-10489
- Fig. II.14 Schematic of the critical current variation vs. the applied magnetic field. (a) A better composition or less strain increases H_{c2} and increases J_c at high fields. A smaller grain size increases J_c at low fields. (b) Combined effect shifts the J_c -H curve out to higher values.
- Fig. II.15 Schematic of the Nb_3Sn layer morphology: Columnar grains at the Nb interface, coarsened grains at the Cu-Sn bronze interface, and a fine layer of equiaxed grains inbetween. XBL 824-5549A

IV. Experimental Procedure

- Fig. IV.1 Scanning electron micrograph of an internal tin wire fabricated by IGC Corp. (a) The sample has been deeply etched to reveal the Nb diffusion barrier and the 61 filament bundles. (b) and (c) Higher magnification of the filament array and the partially reacted filaments. XBB 841-650
- Fig. IV.2 Scanning electron micrograph of the internal tin wire used to measure the critical current and critical current density. XBB 858-6103A

- Fig. IV.3 The bronze-processed wire fabricated by Hitachi Corp. The top optical micrograph shows one of the 31 bundles in the wire. The bundle contains 331 filaments and has a Nb diffusion barrier. In the lower SEM micrograph, the sample has been etched to reveal the thin layer of Nb_3Sn that formed during fabrication. XBB 858-6695A
- Fig. IV.4 Rotation calibration chart for EM301.
- Fig. IV.5 Rotation calibration chart for EM400.
- Fig. IV.6 TEM micrograph of through the center plane of a filament. Nb in the center with Nb_3Sn layer on each side. XBB 867-5947
- Fig. IV.7 Schematic of TEM viewing plane for the sample of Fig. IV.6.
- Fig. IV.8 Probes used to measure critical current. (a) The top probe is for low current measurements ($<25A$) and the bottom probe is for high current measurements. (b) The sample mounting zone of the high current probe. Two samples can be measured per test. (c) The sample mounting zone of the low current probe. Five samples can be measured per test. XBC 870-10492

V. Internal Tin Process - IGC Wire

- Fig. V.1 Comparison of the current density at 4.2K vs. applied magnetic field in the internal tin wire (IGC) of this study and the bronze-processed wire (Airco) studied by Wu et al. (1983).
- Fig. V.2. The average grain size as a function of heat treatment temperature (measured near complete reaction of the Nb). This work and that of Wu et al (1983) averaged over the equiaxed grain region. Data of Scanlan (1975) and Shaw (1976) are included for a comparison.
- Fig. V.3 Kramer plot to determine the extrapolated upper critical field, H_{c2}^* , of the internal tin wire (IGC) of this study and the bronze-processed wire (Airco)

investigated by Wu et al (1983). H_{c2}^* for the internal-tin-processed wire and the bronze-processed wire are 18.9 and 20.7, respectively.

- Fig. V.4 Overall critical current density (10T, 4.2K) of the internal tin wire vs heat treatment time for different treatment schedules. The open points are for heat treatment A+700°C and the solid points are for direct to the high temperature designated in the figure, 650, 700, or 730°C.
- Fig. V.5 SEM micrographs of the internal tin wire at different stages of heat treatment A shown in the figure. (a) The intermetallic layers ϵ and η have formed. (b) The core is all ϵ phase. (c) A β or γ core with Cu-Sn solid solution. XBB 844-2589
- Fig. V.6 Cu-Sn intermetallic, either β or γ , in the internal tin core (top) and filament region (bottom) formed during heat treatment schedule A which was interrupted after 48h at 580°C. A dichromate etchant was used to reveal the internal structure of the intermetallic. XBB 870-10487
- Fig. V.7 TEM micrograph of the Cu-Sn region between to Nb filaments. The sample was given heat treatment A that was interrupted after 12h at 580°C. (a) Low magnification of the Cu-Sn region between the filaments. (b) High magnification of Cu-Sn phase in contact with a Nb-Sn phase. XBB 870-10490
- Fig. V.8 SEM micrograph of a partially reacted filament for a wire that has received heat treatment I. The sample was etched to reveal the Nb_3Sn . Note the large grains at the filament periphery. XBB 858-6105
- Fig. V.9 Schematic of the Cu-Nb-Sn ternary diagram at $\sim 580^\circ\text{C}$. The existence of a two phase region from the Cu-Sn ϵ phase to Nb_6Sn_5 is proposed.
- Fig. V.10 SEM micrograph of a sample given heat treatment A. Porosity is visible through out the filament array. XBB 870-10488

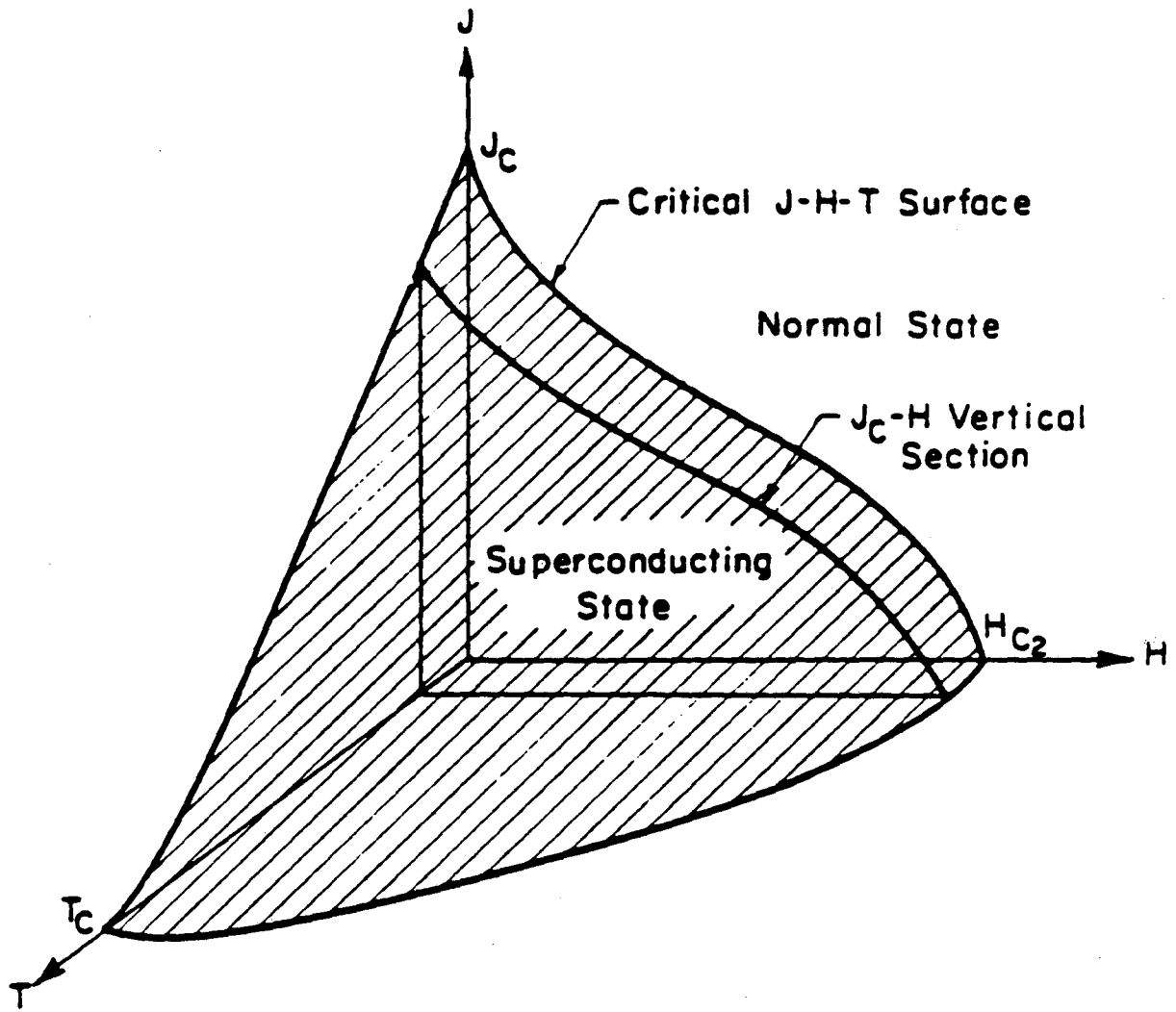
- Fig. V.11 SEM micrograph of a wire (axial view) heat treated directly to 700°C for 2d. XBB 840-7437
- Fig. V.12 SEM micrograph of a wire (longitudinal view) heat treated directly to 700°C for 2d. XBB 858-6101
- Fig. V.13 Overall J_c vs. total heat treatment time the sample received for the heat treatments of this study. XBL 858-3756

VI. Bronze Process - Hitachi Wire

- Fig. VI.1 The Nb_3Sn layer thickness vs. log of heat treatment time at 700°C.
- Fig. VI.2 TEM micrograph of the columnar grains at the Nb interface (bottom of figure) after 2hrs. at 700°C. XBB 872-1129
- Fig. VI.3 TEM micrograph of the Nb- Nb_3Sn interface (bottom of figure) after 2hrs. at 700°C. Nucleation of new grains has ceased and only columnar grains are present. Even three grain junctions reveal no small grains. XBB 872-1127
- Fig. VI.4 Schematic of the previous micrograph with the favorable nucleation sites noted. The sites are three grain junctions.
- Fig. VI.5 TEM micrograph of the Nb_3Sn layer after 7hrs. at 700°C. Columnar grains are present at the Nb interface. The columnar grains that formed during the 2 hour stage (marked in figure) have reconfigured. XBB 867-5951A
- Fig. VI.6 A plot of the Nb_3Sn grain width vs. the distance from the Nb interface for a heat treatment of 700°C for 7hrs. (grain width uncorrected for columnar or equiaxed grain shape).
- Fig. VI.7 Dislocation accommodating crystallographic mismatch between grains. XBB 824-4086
- Fig. VI.8 Bright field TEM of the Nb_3Sn layer with one columnar grain in a zone axis orientation. The convergent beam diffraction pattern is from a 100 zone.

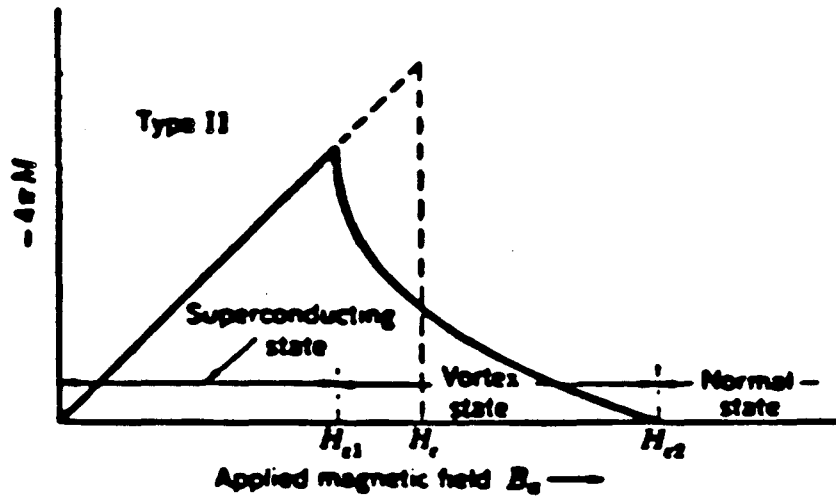
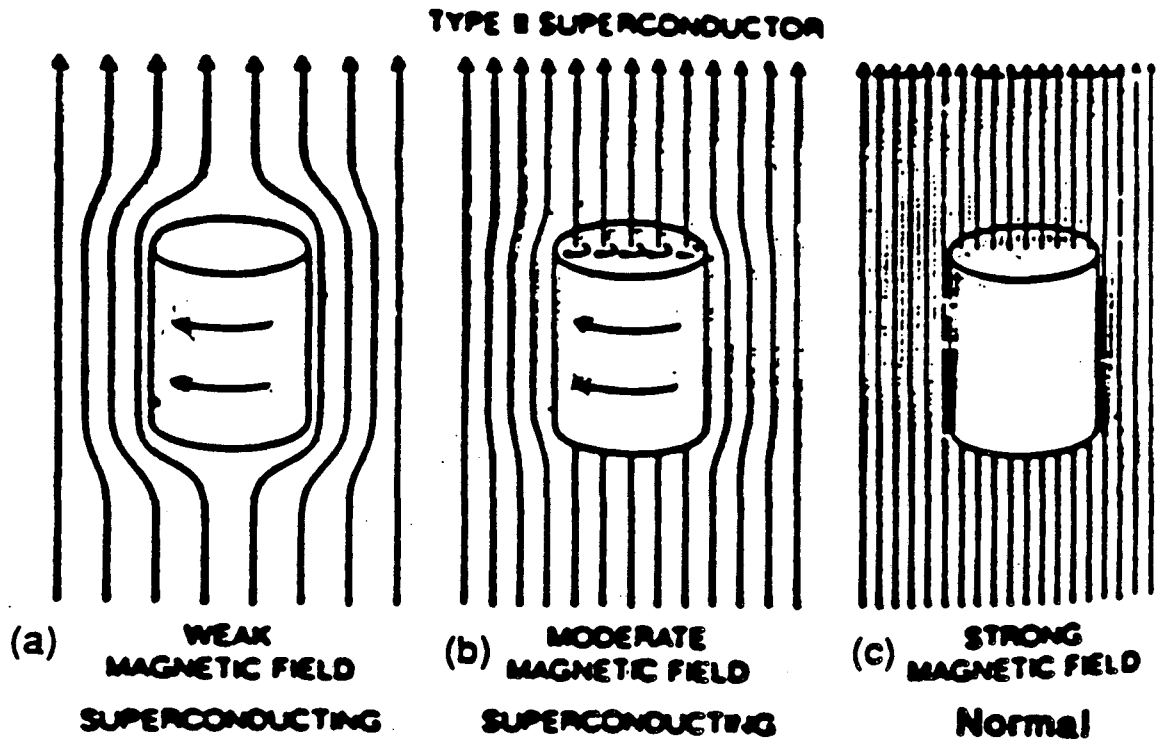
When it is properly oriented with the image, the columnar grain aligns with the [210] direction. XBB 872-1278

- Fig. VI.9 Schematic of the previous micrograph shows the orientation of the columnar grain relative to the Nb interface.
- Fig. VI.10 Bright field TEM of a Nb filament reveals a homogeneous distribution of dislocations. The SAD of the Nb filament which contains several grains shows a [110] texture. The 110 spot along the filament axis is split into two spots separated by -5° . XBB 870-10486
- Fig. VI.11 X-ray diffraction scan for an axially oriented sample. A strong [110] texture is observed: 110 reflection strong, 200 and 211 absent.
- Fig. VI.12 The geometry of the plane strain elastic model.
- Fig. VI.13 Graph of the stress state obtained in Nb_3Sn during heat treatment if there is no stress relief and the Nb_3Sn layer remains elastic. ($\beta = 12\text{GPa}$, $b = 3\mu\text{m}$)
- Fig. VI.14 Plot of the stress state obtained by Pugh et al (1985) from a shrink fit model.
- Fig. VI.15 No dislocations are visible the interior of grains, only arrays at grain boundaries. XBB 870-10491
- Fig. VI.16 Crystallographic misorientation between a columnar grain and the adjacent equiaxed grains. Data was obtained from the sample of figure VI.8. The misorientation of the equiaxed grains is relative to the columnar grain.
- Fig. VI.17 The Gibbs-Thomson relation for the columnar grains that form in Nb_3Sn .
- Fig. VI.18 The number of lateral sides which the columnar grain has determines the direction of boundary motion.



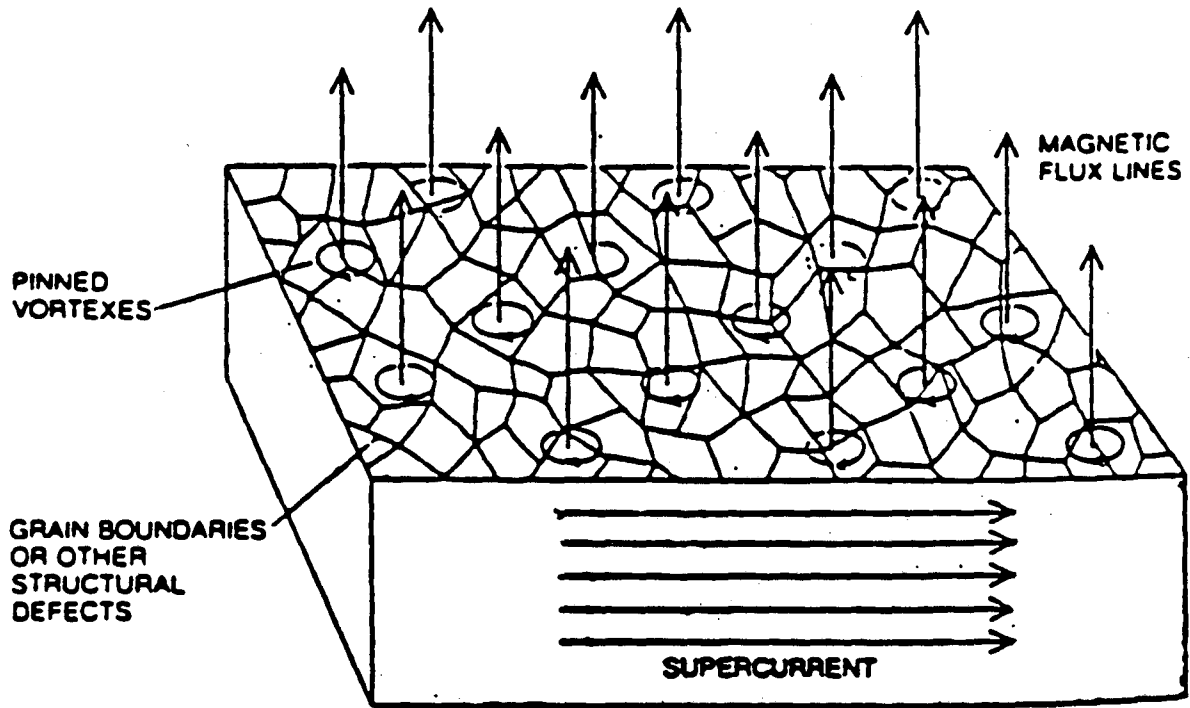
XBL 836-5778

Fig. II.1



(d)

Fig. II.2



HIGH-CRITICAL-CURRENT TYPE II SUPERCONDUCTOR

LORENTZ FORCE $F = J \times B$

OPPOSED BY PINNING FORCE $F_p = J_c \times B$

Fig. II.3

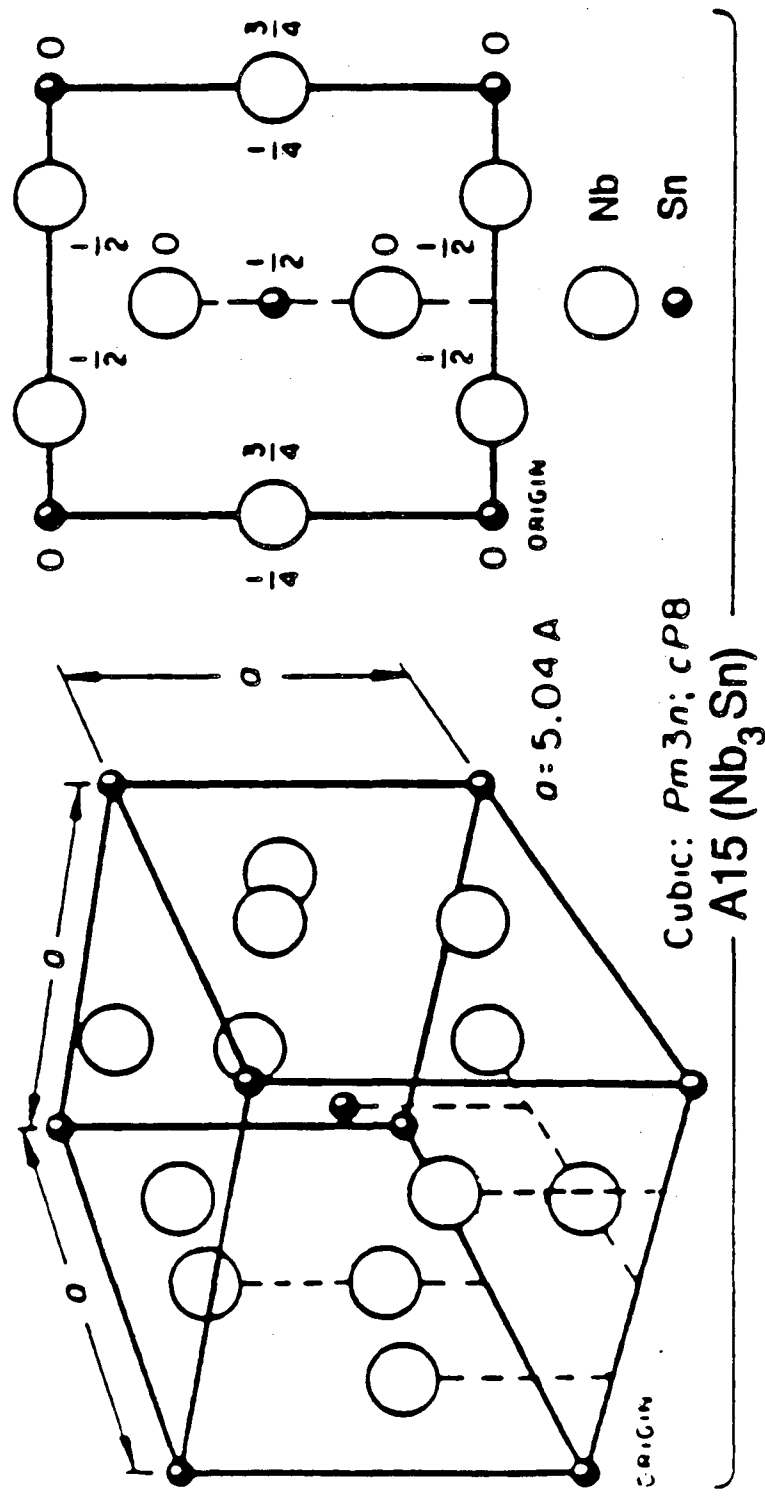
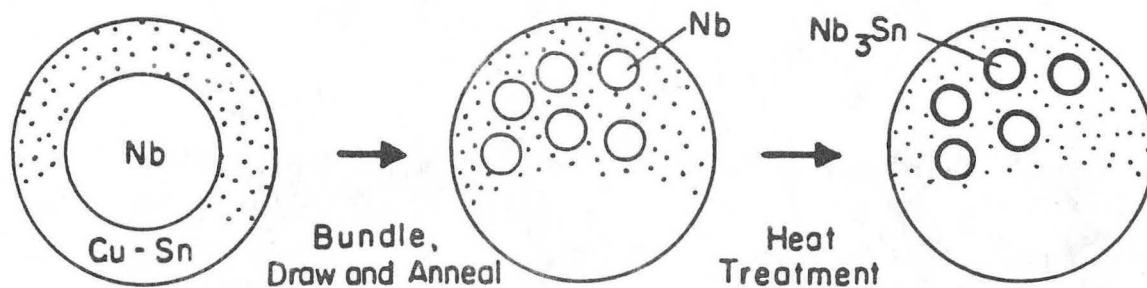
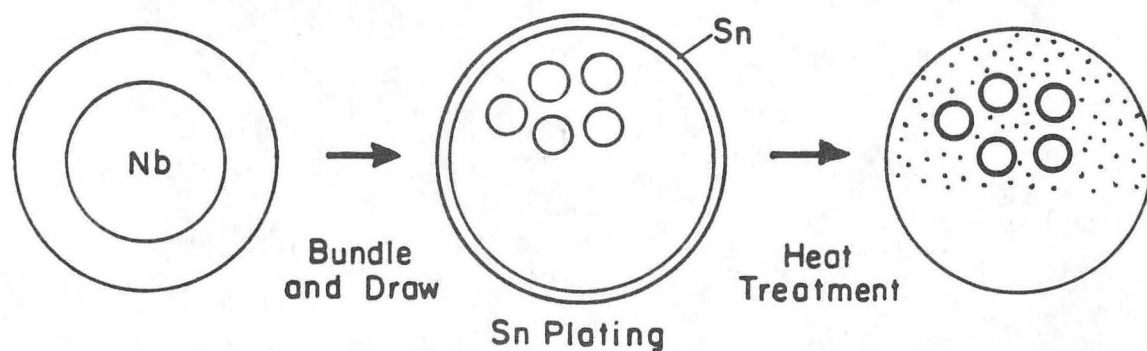


Fig. II.4

1. INTERNAL BRONZE (1969)



2. EXTERNAL BRONZE (1972)



3. INTERNAL Sn DIFFUSION (1974)

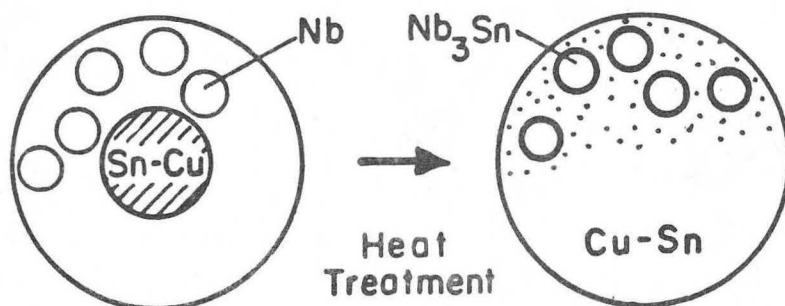
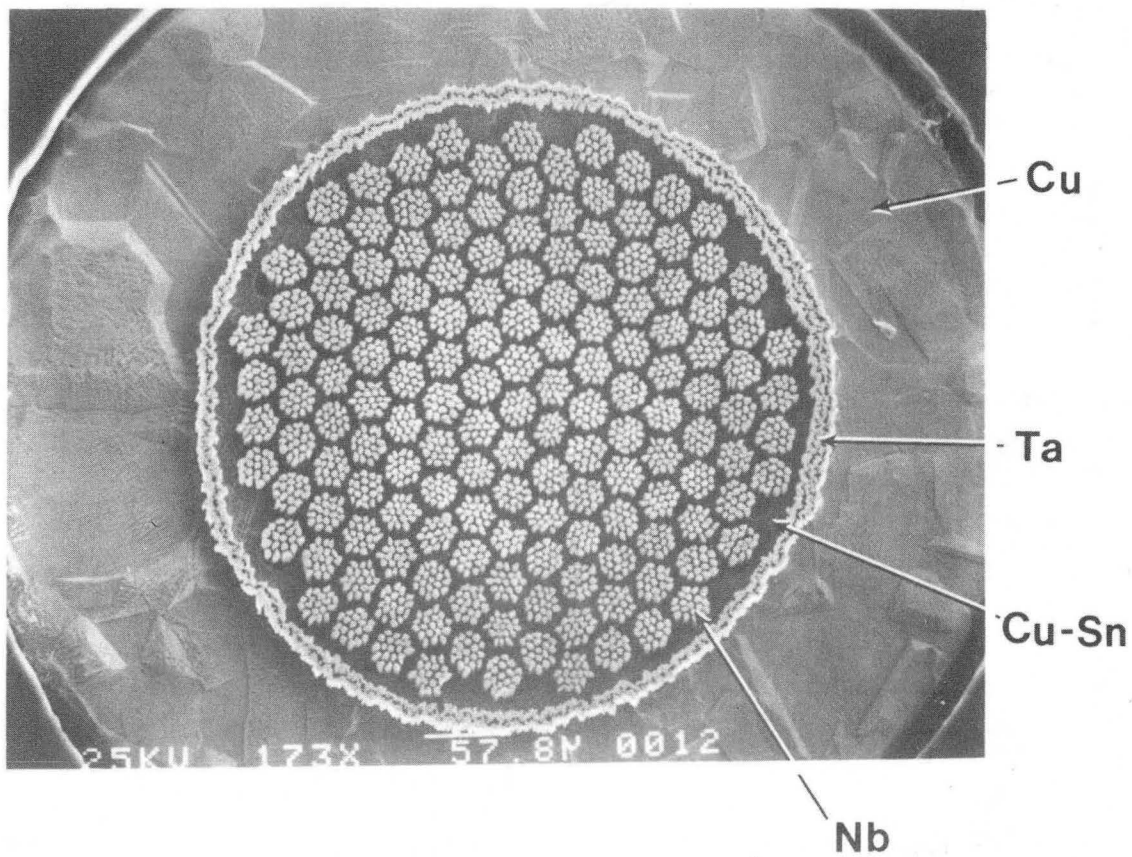


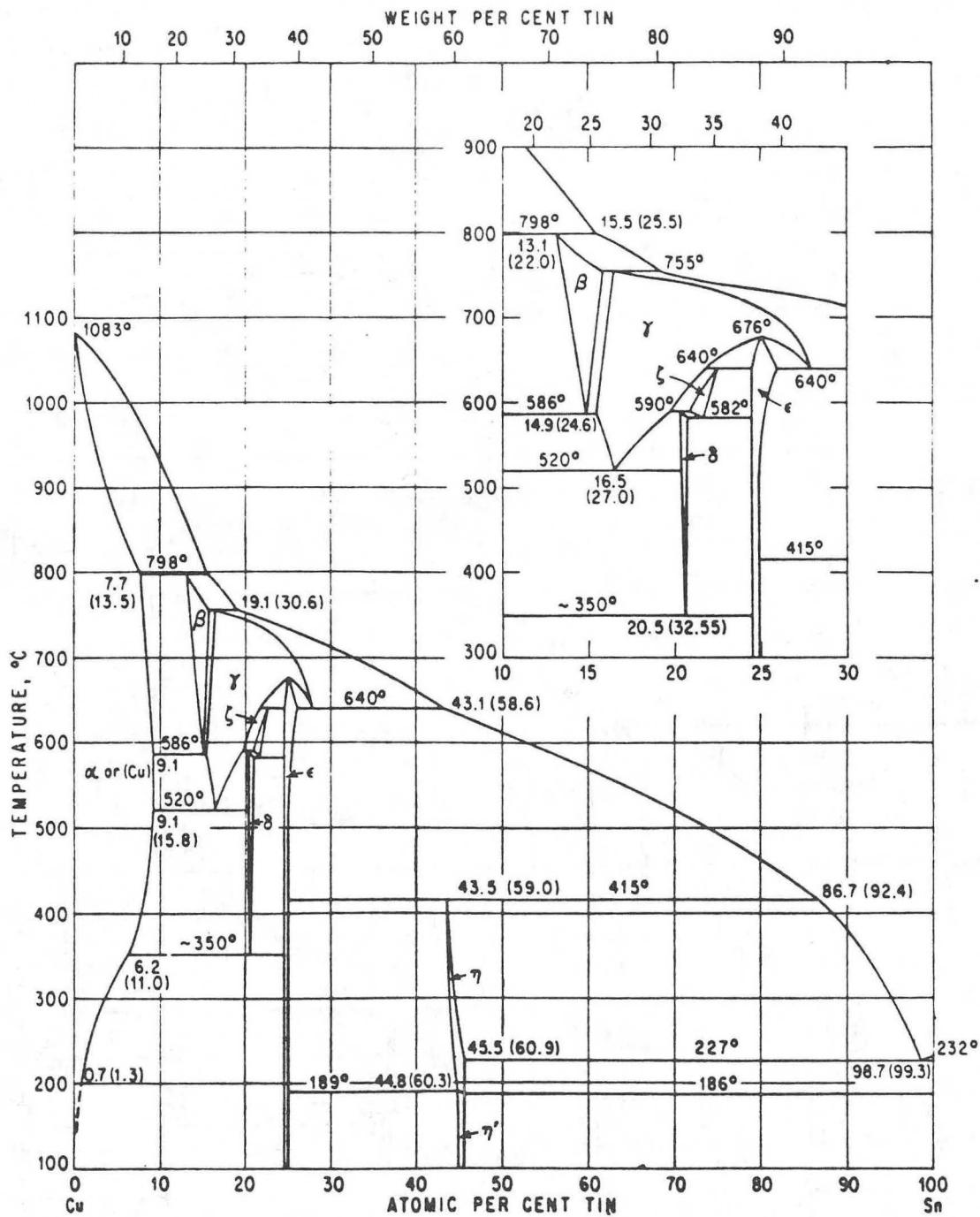
Fig. II.5

AIRCO Internal Bronze Wire



XBB 831-546A

Fig II.6



XBL 849-3701

Fig. II.7

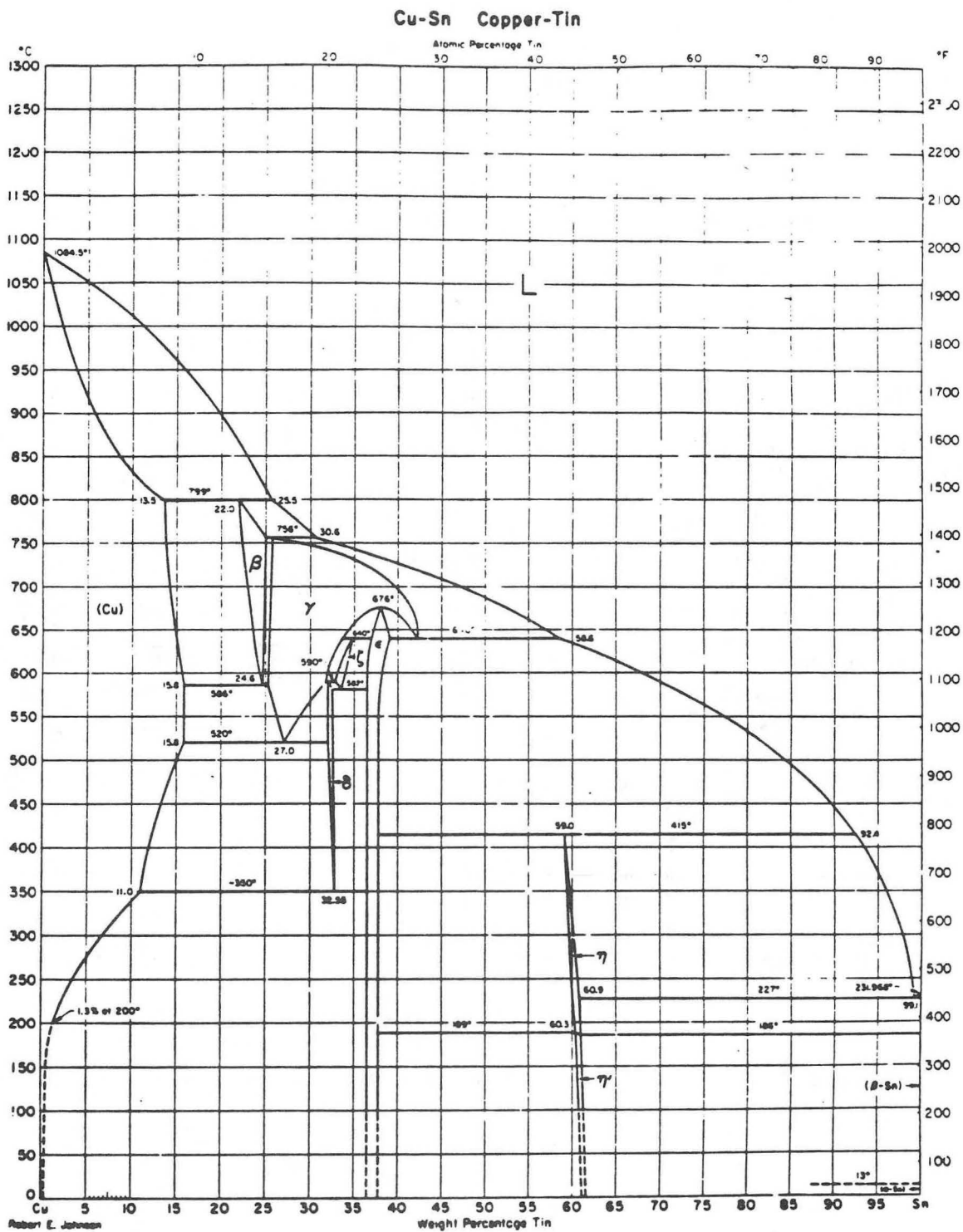


Fig. II.8

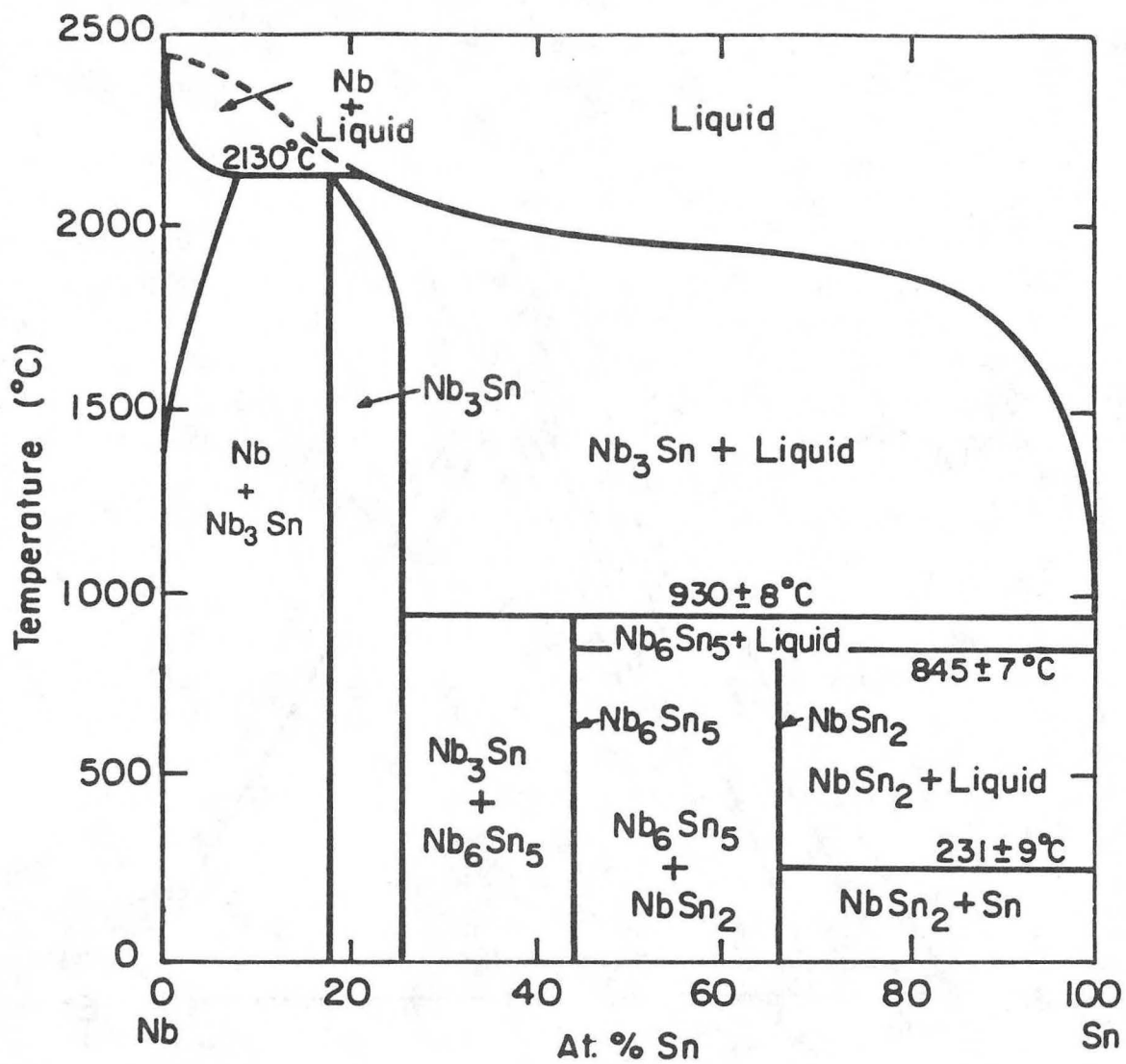


Fig. II.9

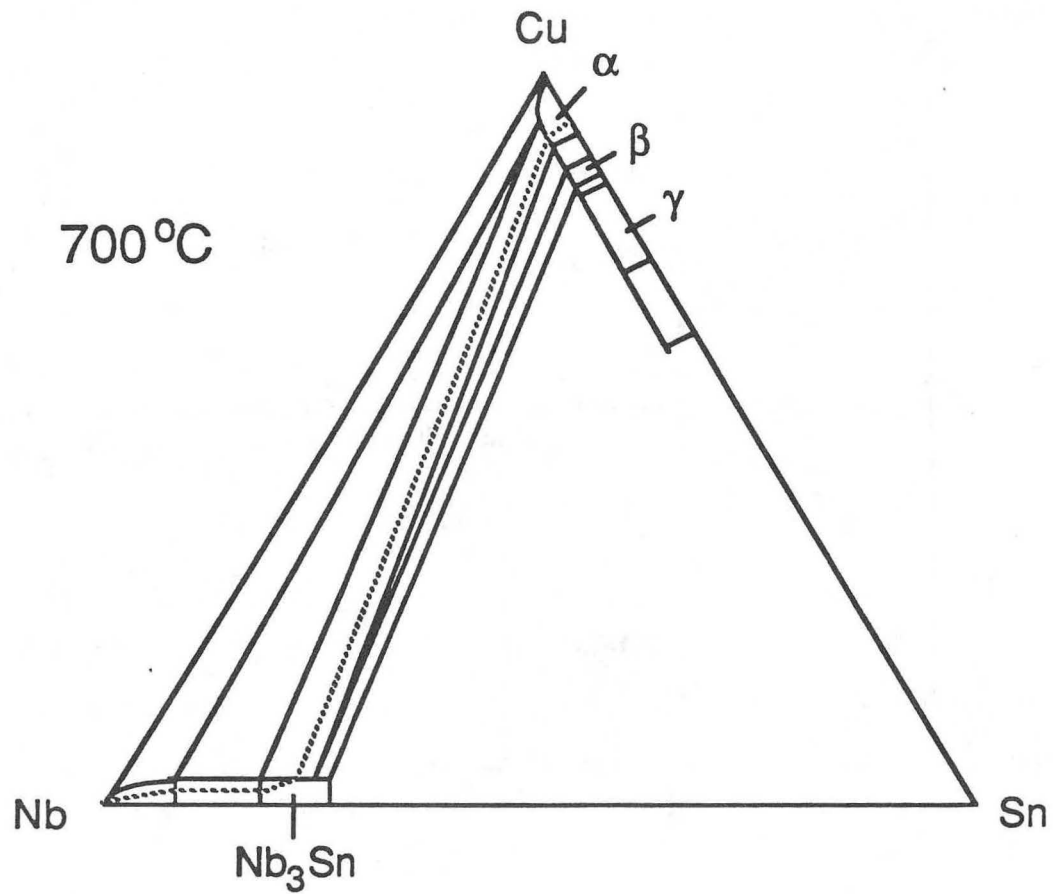


Fig. II.10

IGC Internal Tin Wire

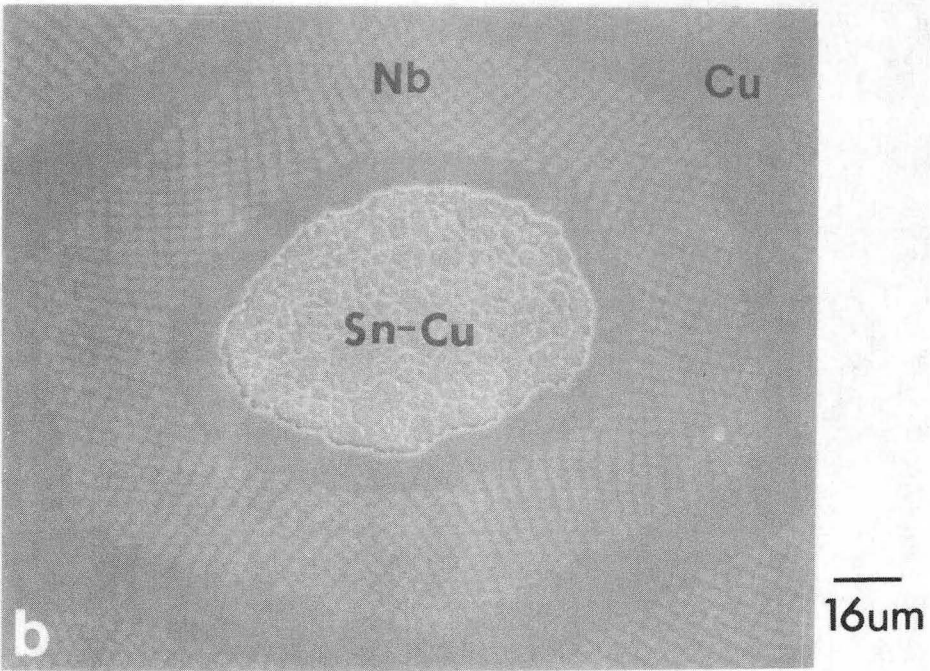
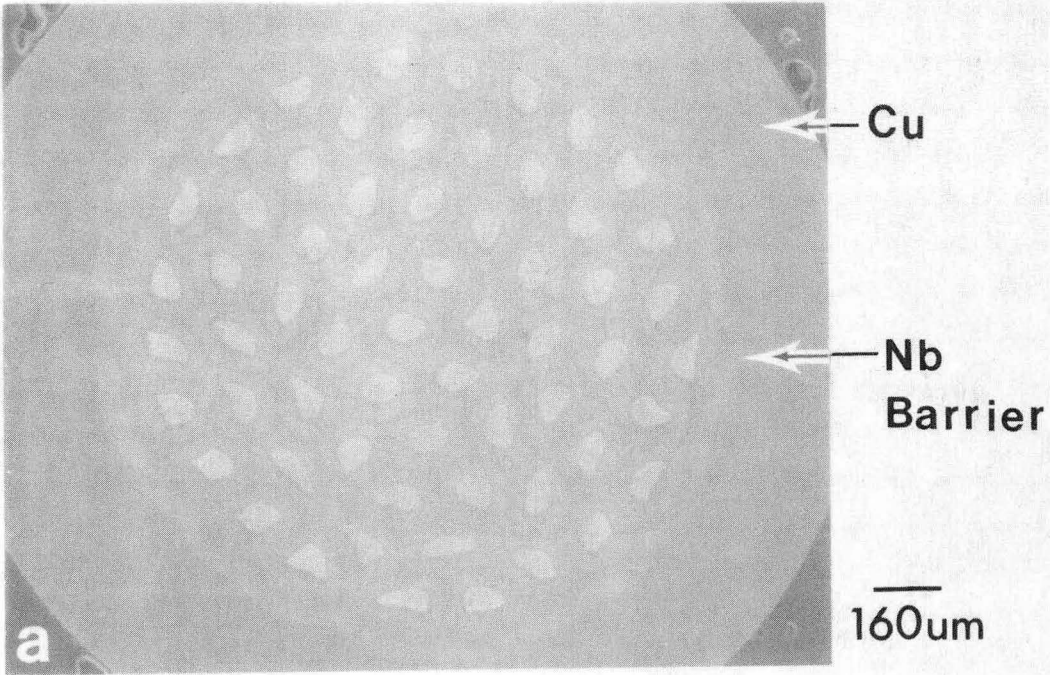
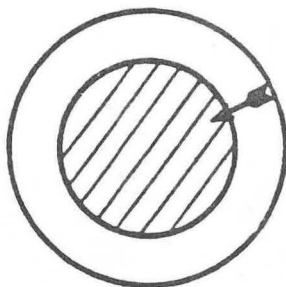


Fig II.11

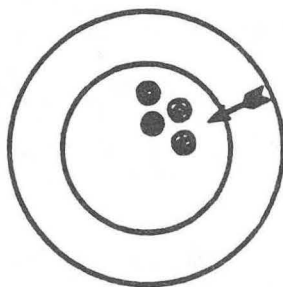
$$J_c = I_c / \text{Area}$$

J_c
(overall)



area inside Ta barrier

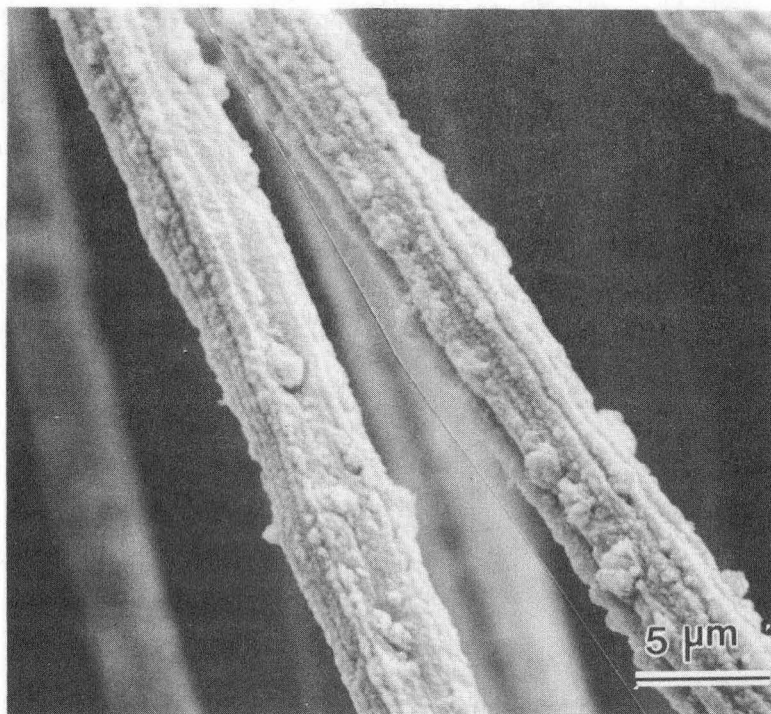
J_c
(Nb_3Sn)



Nb_3Sn cross-sectional area

Measure of Nb_3Sn "Quality"

Fig. II.12



XBB 870-6489

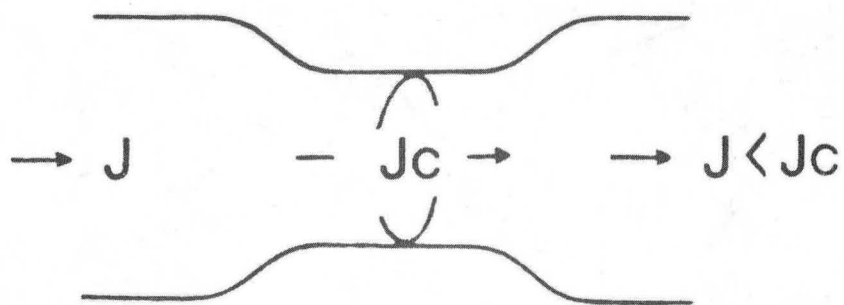


Fig.II 13

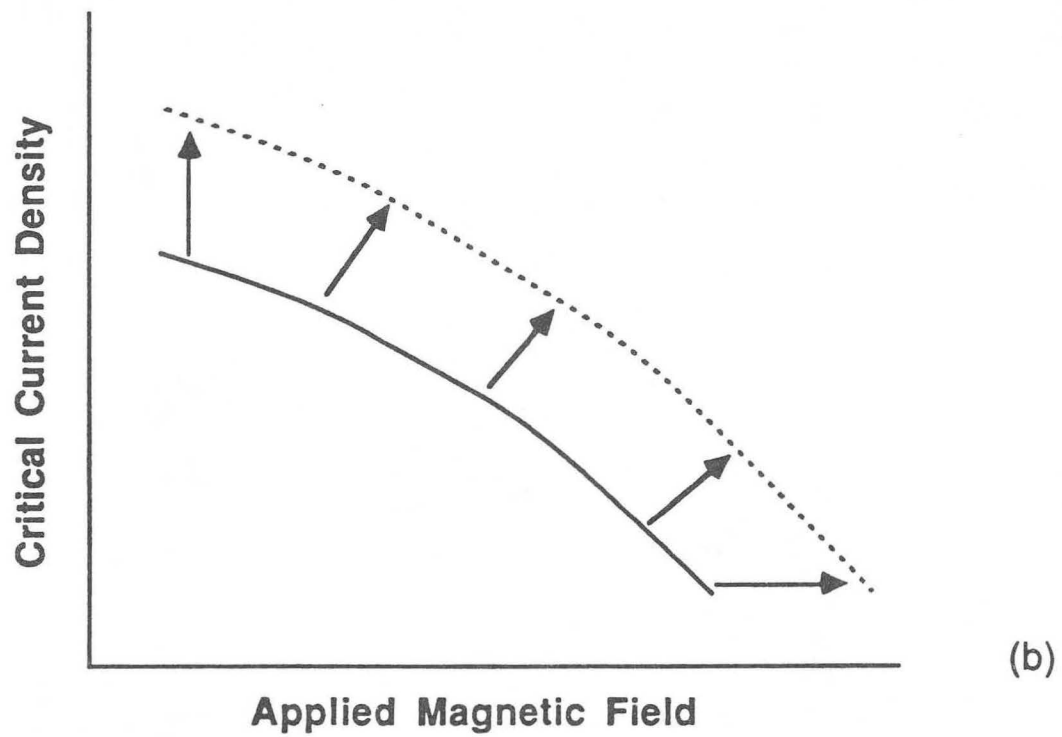
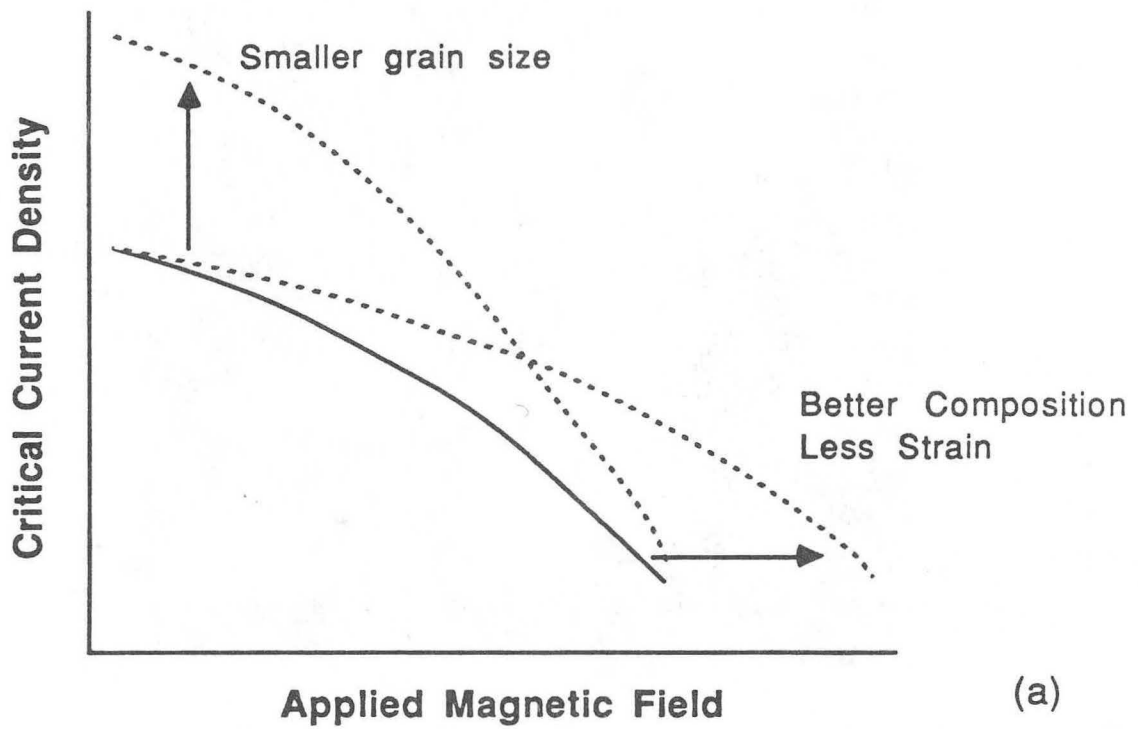
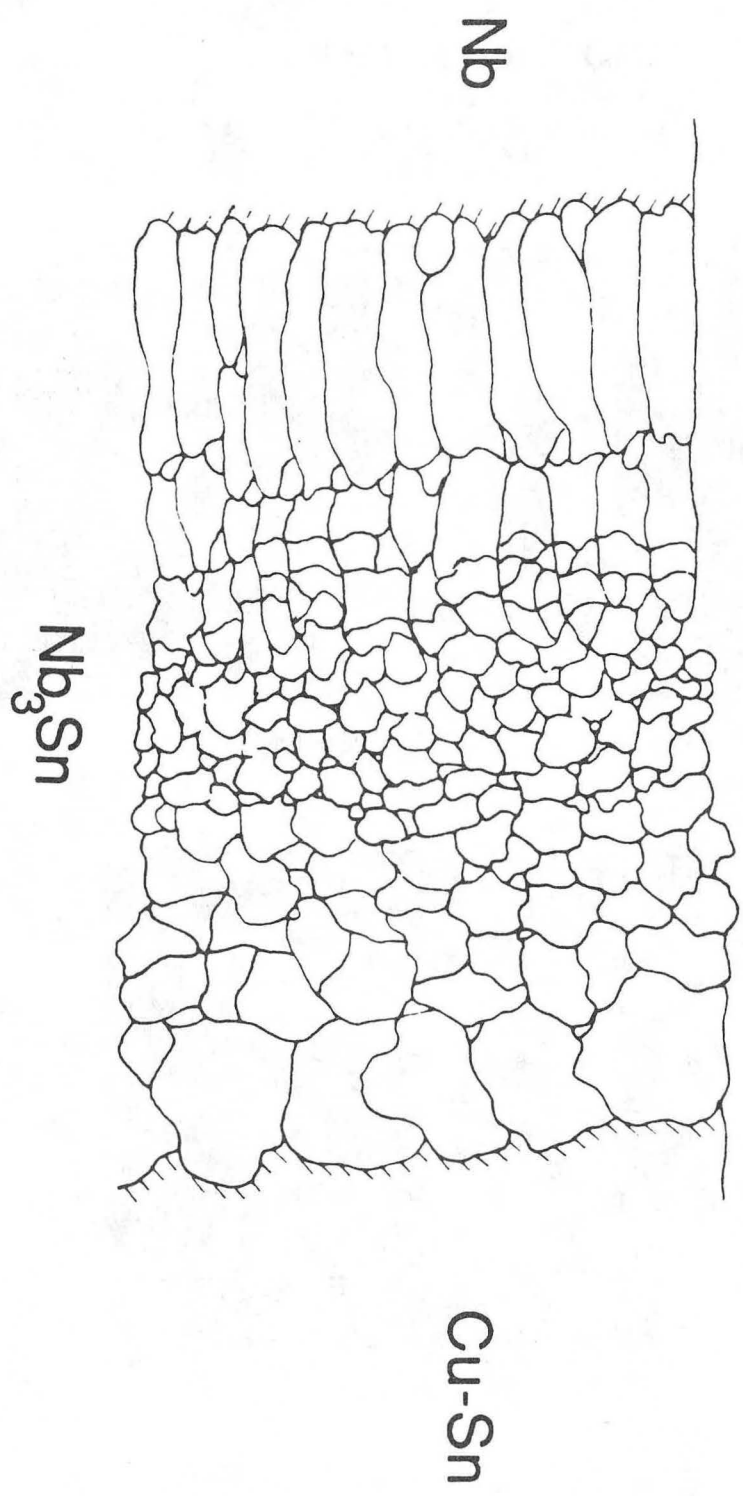



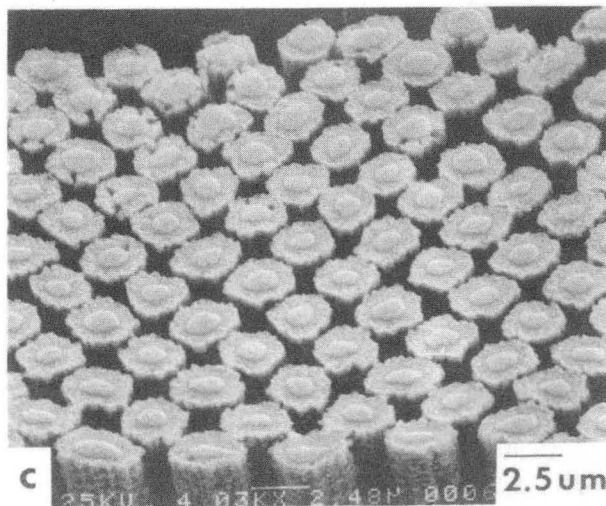
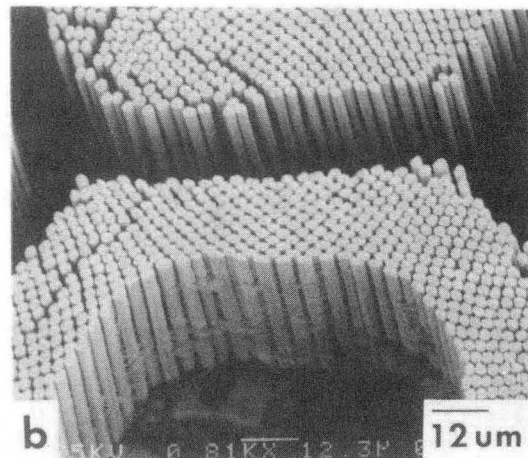
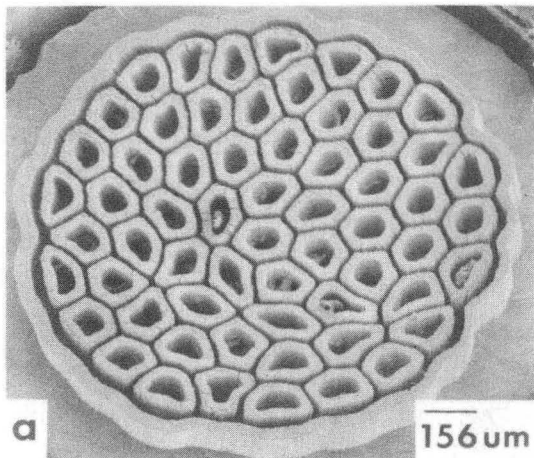
Fig. II.14



XBL 824-5549A

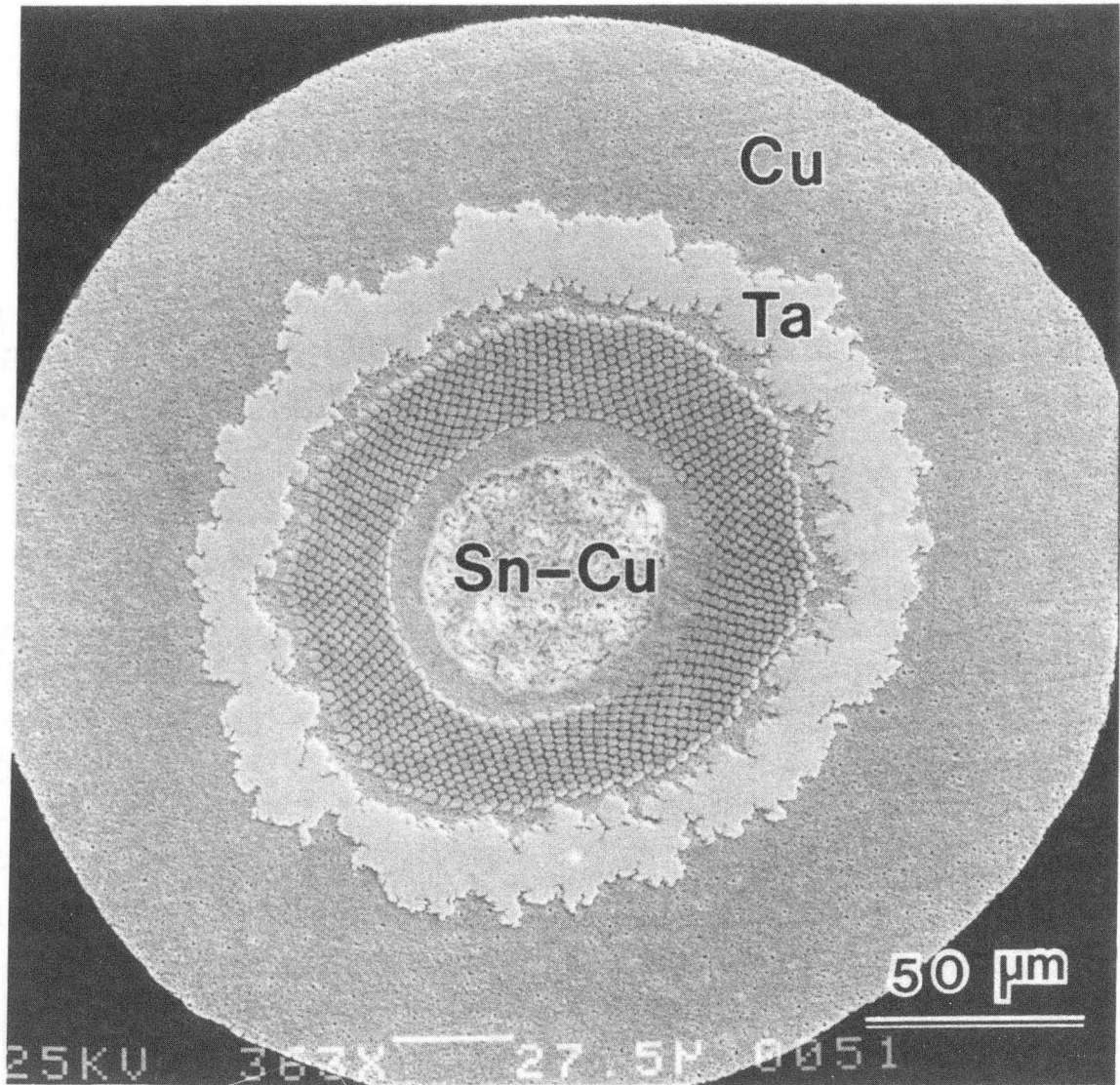
Fig. II.15

IGC Internal Tin Wire
200°C/200hrs.
375°C/33hrs.
580°C/218hrs.  **A**



XBB 941-650

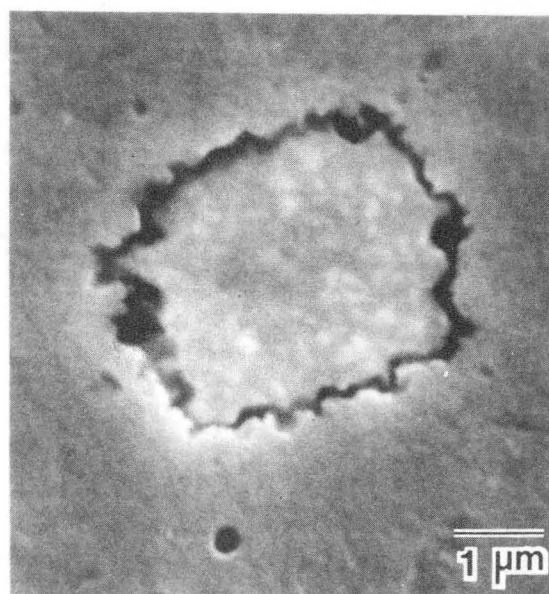
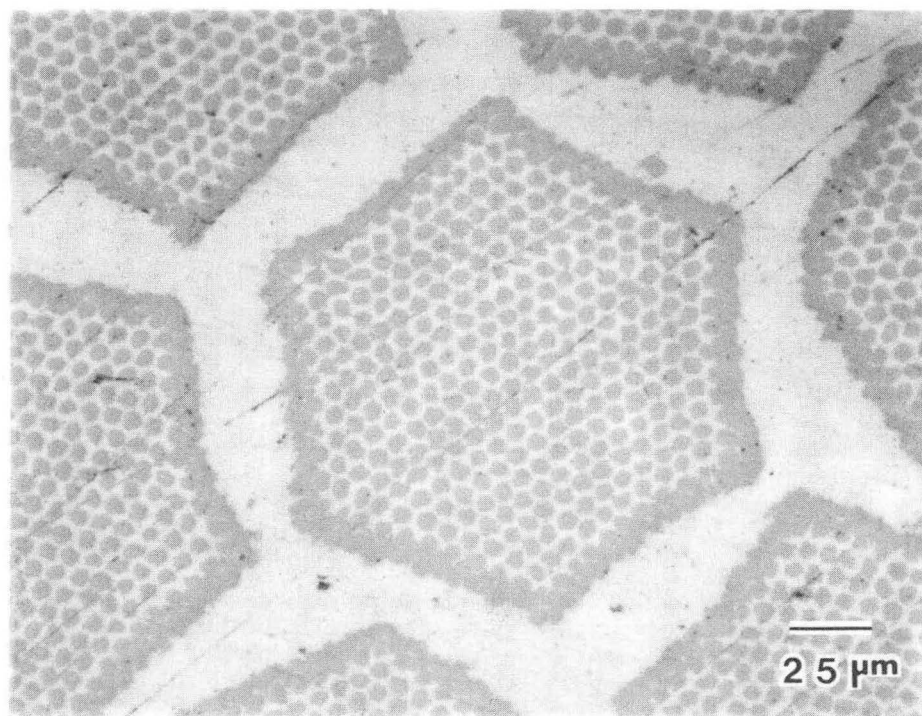
Fig. IV.1



XBB 858-6103A

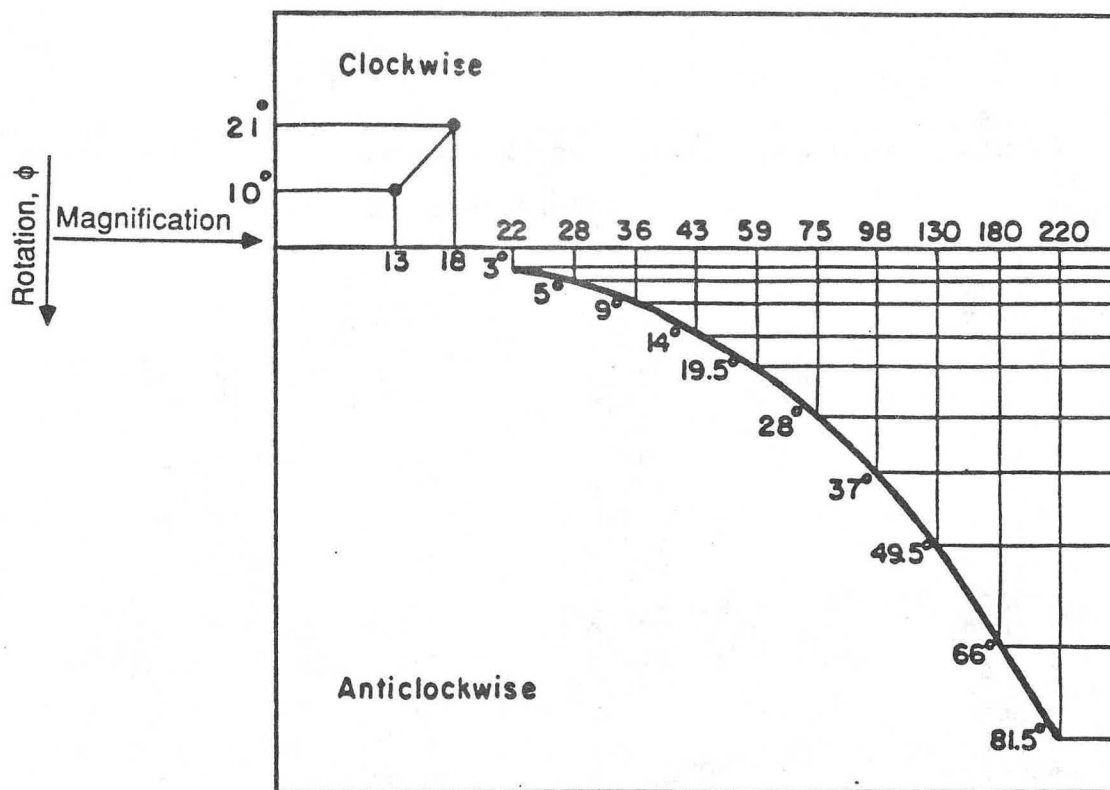
Fig. IV .2

Bronze-Processed Wire (Hitachi)



XBB 858-6695A

Fig IV.3



Rotation Calibration Phillips Goniometer Stage

- 1) Place micrograph with emulsion side up (numbers reversed).
- 2) Rotate SAD by 180° with respect to the image.
- 3) Rotate SAD additionally by degrees as seen in the graph depending on the magnification.

Lens Settings

Proj.: 3.01
Int. : 0.67
Diff.: 1.62

Fig. IV.4

ROTATION CALIBRATION

Rotate image with respect to diffraction pattern with emulsion side down. Camera length 575 mm.

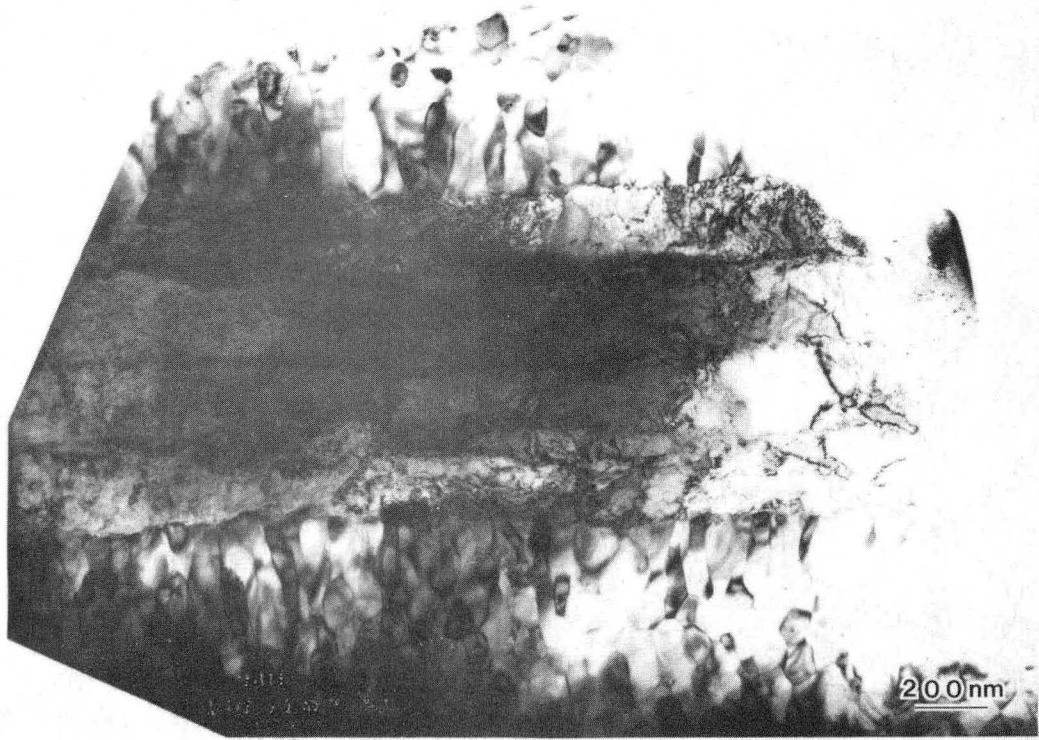
Magnification	Rotation(degrees)	Direction of Rotation
3600	112.5	counter-clockwise
4600	90.0	"
6000	47.5	"
8000	41.5	"
10000	39.5	"
13000	37.5	"
17000	38.0	"
22000	44.0	"
28000	71.0	"
36000	146.0	clockwise
46000	145.5	"
60000	148.0	"
80000	156.0	"
100000	162.5	"
130000	178.5	"
170000	170.5	counter-clockwise
220000	148.5	"
280000	113.0	"
360000	100.5	"
410000	124.0	"
480000	102.0	"

For other camera lengths rotate the image additional degrees.

Camera length	Rotation(degrees)	Direction of rotation
210	11.5	counter-clockwise
290	4.0	counter-clockwise
400	3.5	clockwise
800	7.5	clockwise
1150	19.0	clockwise
1600	37.5	clockwise

EG 6/85

Fig. IV.5



XBB 867-5947

Fig. IV. 6

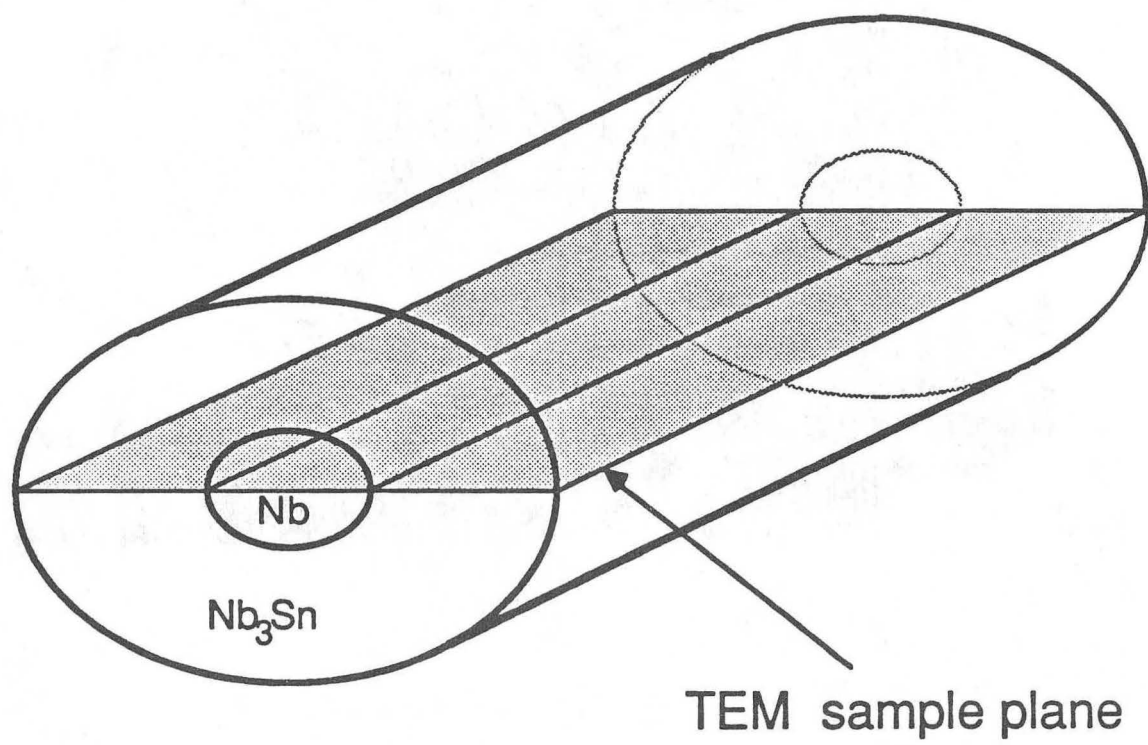
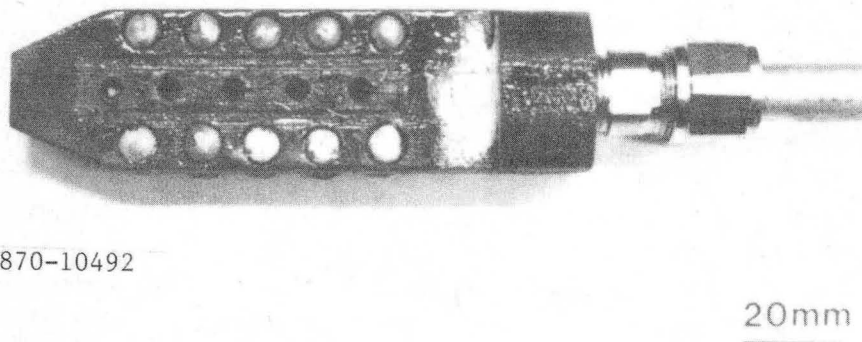
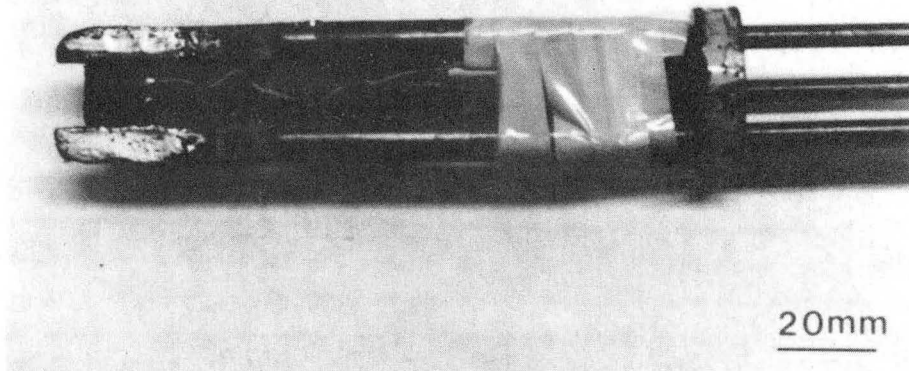
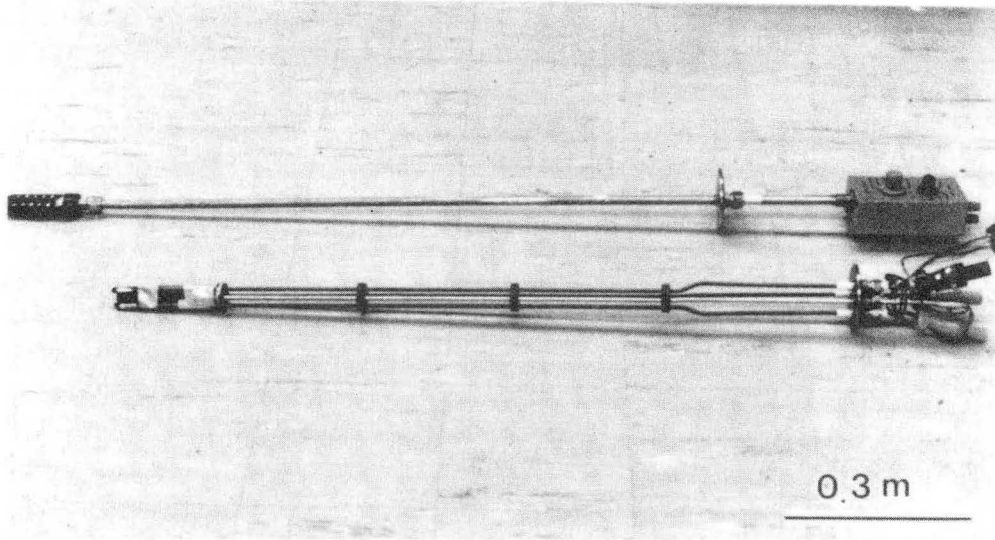


Fig. IV.7



XBB 870-10492

Fig IV.8

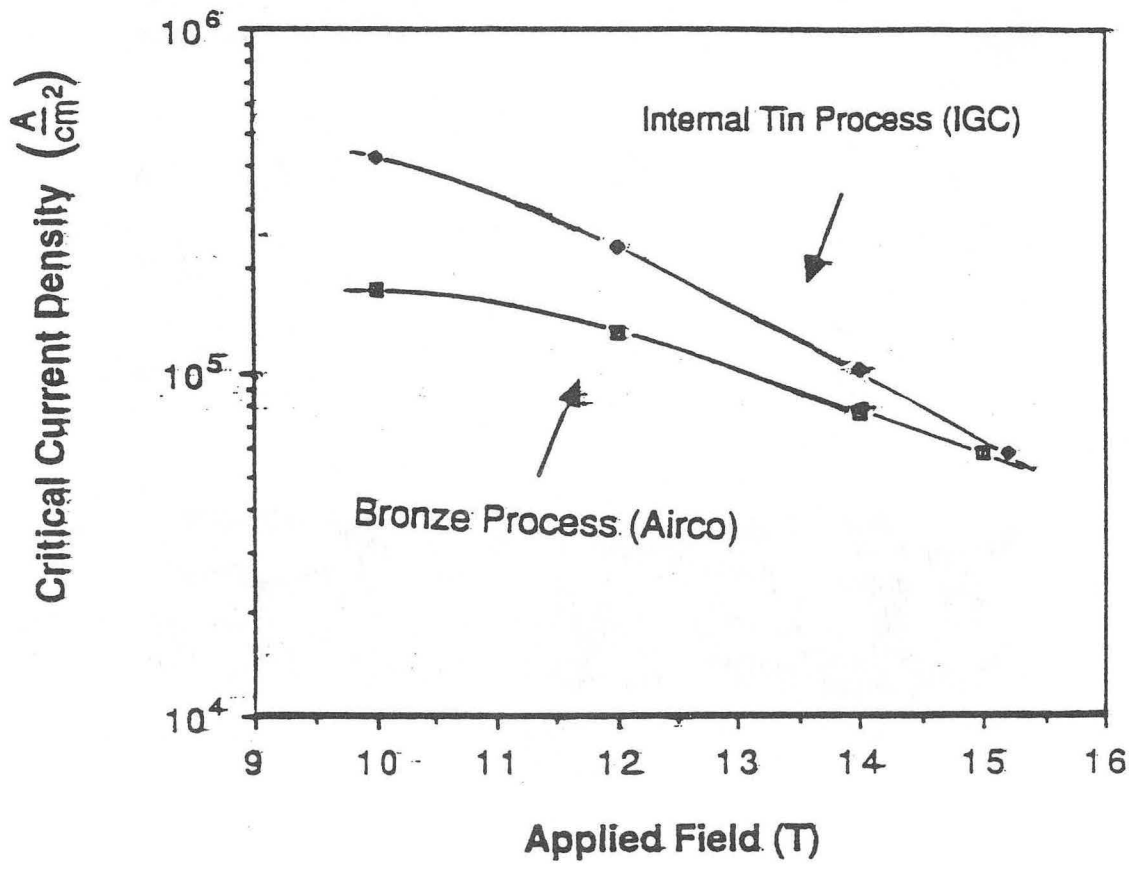


Fig. V.1

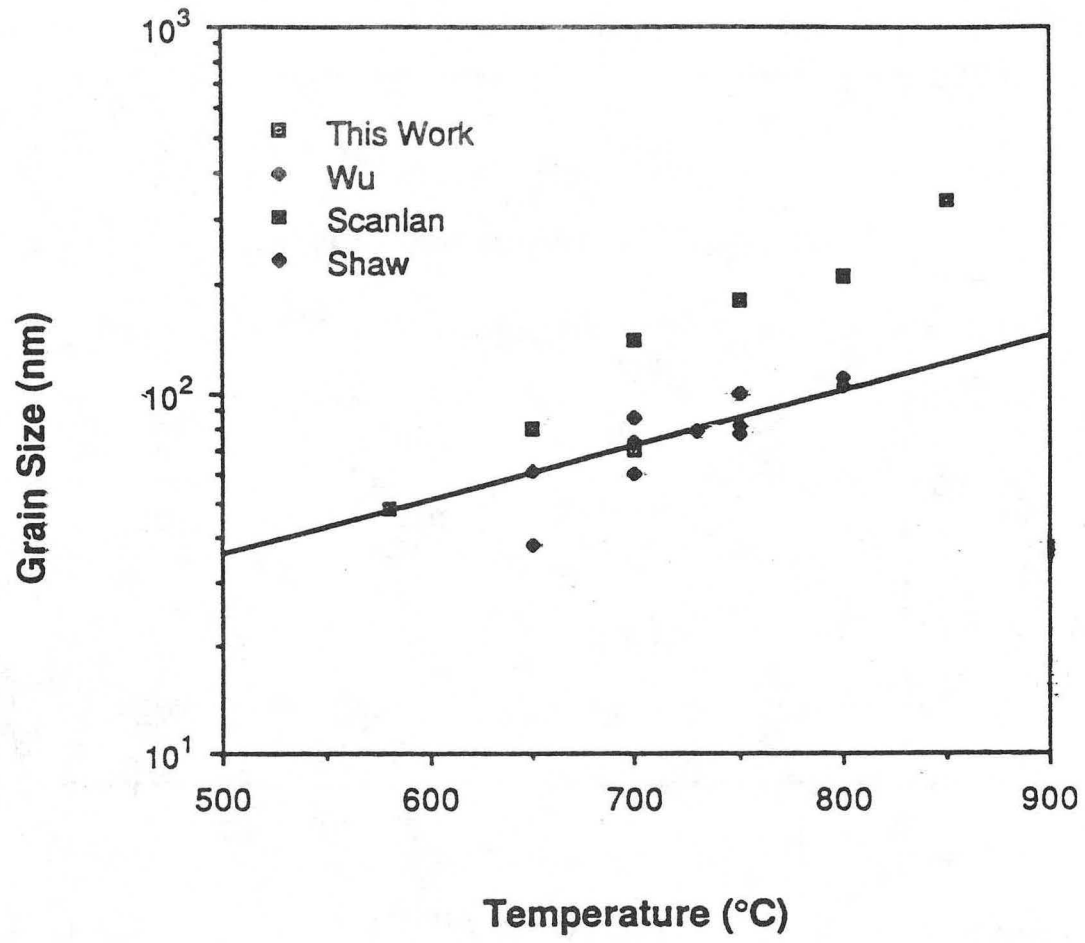


Fig. V.2

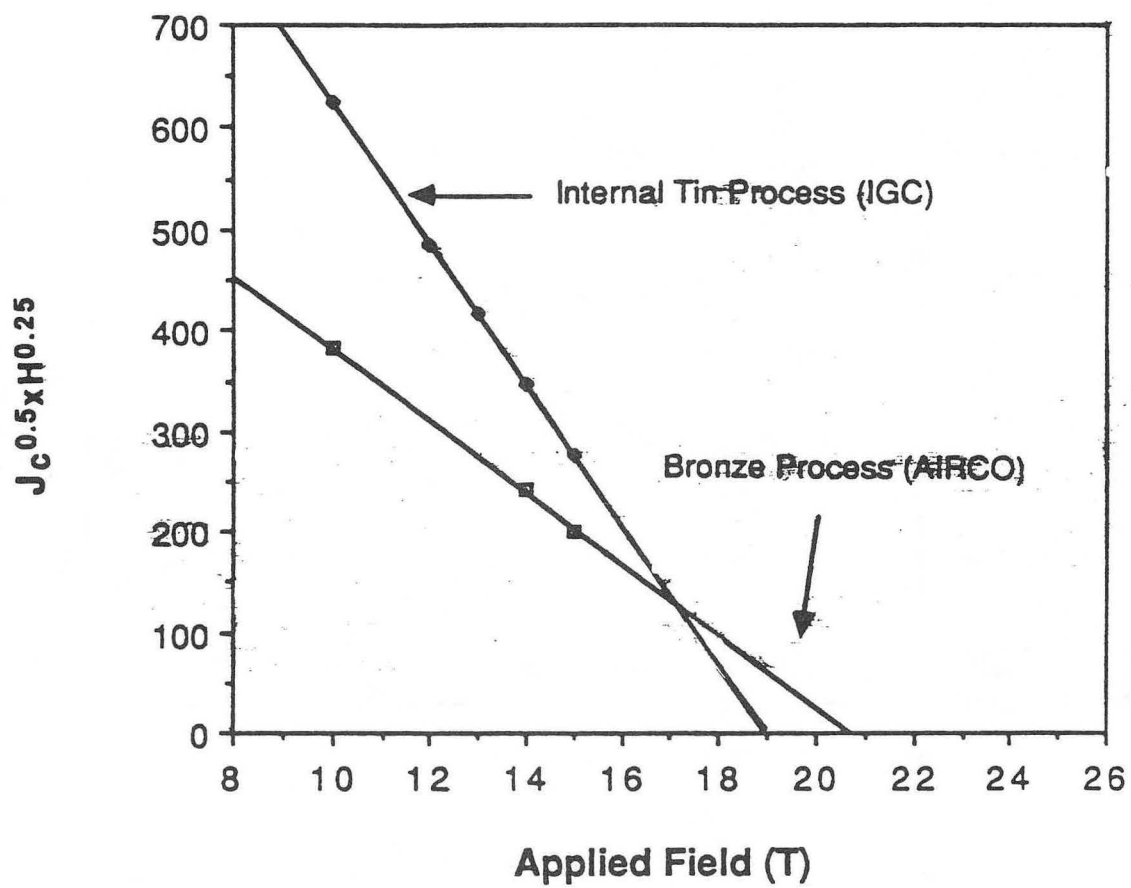


Fig. V.3

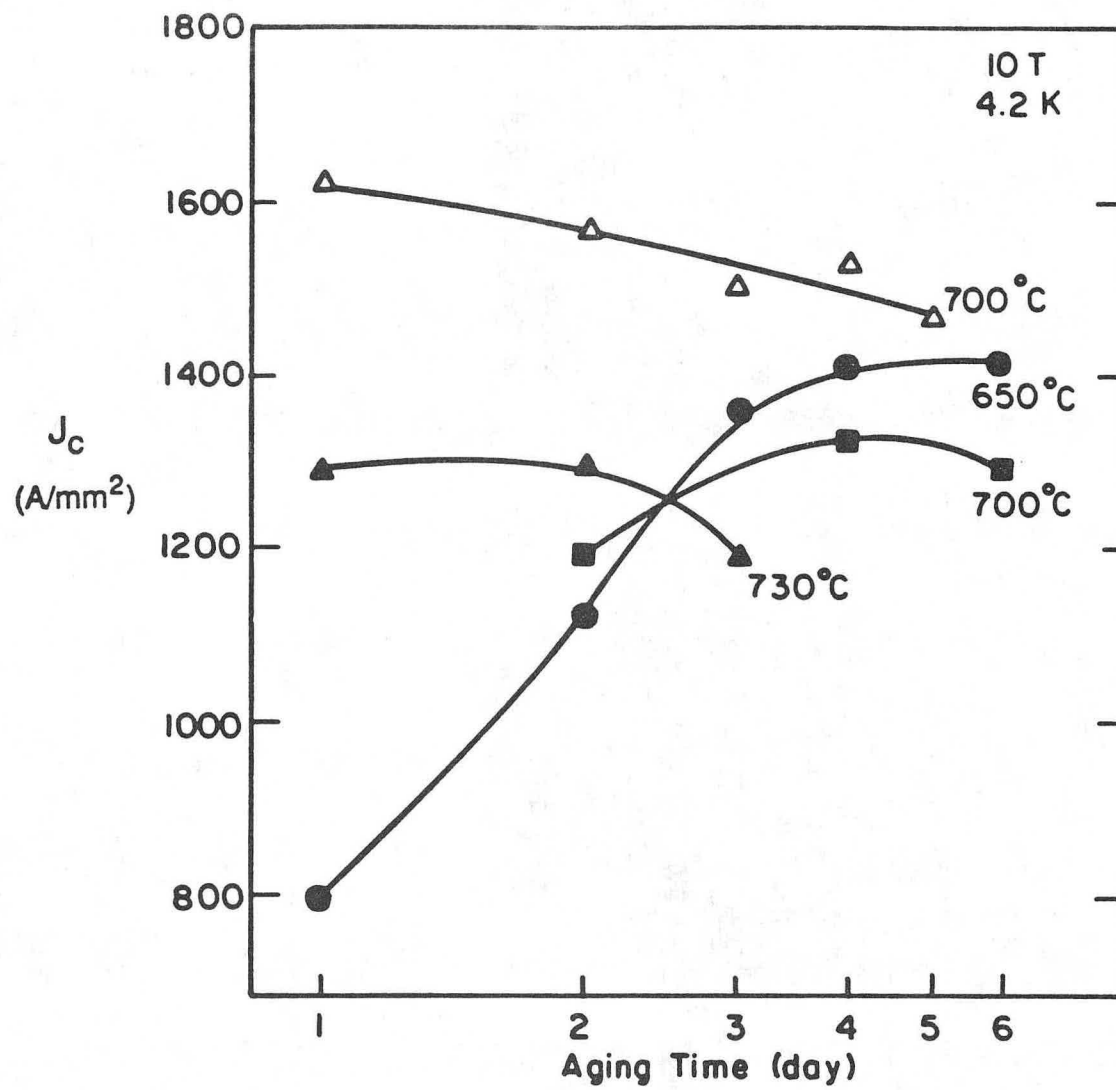
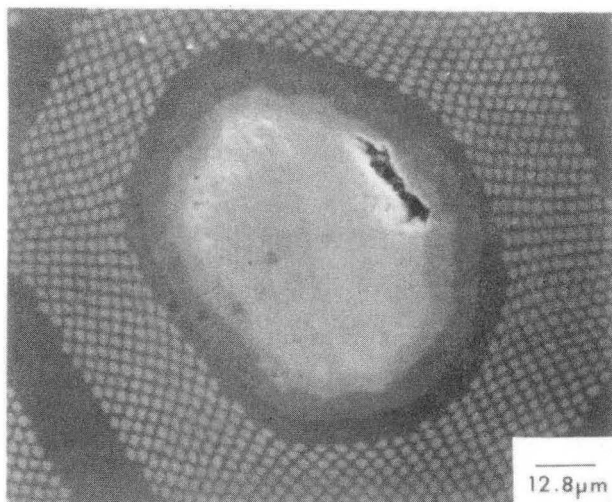


Fig. V.4



IGC

200° C/200hrs.



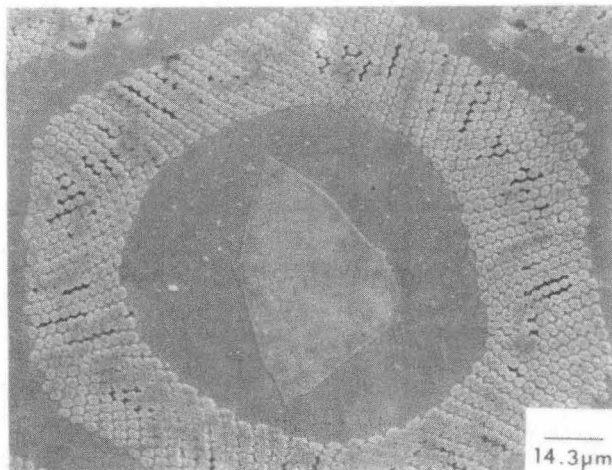
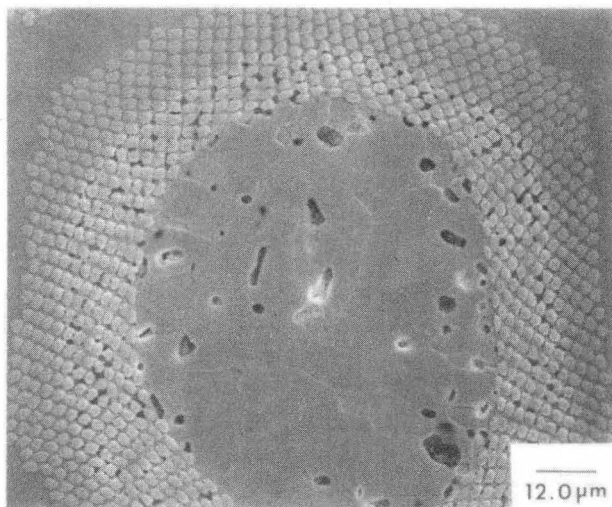
+

375° C/33hrs.



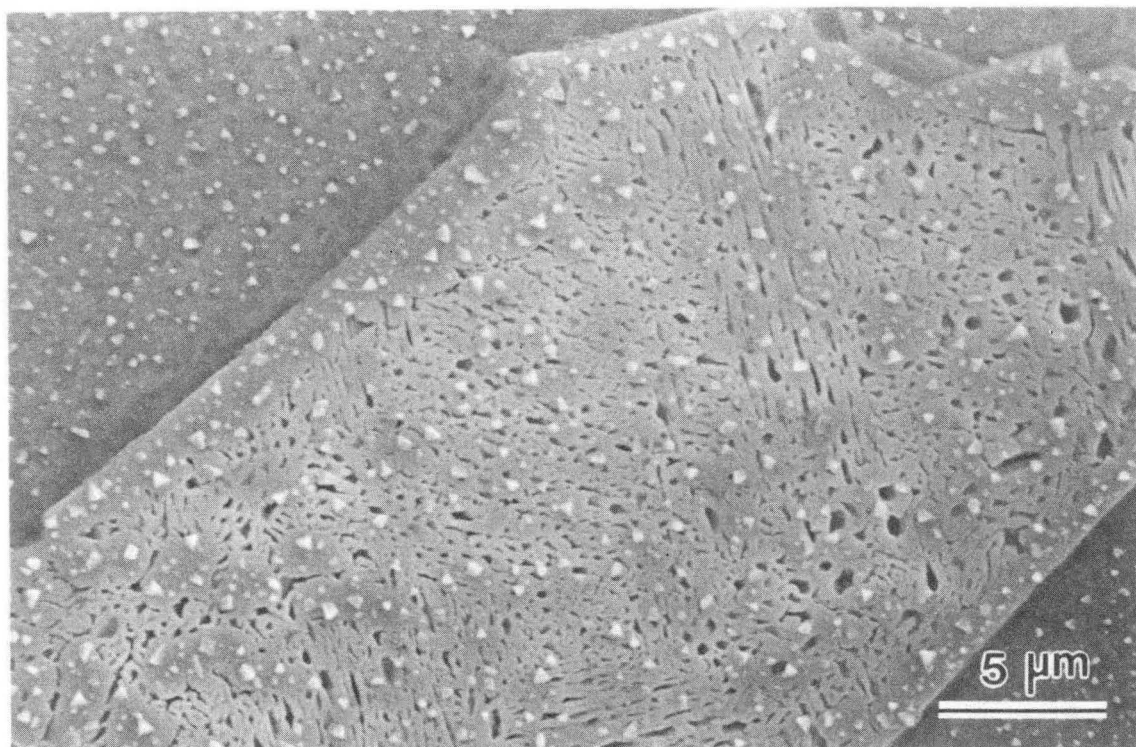
+

580° C/48hrs.



XBB 844-2589

Fig. V. 5



XBB 980-10487

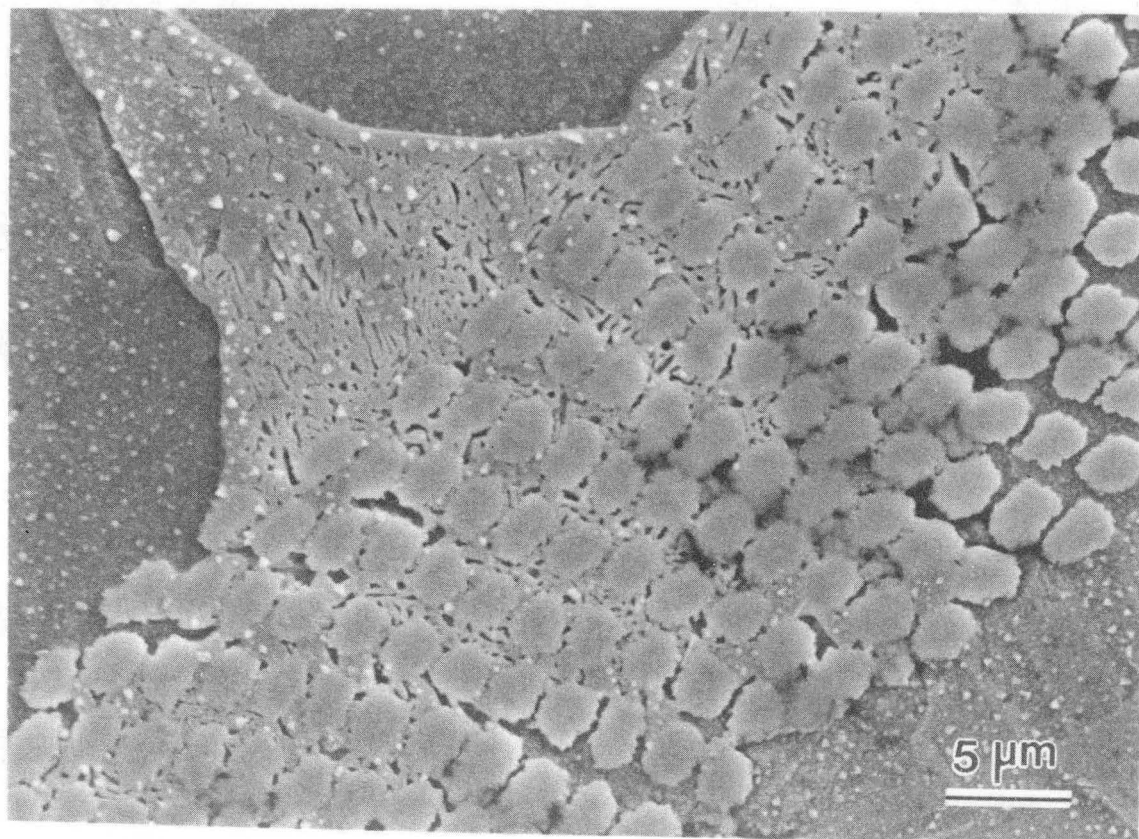


Fig. V.6



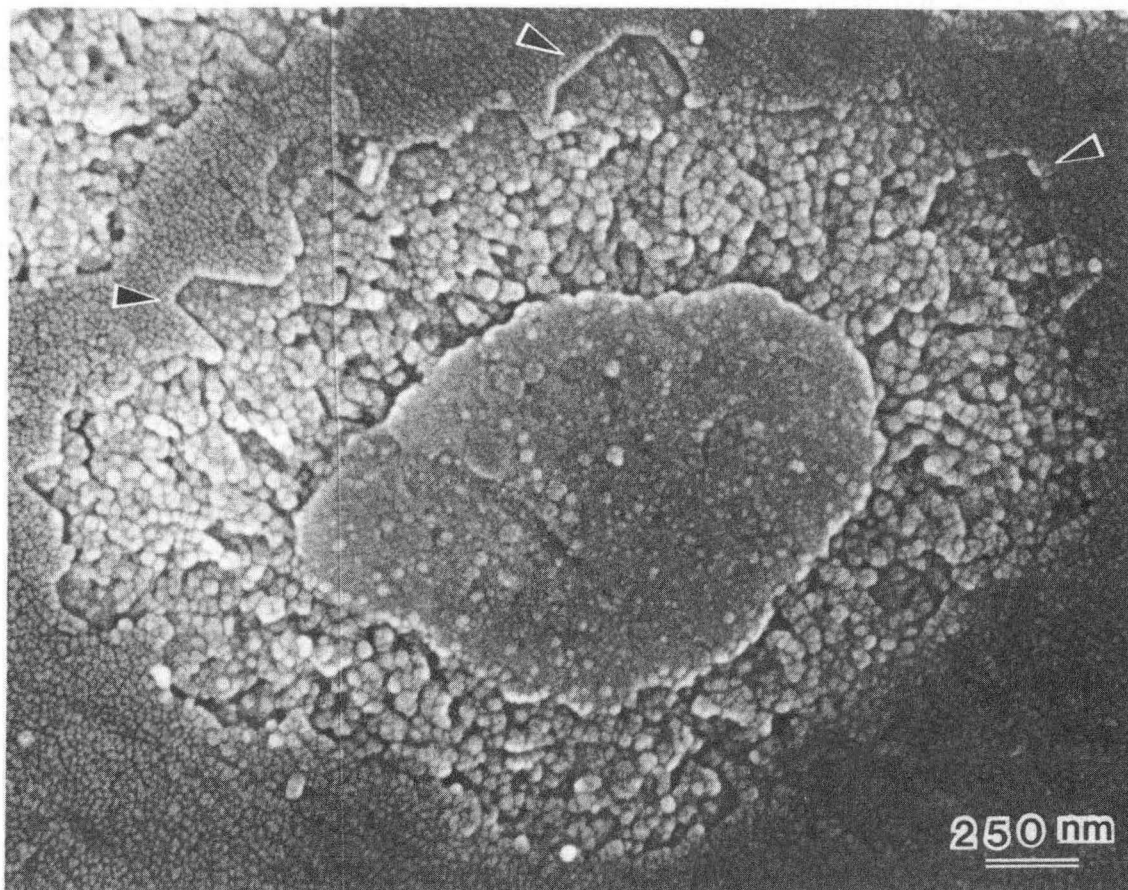
(a)



(b)

XBB 870-10490

Fig. V. 7



XBB 858-6105

Fig. V.8

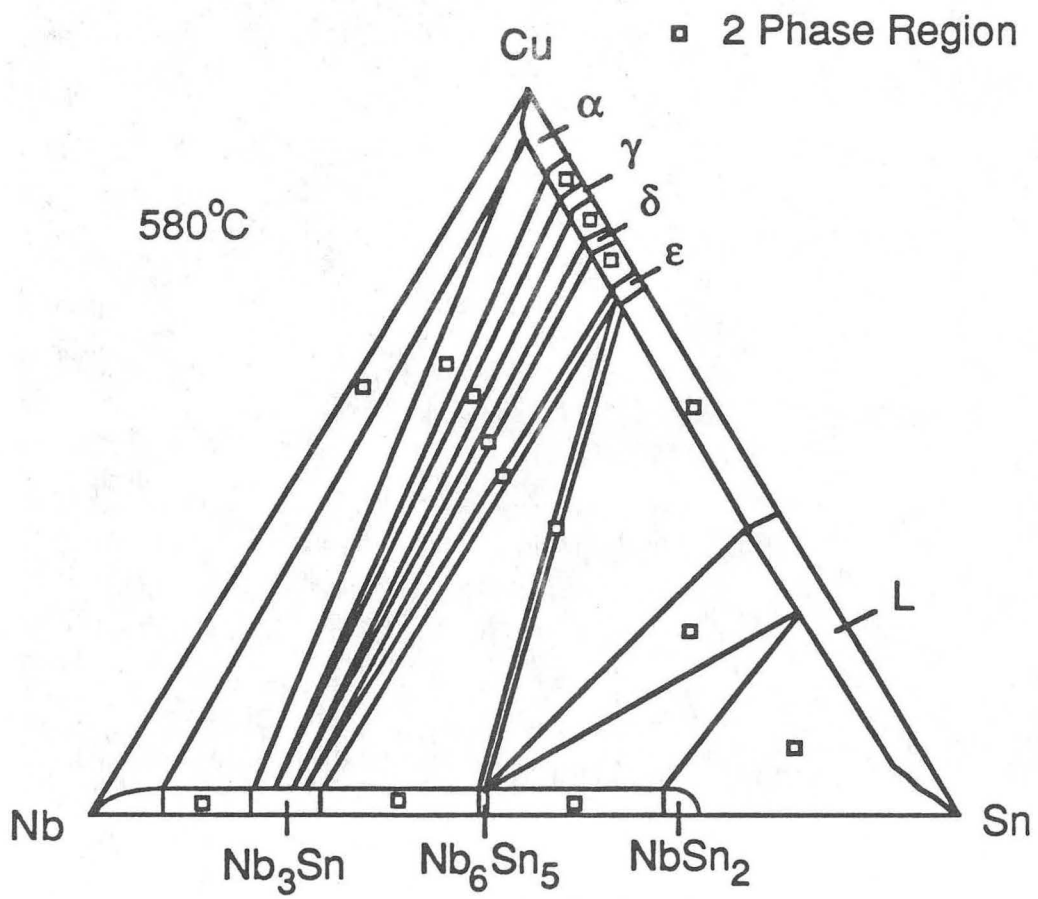
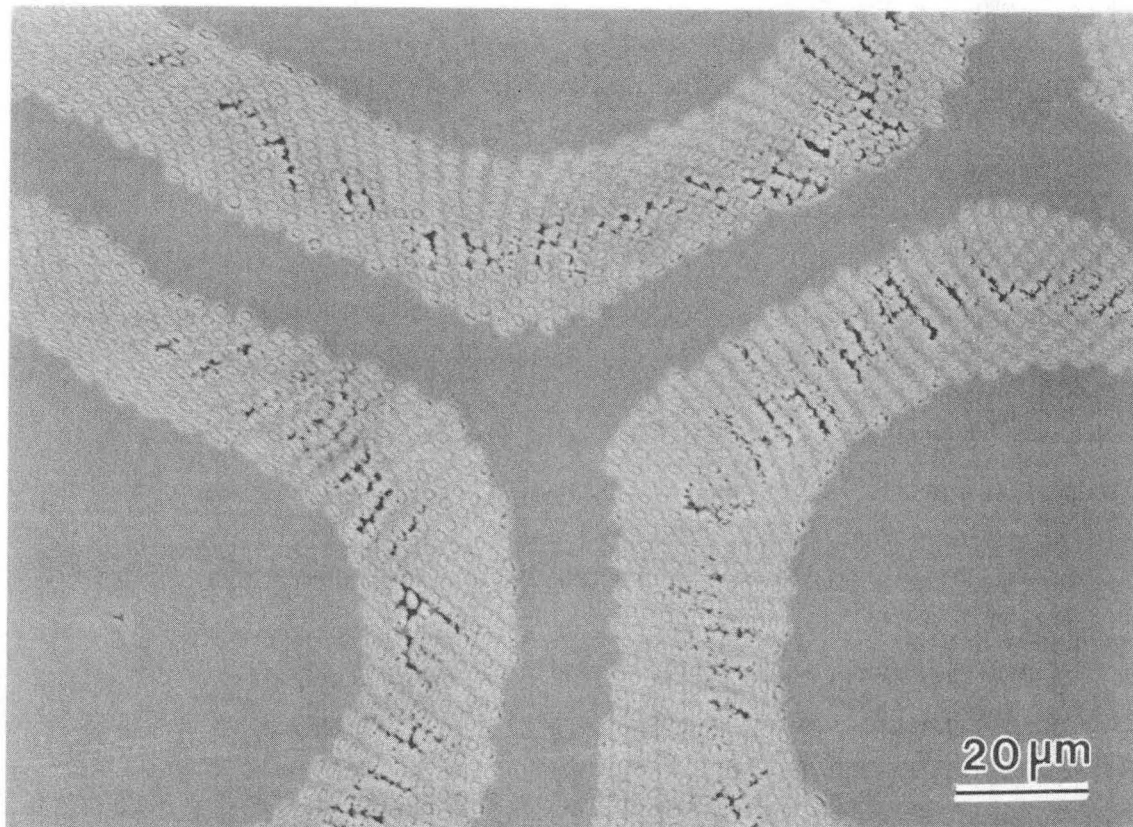
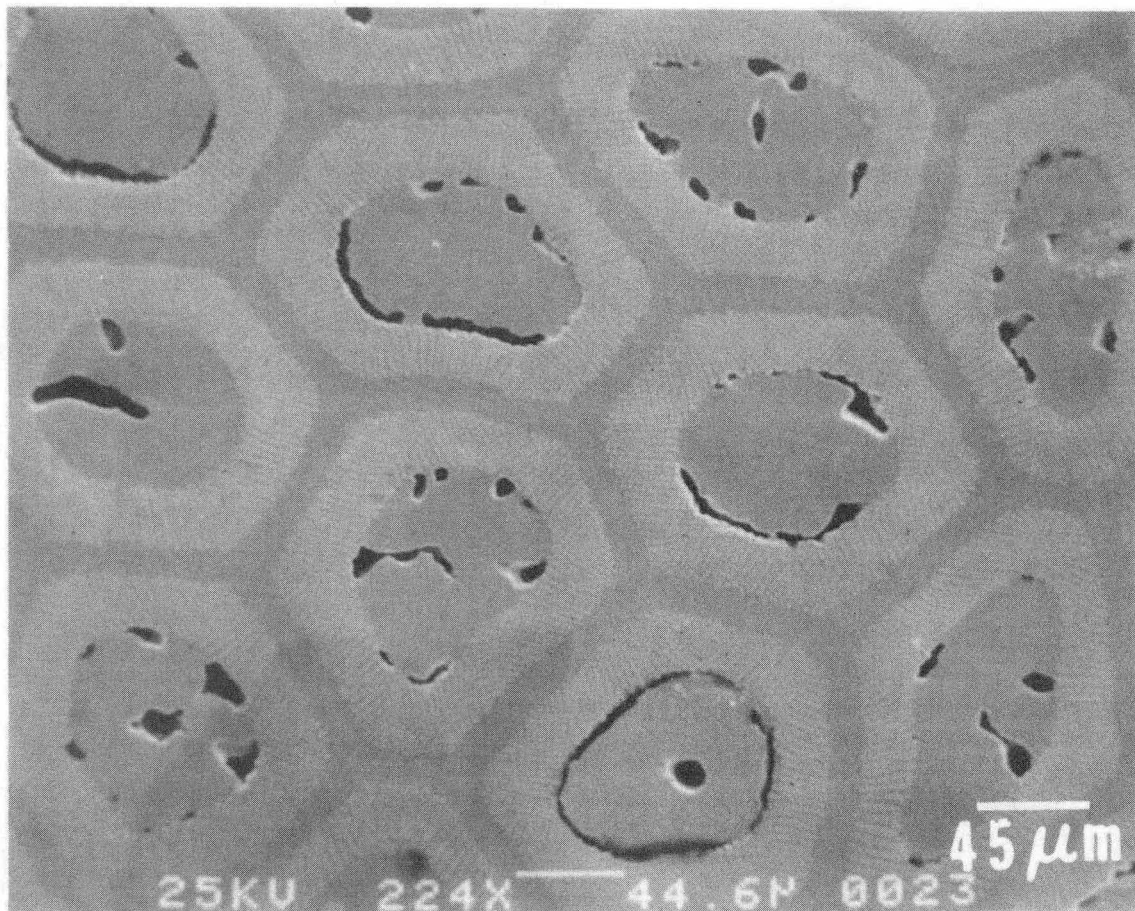


Fig. V.9



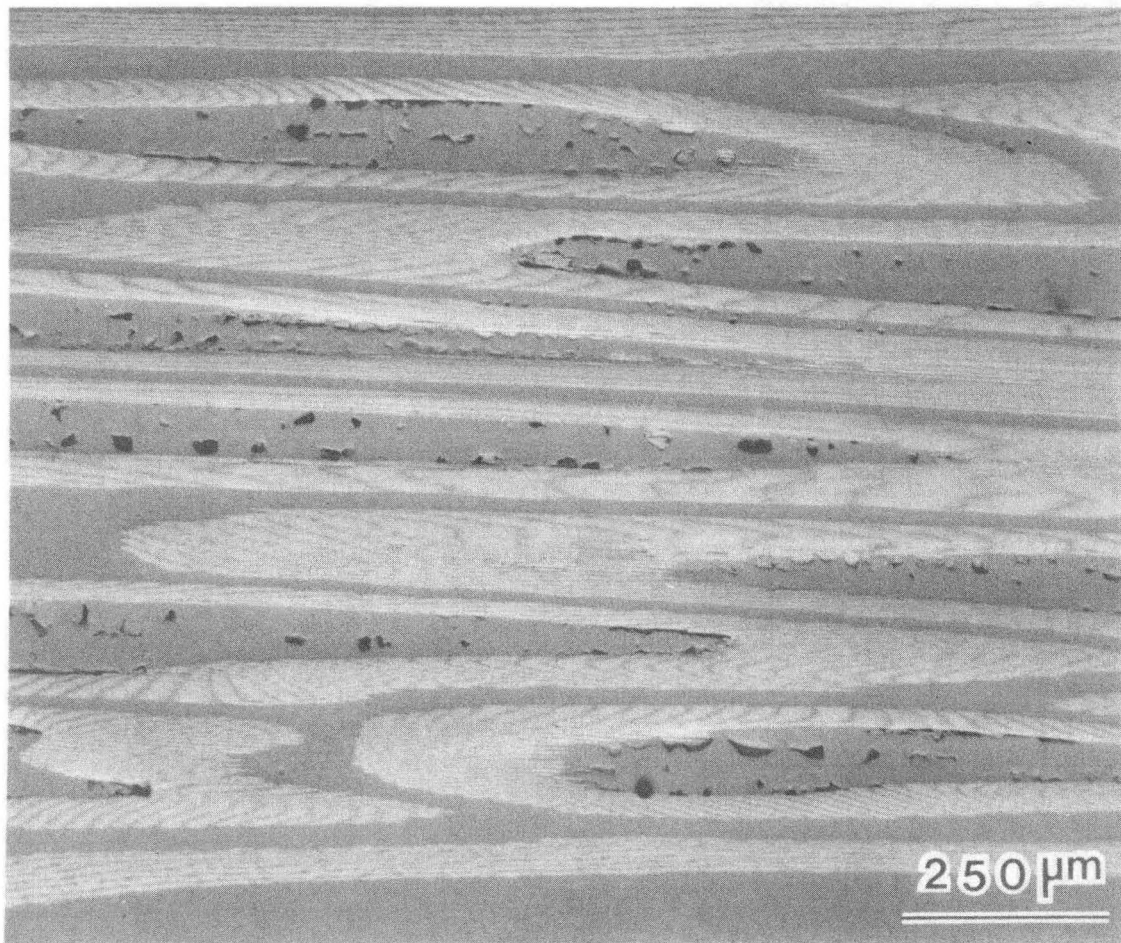
XBB 870-10488

Fig. V.10



XBB 840-7437

Fig. V.11



XBB 858-6101

Fig. V.12

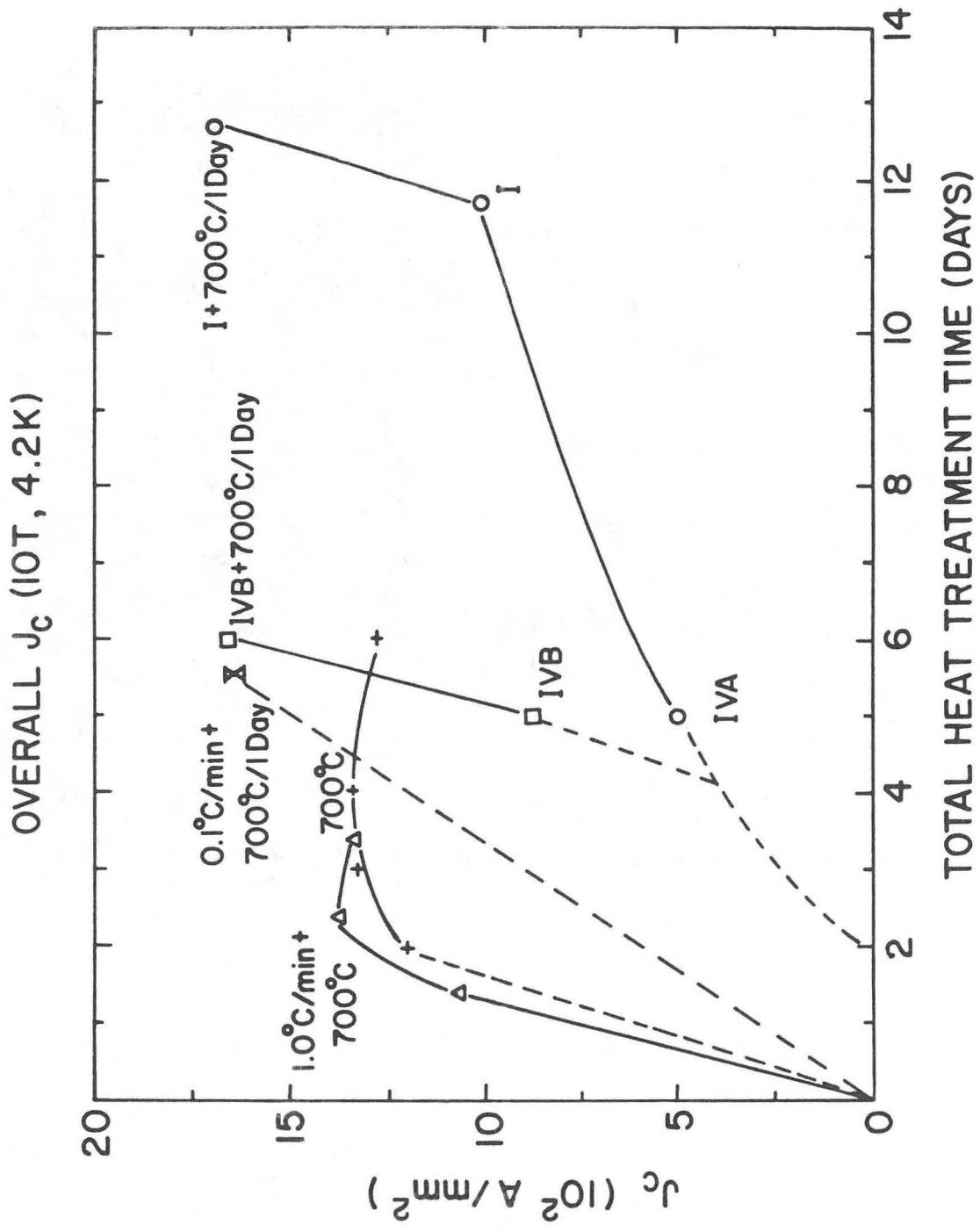


Fig. V.13

Table 4. Critical current, overall J_c , and J_c vs. heat treatment.
All currents measured at 10T and 4.2K.

Heat Treatment	Amount Reacted* (%)	I_c (Amperes)	Overall J_c ($\times 10^2$ A/mm ²)	J_c of Nb ₃ Sn ($\times 10^3$ A/mm ²)
IVA	60	6.5	5.0	2.4
IVB	75	11.4	8.8	3.0
I	85	13.0	10.0	2.8
IVB + 700°C/1 day	100	21.6	16.6	3.9
I + 700°C/1 day	100	21.9	16.9	4.0
0.1°C/min. + 700°C/1 day	100	21.2	16.3	3.8
700°C/4 days	100	18.2	14.0	3.3

$$* \text{ (Amount Reacted, \%)} = \frac{A_{15}}{A_{15} + Nb} \times 100$$

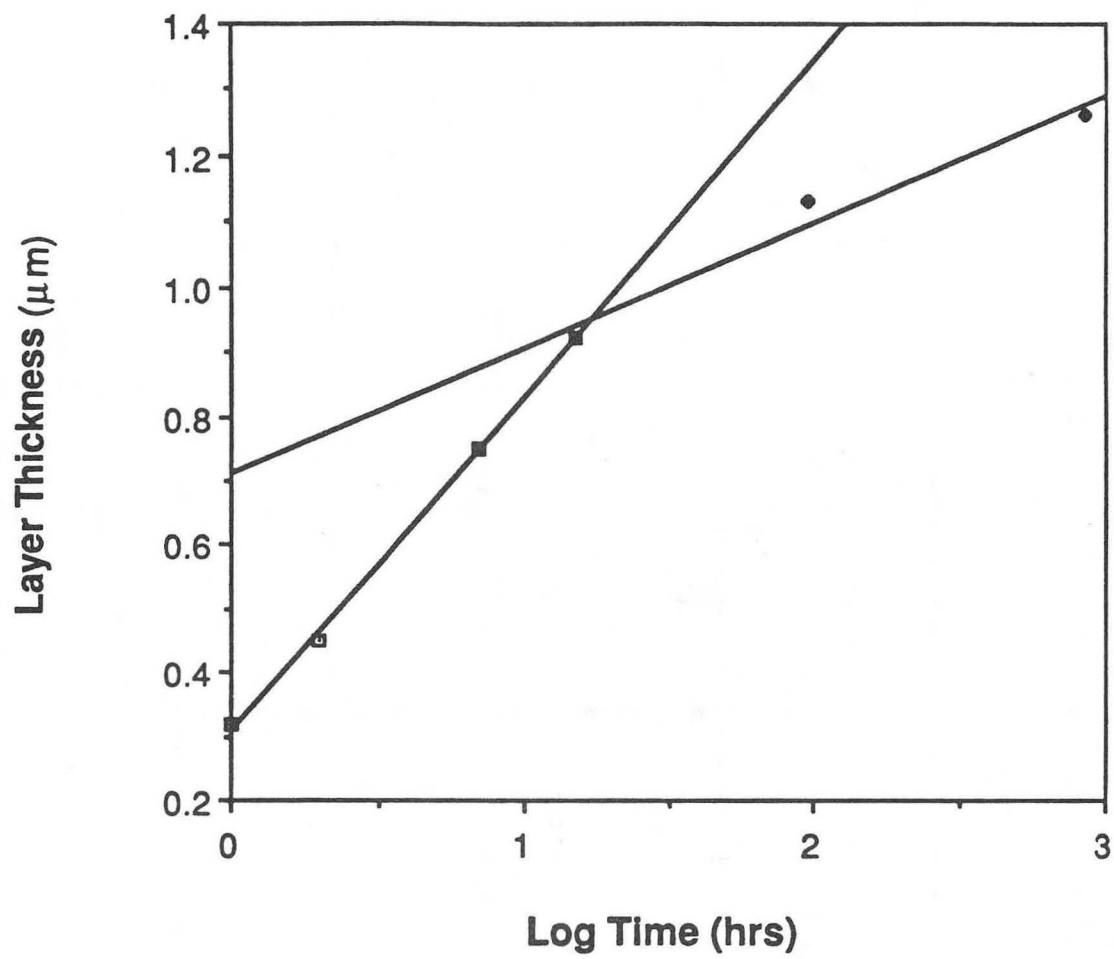
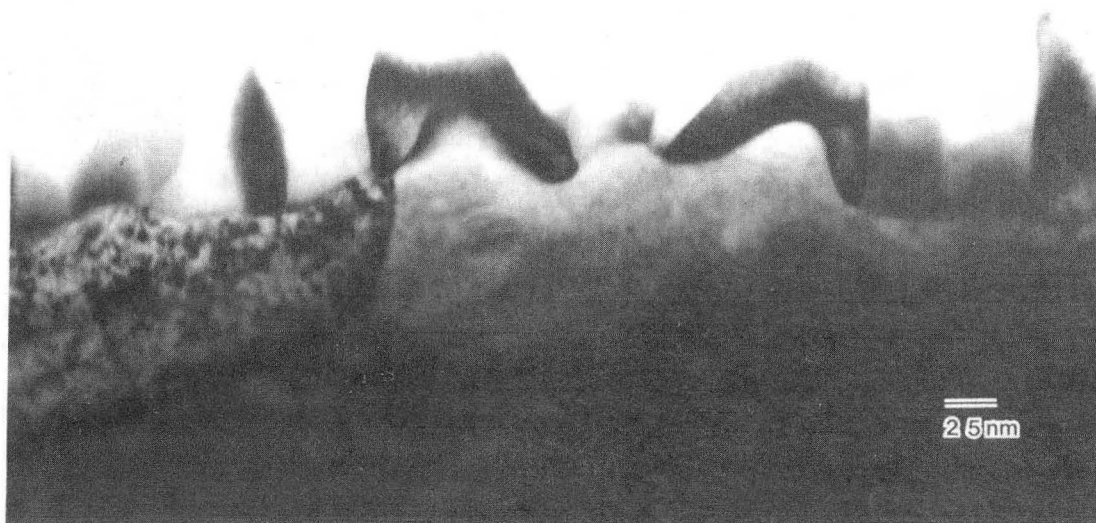


Fig. VI.1



XBB 872-1129

Fig. VI.2



XBB 872-1127

Fig. VI.3

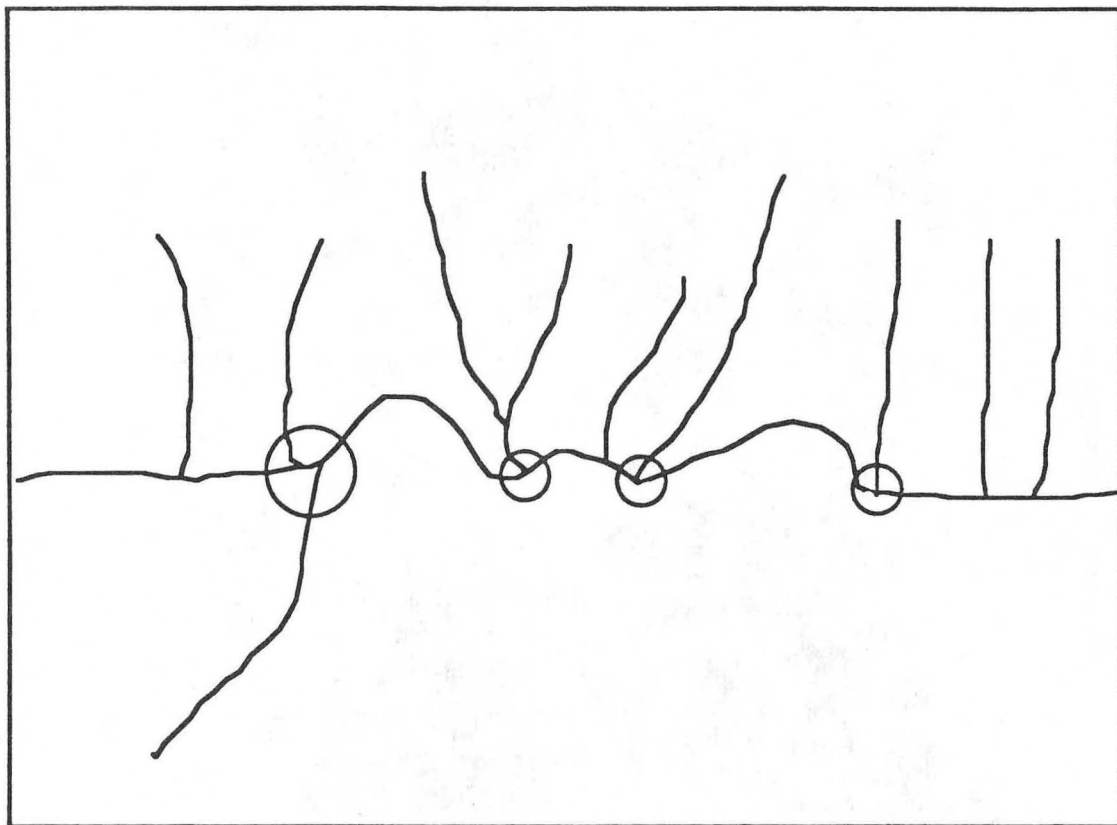
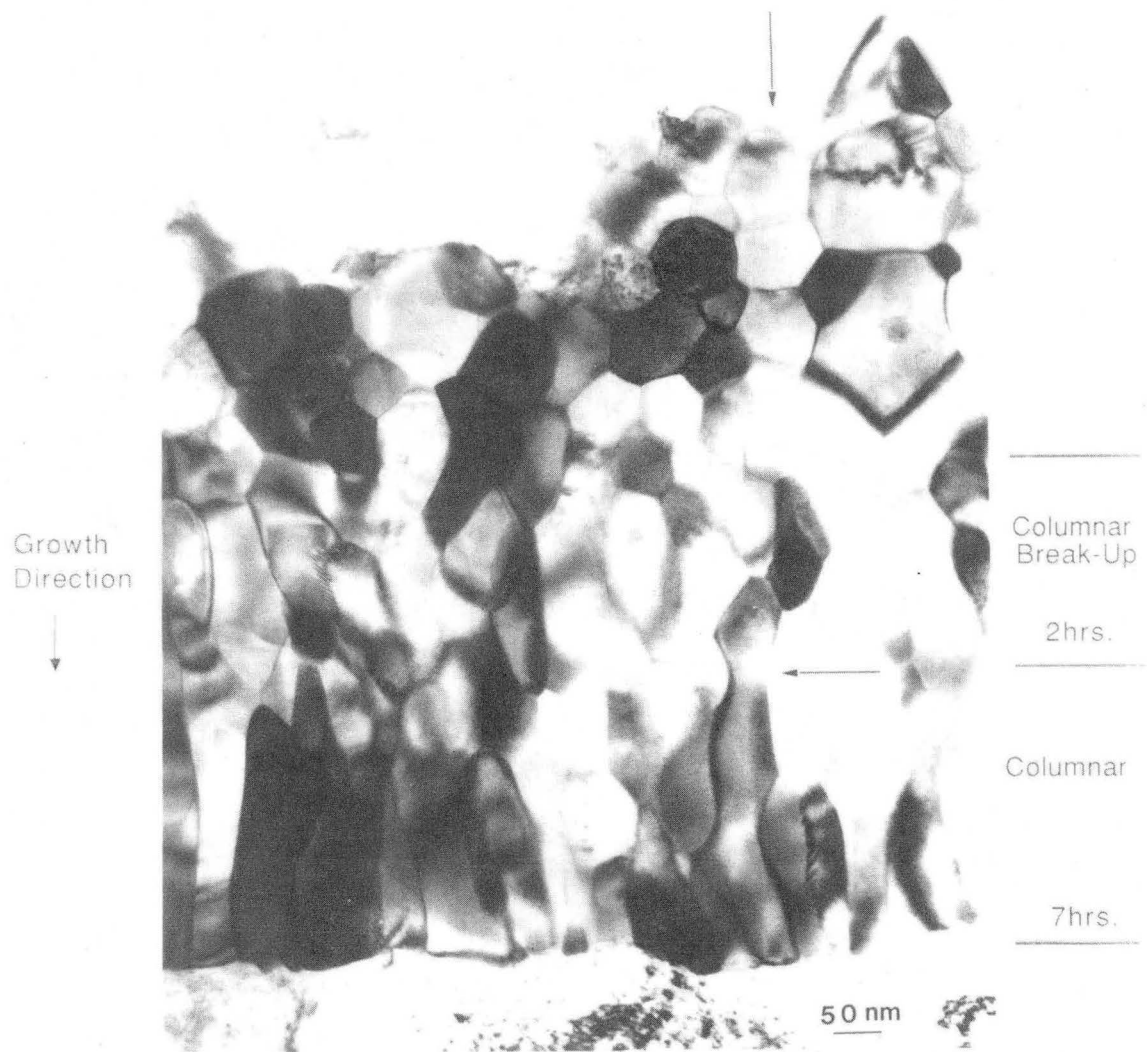


Fig. VI.4



XBB 867-5951A

Fig. VI.5

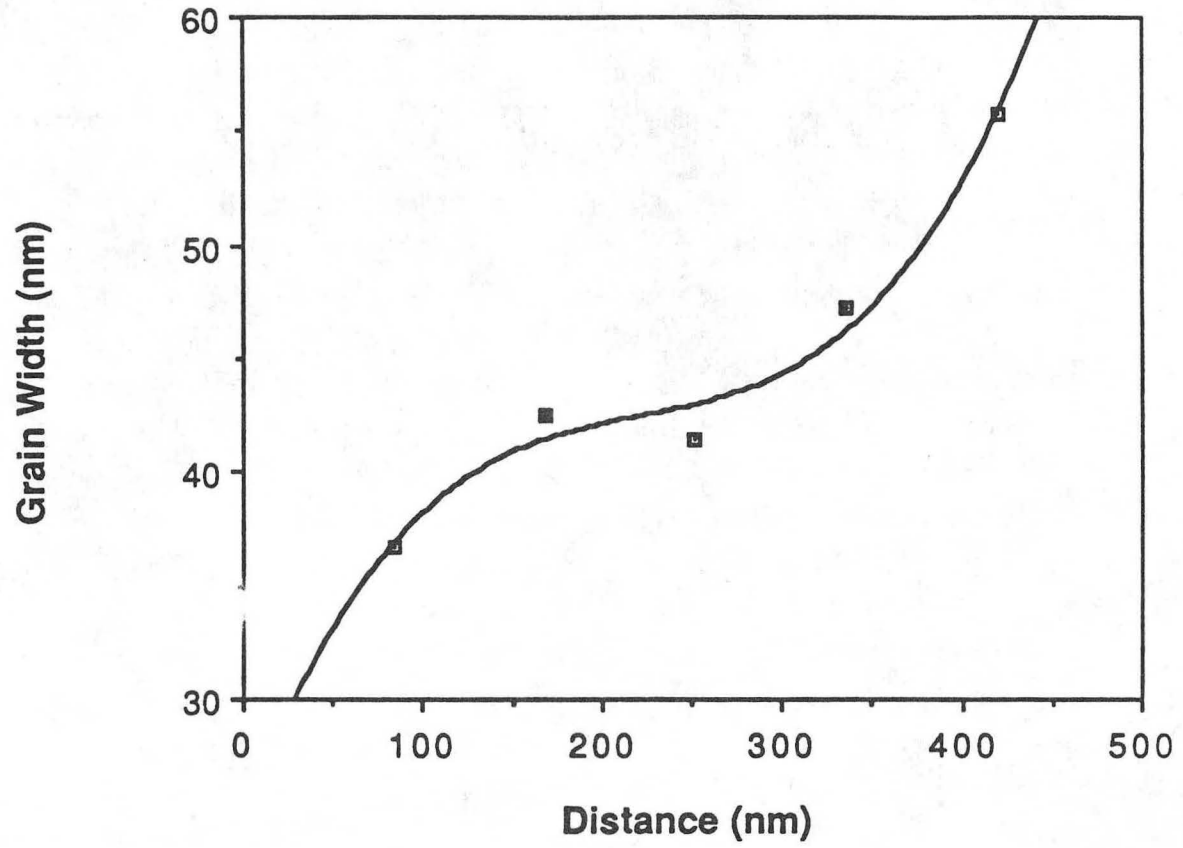
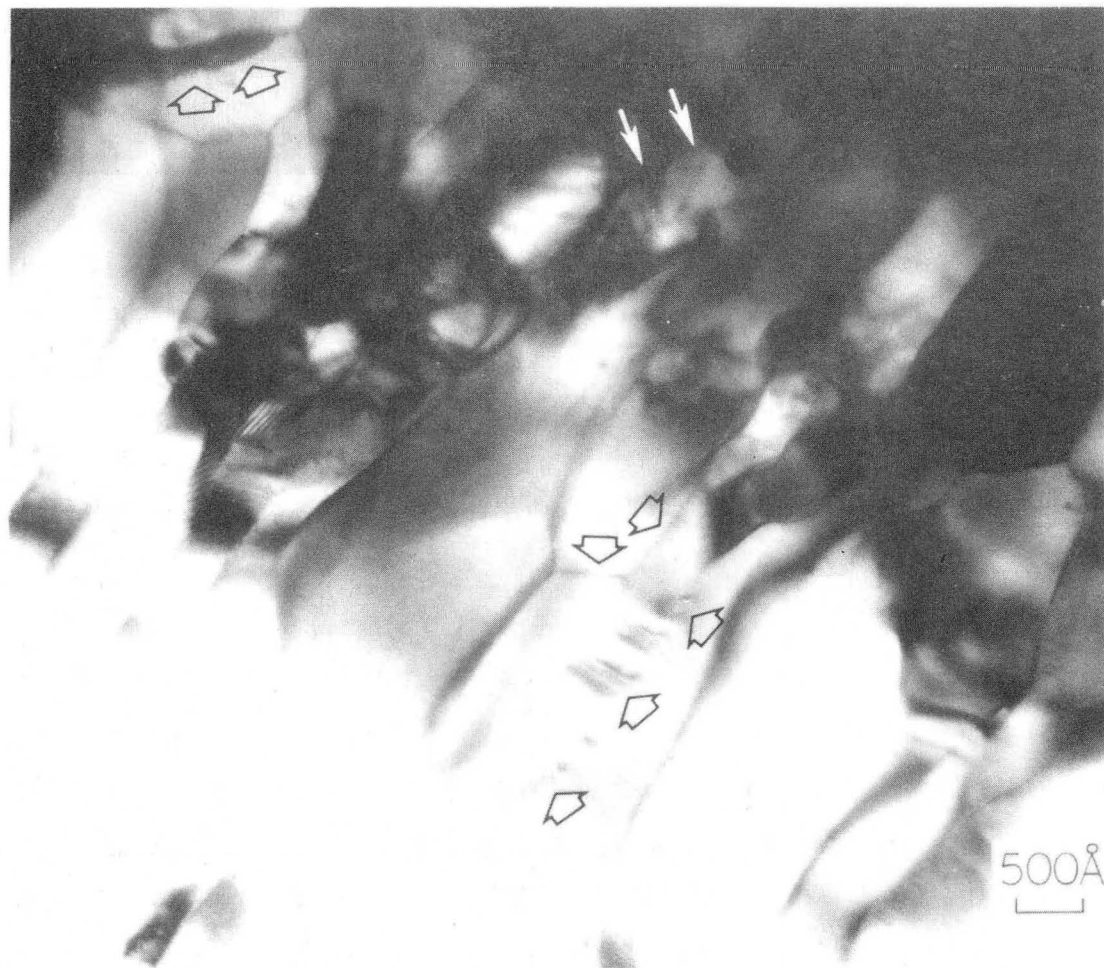
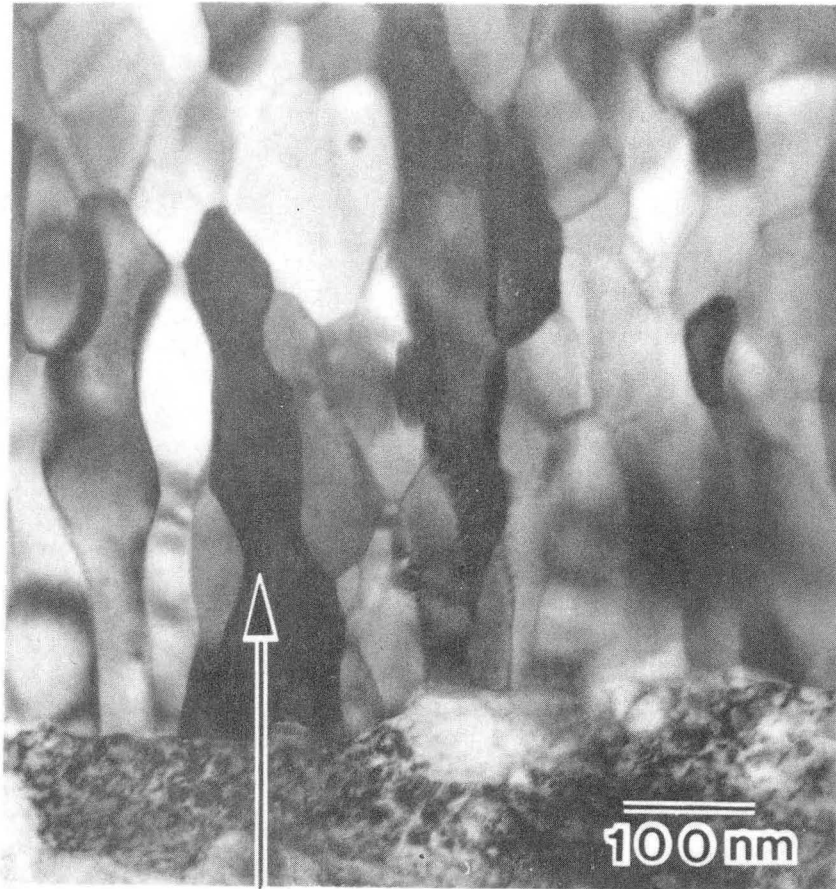


Fig. VI.6

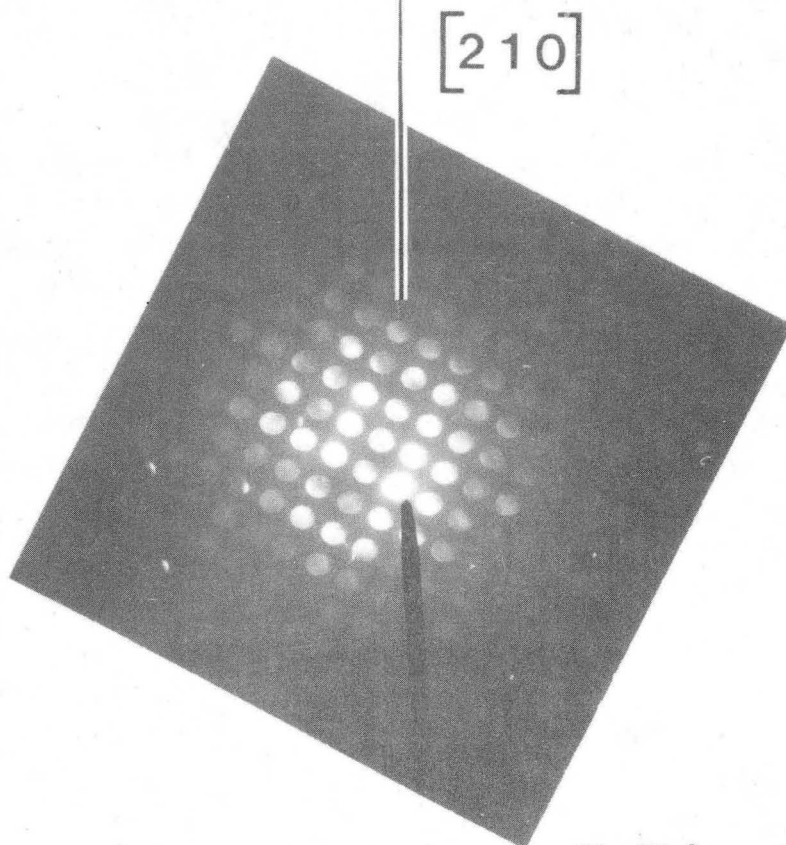


XBB 824-4086

Fig IV.7



XBB 872-1278



100
Pattern

Fig VI.8

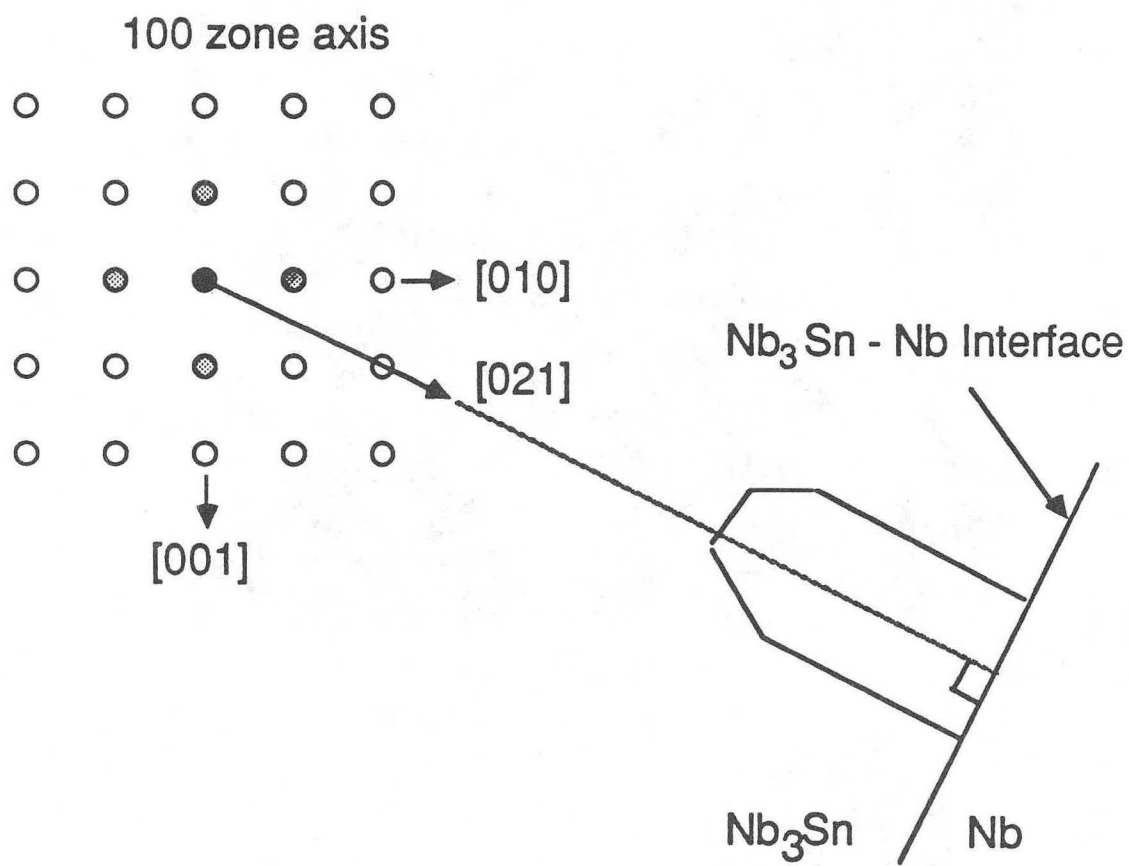


Fig. VI.9

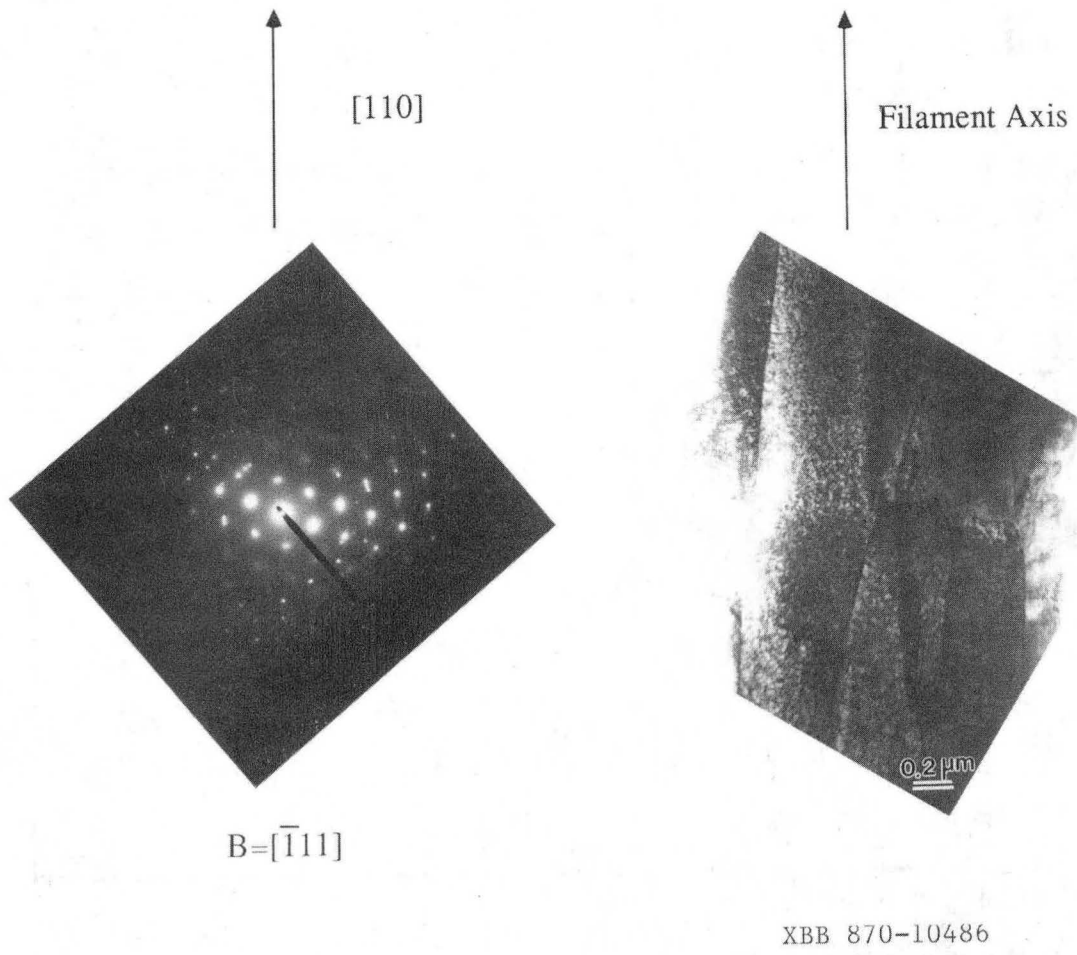


Fig.VI.10

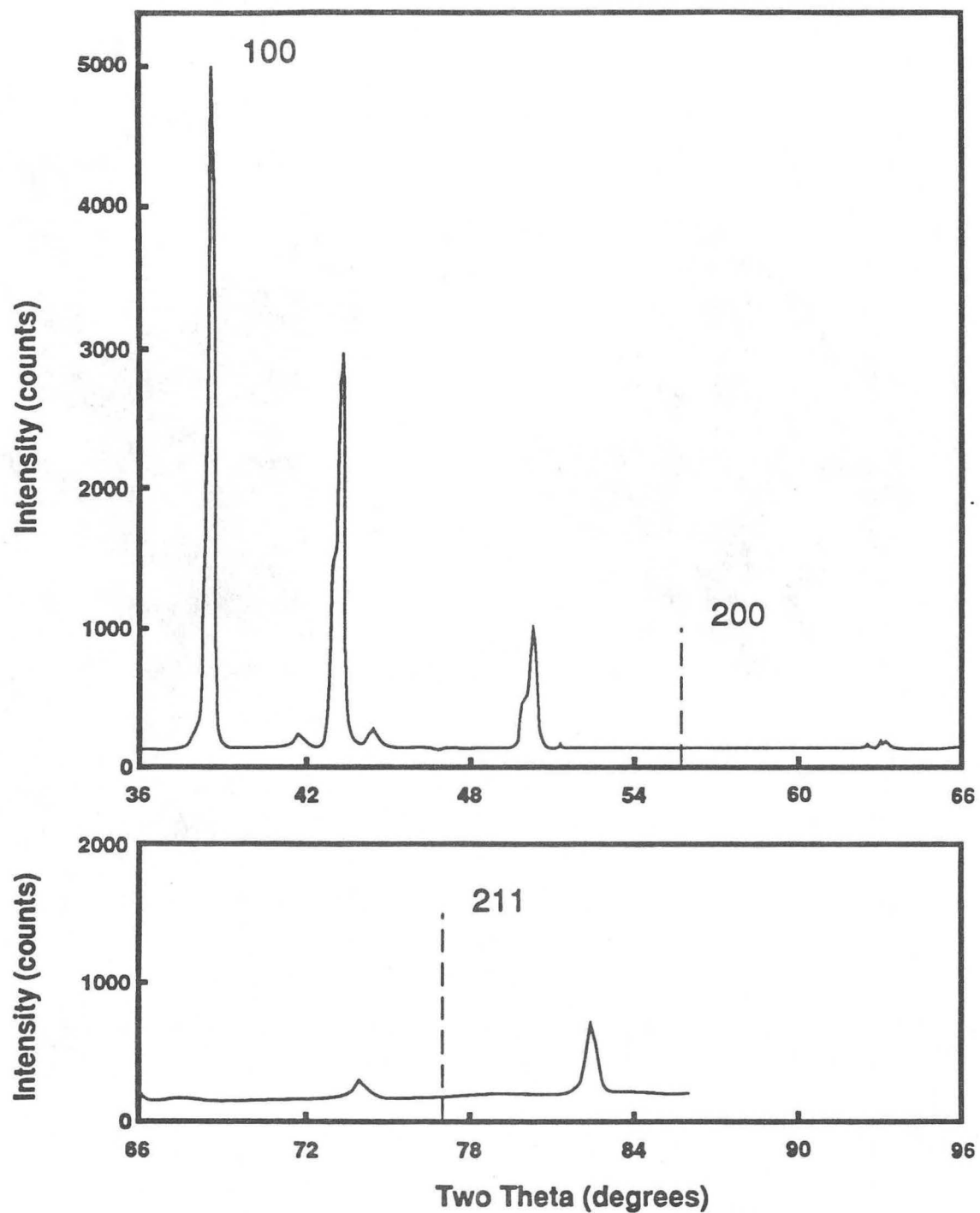


Fig. VI.11 X-ray diffraction scan for an axially oriented sample. A strong [110] texture is observed: 110 reflection strong, 200 and 211 absent.

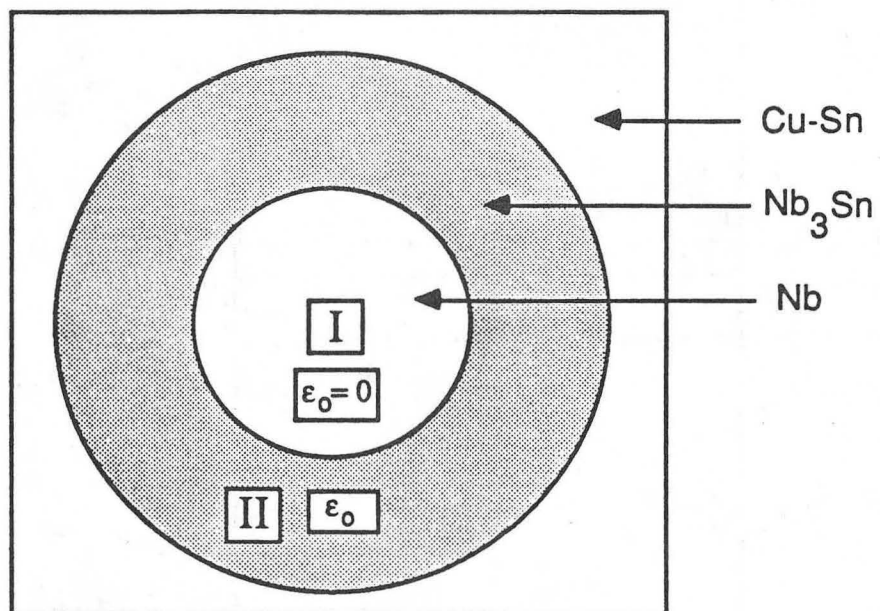


Fig. VI.12

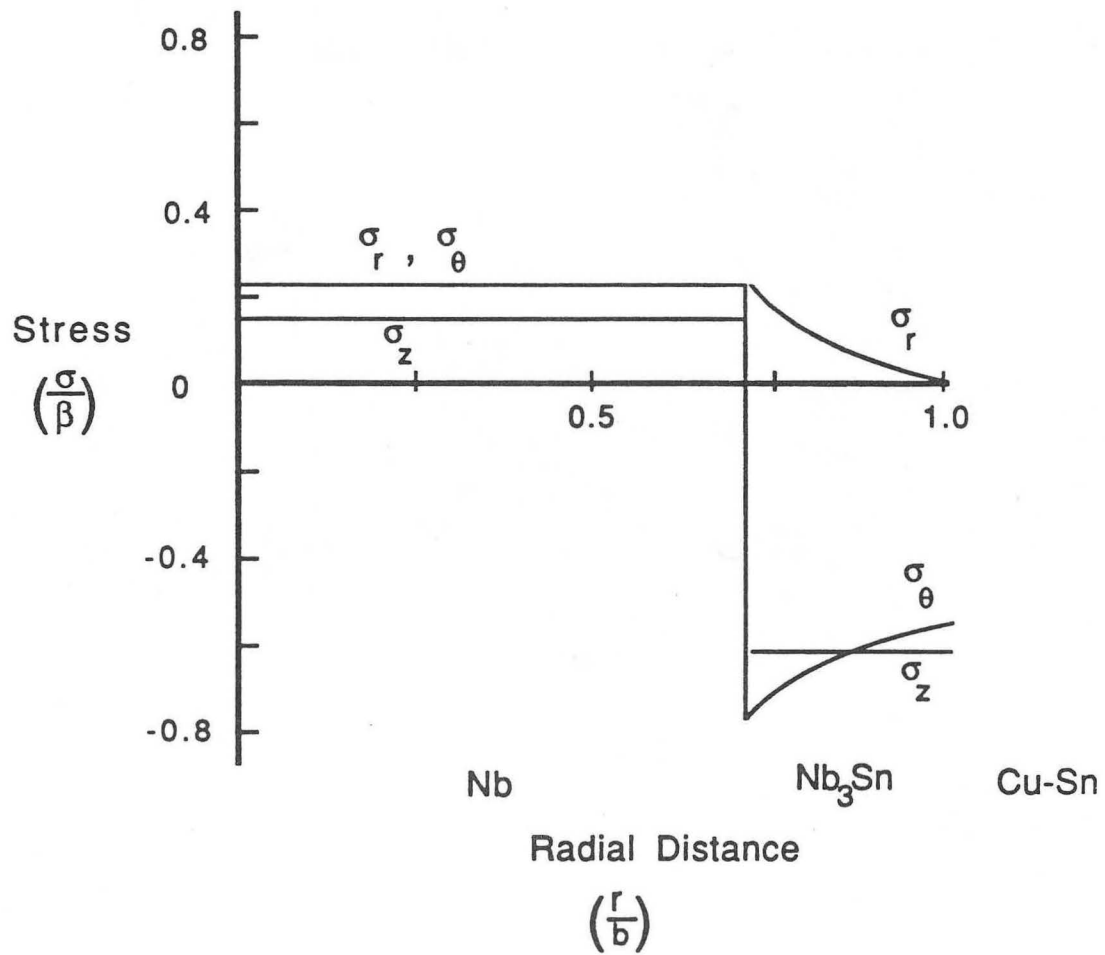


Fig. VI.13

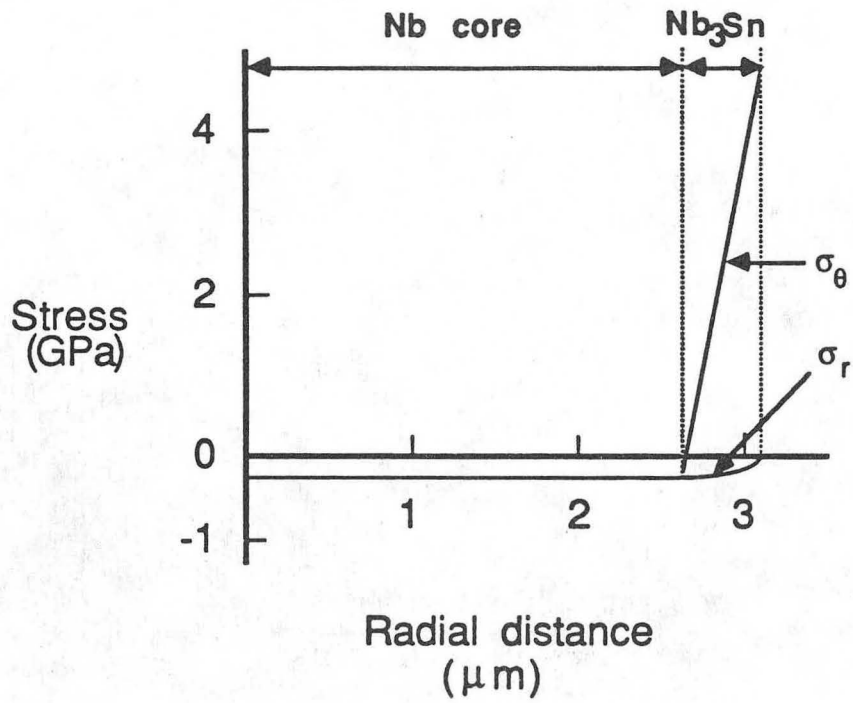
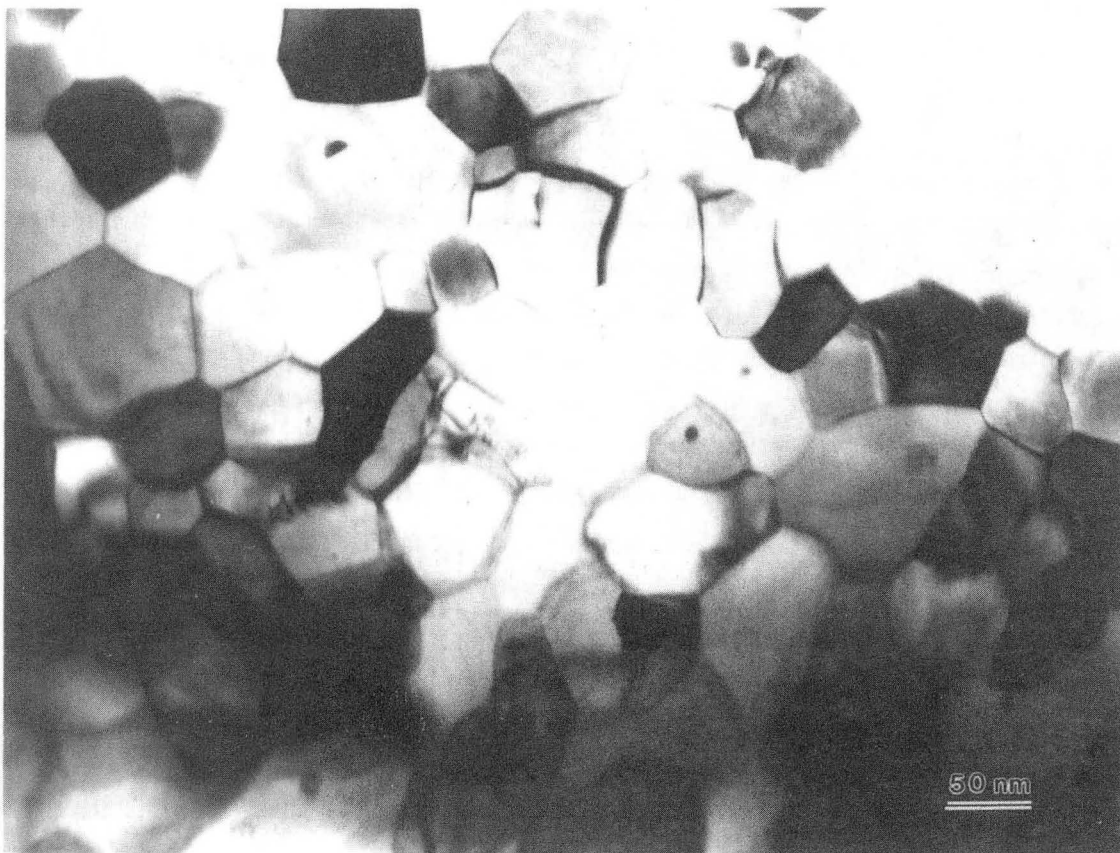


Fig. VI.14



XBB 870-10491

Fig. VI.15

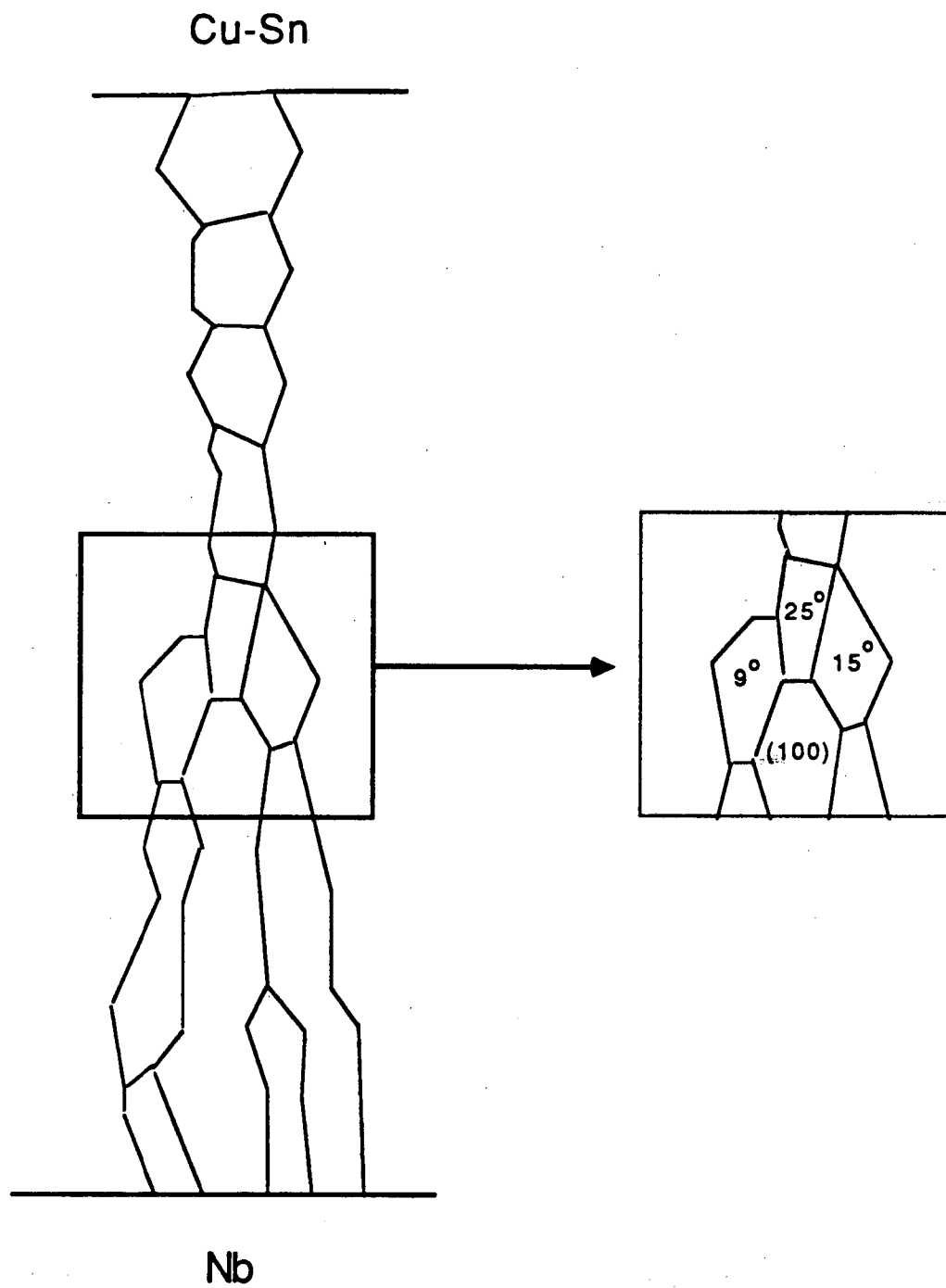


Fig. VI.16

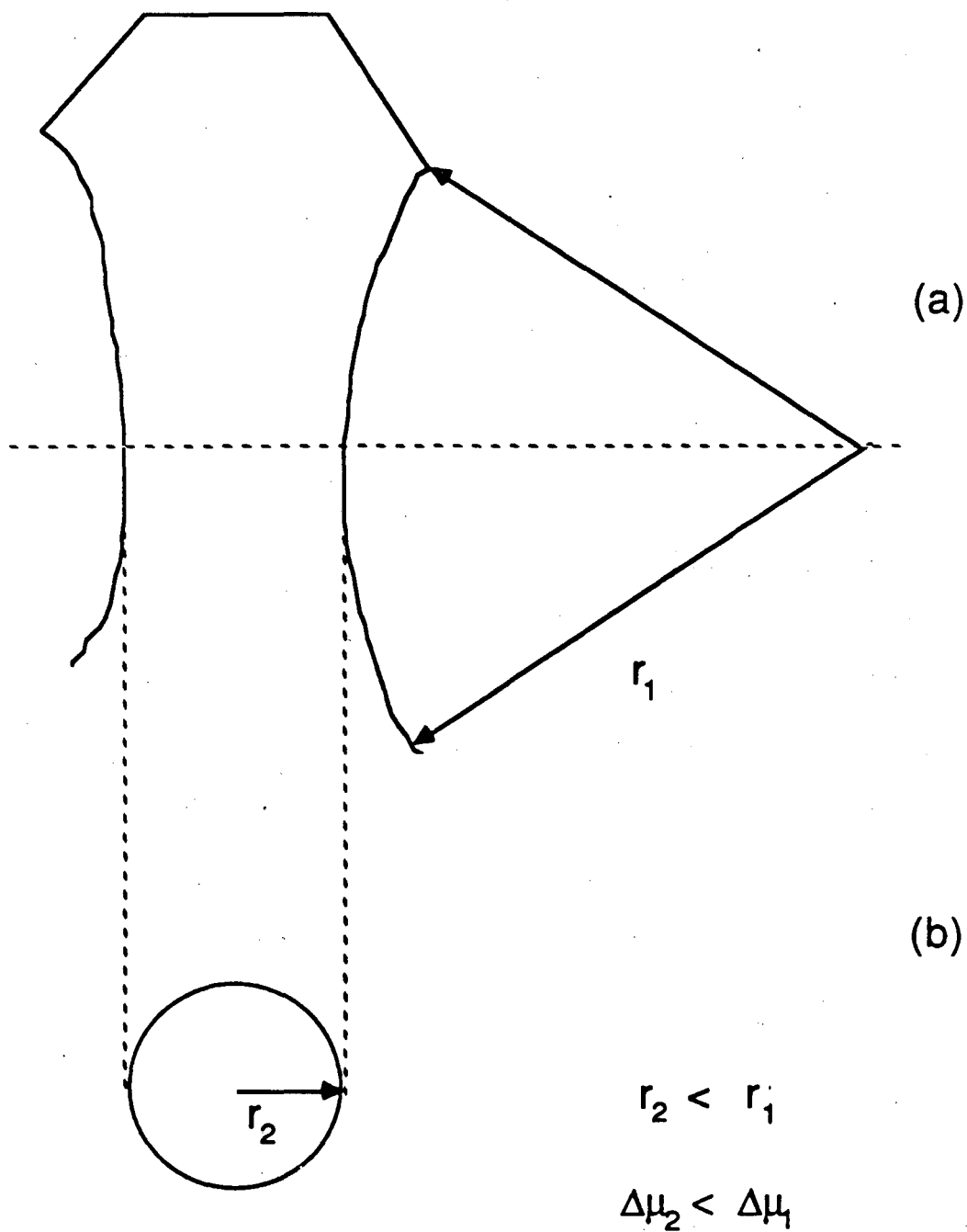


Fig. VI.17

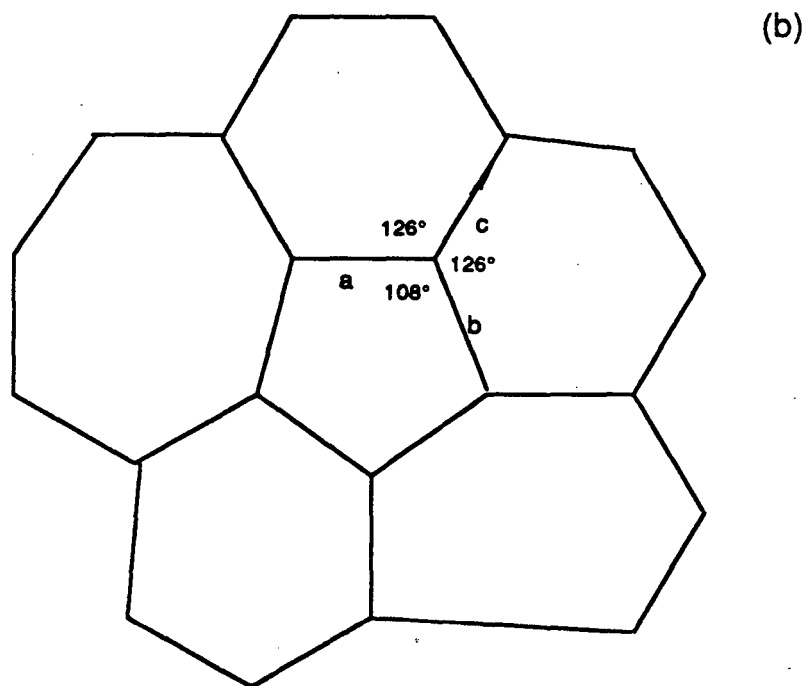
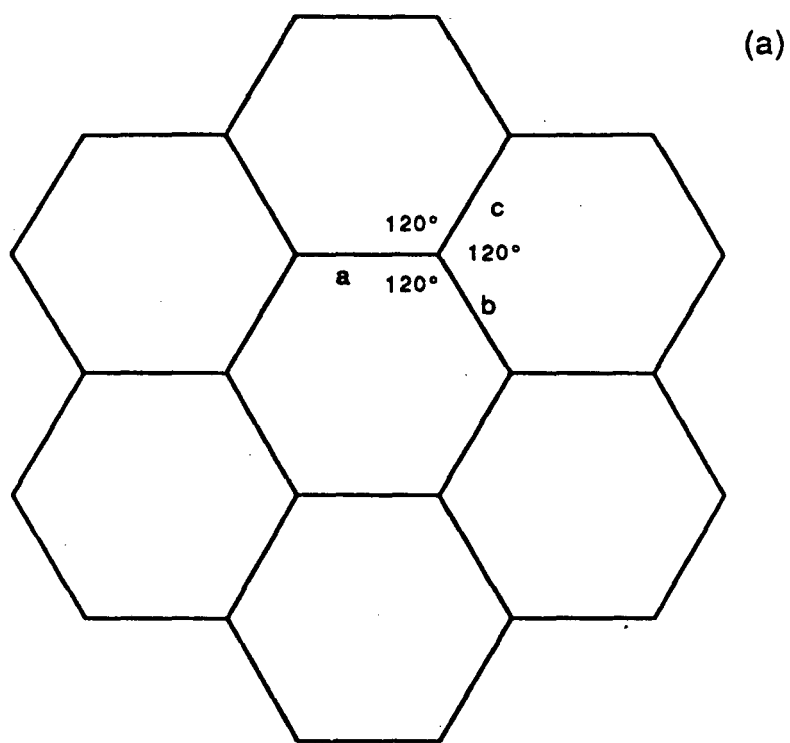


Fig. VI.18

*LAWRENCE BERKELEY LABORATORY
CENTER FOR ADVANCED MATERIALS
1 CYCLOTRON ROAD
BERKELEY, CALIFORNIA 94720*